Imperial College London

Department of Electrical and Electronic Engineering

The Effect of Renewable Power Interface Electronics on Grid Monitoring Systems

Author:

Aditya Joshi (CID:01519308)

Supervisors:

Professor Tim Green
Dr Caspar Collins

Final year thesis report
For MEng Electrical and Electronic Engineering

1 Final report Plagiarism Statement

I affirm that I have submitted, or will submit, an electronic copy of my final year thesis report to the provided EEE link.
I affirm that I have submitted, or will submit, an identical electronic copy of my final year thesis to the provided Blackboard module for Plagiarism checking.
I affirm that I have provided explicit references for all the material in my Final Report that is not authored by me, but is represented as my own work.

Contents

List of Figures

2 Acknowledgements

I would like to thank my supervisor Professor Tim Green for introducing me to the topic and for his guidance and support throughout the thesis. I would like to give a special thanks to my co-supervisor Dr Caspar Collins for his continued technical help and support, without whom this thesis would not be possible. I also wish to thank my friends and family for supporting me through all the tough times.

3 Abstract

Increasing climate concerns push for the further decarbonisation of the electricity grid through increased penetration of renewables which interface with the grid through power converters. Electricity grid distance protection systems were designed for use with traditional synchronous generators thus power converters can cause maloperation and worsen the accuracy of fault detection. This thesis investigates how and why converters show worse performance in distance protection systems and evaluates the effectiveness of two potential solutions. It is shown that the maloperation is due to current limits on converters, which synchronous generators do not have. By injecting current at a specific phase angle, maloperation was found to reduce and become easier to mitigate for line to line faults, though improvements were limited by magnitude errors. Injecting current at higher order harmonics significantly reduced maloperation for line to line and line to ground faults but showed difficulties in scalability due to issues with multi-frequency current injection.

4 Introduction

The increasing pressures of climate change and the need to dramatically reduce global carbon emissions is leading to drastic changes in the energy, transport and heat sector. One such change is in the UK electricity supply, where the government aims to fully decarbonise power by 2035[5]. To achieve this the share of electricity generated from renewable net zero energy sources such as solar and wind energy must dramatically increase, resulting in increasing penetration of renewable energy in the electricity grid. Since these energy sources are entirely dependent on weather they require power converters such that they can supply power at a regulated frequency and voltage. For example, solar panels output energy at DC current, whereas the grid operates at 50 or 60 Hz. An inverter is thus required. Similarly, wind turbines are increasingly using power converters to interface with the grid so that they can rotate at a variable speed to efficiently capture wind energy while still generating electricity at a rated voltage and 50-60 Hz frequency.
Current UK and global electricity grid infrastructure, including fault protection and frequency control systems, was designed assuming that the majority of the energy would be originating from spinning or synchronous generators[6]. These include hydroelectricity, nuclear power and traditional fossil fuel generators such as coal and natural gas steam turbines. Power converters however behave differently to synchronous generators in terms of their electrical and stability properties, since they are based on semiconductor technology whereas generators are electro-mechanical. A particularly important difference is that power converters are current limited to a rated value so that the transistors do not risk overheating. As a result there are now many challenges in updating electricity transmission infrastructure to ensure a reliable and secure supply of energy for a grid heavily penetrated by converter technology[7]. One of these challenges involves distance protection systems for transmission line faults, where the properties of power converters can lead to maloperation and fault detection errors. Studying and finding solutions to this problem forms the main content of this thesis.

5 Background theory

Understanding the principles of distance protection and its implementations is key to the background for this thesis. Distance protection utilises voltage and current measurement relays to determine the impedance to a fault to determine how far away and in which zone of the transmission line the fault resides. This allows the correct section of the transmission line to be disconnected to clear the fault, while ensuring the unaffected lines remain in operation.

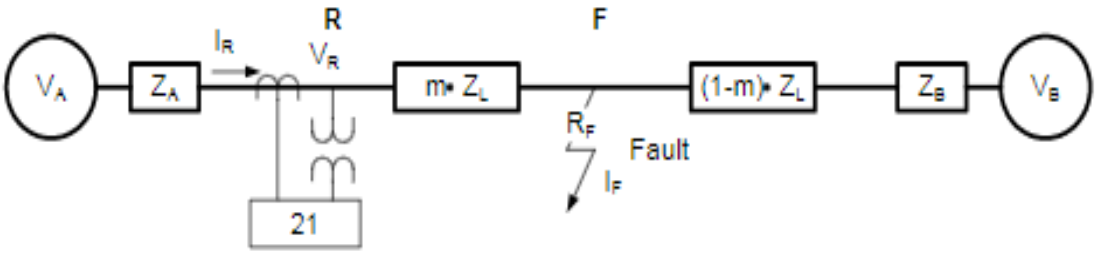

Figure 1: Three phase fault [1]

Figure 1 shows a three phase fault for a simple transmission network. Here Z_{AB} represents the source impedances of the two generators and Z_L represents the line impedance, where m determines where on the line the fault has occurred. The relay current is denoted by I_R. It is shown that

$$V_R - I_R \cdot mZ_l - R_{fault} \cdot I_{fault} = 0[1] \tag{1}$$

If we assume a bolted three phase fault, then the impedance to the fault mZ_l is directly given by the measured impedance at the relay, thus allowing us to calculate its distance. However, if the fault impedance is included, the measured relay impedance gives us

$$mZ_1 + \frac{I_{fault}}{I_R} R_{fault}[1] \tag{2}$$

In order to analyse asymmetric unbalanced faults and circuits, where at most two lines are affected, sequence decomposition must be used.This allows the expression of unbalanced phase terms using a conversion matrix in terms of a sum of positive, negative and zero sequences. For example $V_A = V_0 + V_1 + V_2$, where V_A is the A phase voltage expressed as sum of sequence voltages. .(For more information see [8]. In figure 2 a sequence representation of a line to ground fault is shown. Performing Kirchhoff's voltage law around the relay voltage for the positive sequence phase gives us

$$V_{r1} - V_{f1} - I_{r1} \cdot mZ_{L1} = 0[1] \tag{3}$$

We similarly obtain

$$V_{r0} - V_{f0} - I_{r0} \cdot mZ_{L0} = 0[1] \tag{4}$$

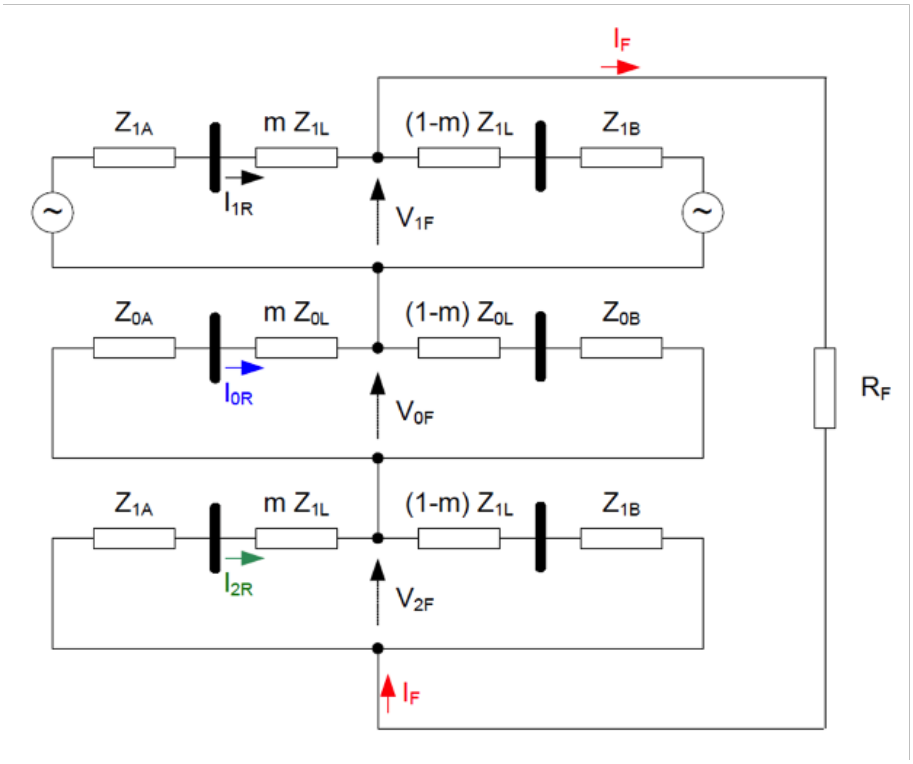

Figure 2: Line to ground fault [1]

and

$$V_{r2} - V_{f2} - I_{r2} \cdot mZ_{l2} = 0[1] \tag{5}$$

By combining these equations and given that $V_{r1} + V_{r2} + V_{r0} = V_{AR}$, the A phase relay voltage, we obtain

$$V_{AR} - I_{fault} \cdot R_{fault} - I_{r1} \cdot mZ_{L1} - I_{r2} \cdot mZ_{L2} - I_{r0} \cdot mZ_{L0} = 0[1] \tag{6}$$

Since

$$mZ_{L1}(I_{r1} + I_{r2} + \frac{Z_0}{Z_1} I_{r0})[1] \tag{7}$$

can be re-written as

$$mZ_{L1}(I_{AR} + I_{r0}(\frac{Z_{L0}}{Z_{L1}} - 1)[1] \tag{8}$$

This can be written as the zero sequence compensated current

$$I = I_{AR} + I_{r0}(\frac{Z_{L0}}{Z_{L1}} - 1)[1] \tag{9}$$

where I_{r0} can be obtained from phase measurements and $K0 = (\frac{Z_{L0}}{Z_{L1}} - 1)[1]$. This gives us $V_{AR} - Ifault \cdot R_{fault} - mZ_{L1}I = 0$. If we assume a fault impedance of zero, then $\frac{V_{AR}}{I} = mZ_{L1}$ allowing us to determine the location of the fault on the line. Similarly with the three phase fault, if we include the fault resistance we obtain $mZ_{L1} + \frac{I_{fault}}{I_{relay}} \cdot R_{fault}$.

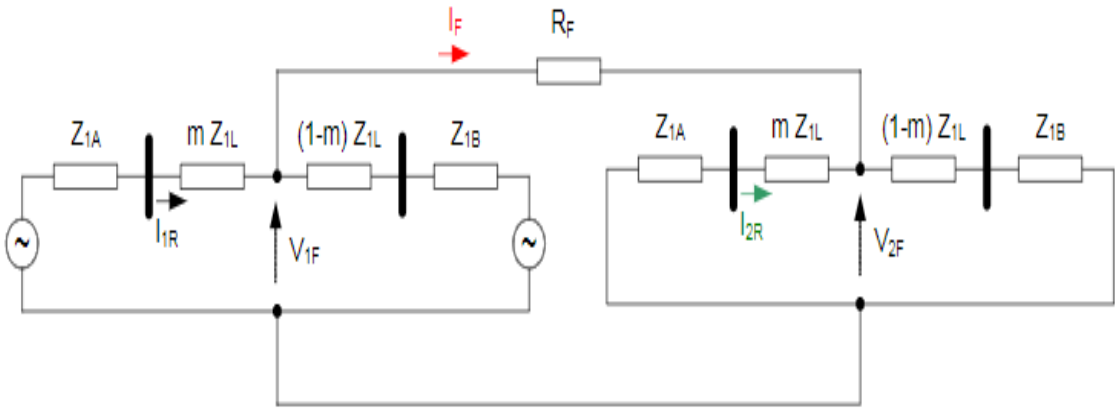

Figure 3: Line to line fault [1]

Finally, in figure 3 we see a line to line representation of the sequence network. Performing a similar analysis we have

$$V_{r2} - V_{f1} = I_{r1} \cdot Z_{L1}[1] \tag{10}$$

and

$$V\_V_{f2} = I_{r2} \cdot Z_{L1}[1] \tag{11}$$

where V_{f1} represents the voltage at the fault location. Since $I_{fault} \cdot R_{fault} = V_{f1} - V_{f2}$, this gives us

$$I_{fault} \cdot R_{fault} + (V_{r2} - V_{r1}) = mZ_{L1}(I_{r2} - I_{r1})[1] \tag{12}$$

With a zero fault impedance, we obtain

$$mZ_{L1} = \frac{V_{r2} - V_{r2}}{I_{r2} - I_{r1}}[1] \tag{13}$$

Since $V_{r2} - V_{r2}$ gives us $(V_b - V_c)(a^2 - a)$, we therefore obtain the impedance to fault as $\frac{V_{bc}}{I_{bc}}$ [1].

For traditional synchronous generators, the relay and fault currents are of similar phase, resulting in mainly resistive deviations in measured impedance from true line impedance to fault. Generators also have a high short circuit capacity, so much more of the fault current is supplied generator side, resulting in smaller magnitude resistive deviations [9]. A key part of the problem statement of this thesis relates to the equation

$$mZ_1 + \frac{I_{fault}}{I_R} \cdot R_{fault} \tag{14}$$

that determines the deviation of our relay impedance from the fault location. We can re-write this as

$$1 + \frac{1}{3} \cdot \frac{I_{grid}}{I_{relay}} \tag{15}$$

for a line to ground fault and

$$\frac{1}{2} \cdot (1 + \frac{I_{grid}}{I_{relay}}) \tag{16}$$

for a line to line fault. From figure 3 and 2 the grid side current can be expressed as a sum of the fault current flowing through the grid for all three sequences subtracted by the pre-fault current flowing through the grid. The relay current can similarly be expressed as a sum of the fault current flowing through the relay for all three sequences plus the pre-fault current. $I_{grid} + I_{relay}$ is then equal to $3I_{fault}$ since the sum of the two currents within the same sequence network must add up to the fault current. Thus the phase equivalent fault current $I_{fault} = 1 + \frac{I_{grid}}{3I_{relay}}$. Similar analysis follows for line to line faults. Two sequence components means $I_{grid} + I_{relay}$ equals $2I_{fault}$.

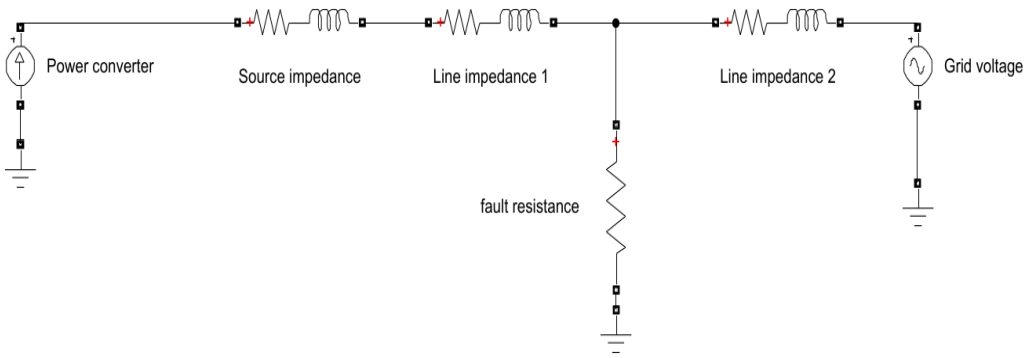

Figure 4: Three phase fault with converter interfacing

Figure 4 shows a basic circuit schematic for a three phase fault with a current source modelling our power converter. The fault current I_{fault} becomes much larger in magnitude than the relay current I_r. This is because most of the fault current is being provided by the grid due to the current limiting of the power converter. This significantly alters the measured fault from mZ_{L1} by increasing the $\frac{I_{grid}}{I_{relay}}$ error term. Currents coming from the grid side can also have a different phase to that from the power converter during a fault, since the converter current phase is heavily dependent on the control mechanisms in use. This can result in overreaching or under-reaching of the measured impedance. This presents serious consequences for the accuracy of fault detection systems, particularly those using traditional techniques, when the use of power converters becomes more widespread.

6 Literature review: Evaluating distance protection technologies

6.1 Traditional methods of distance protection

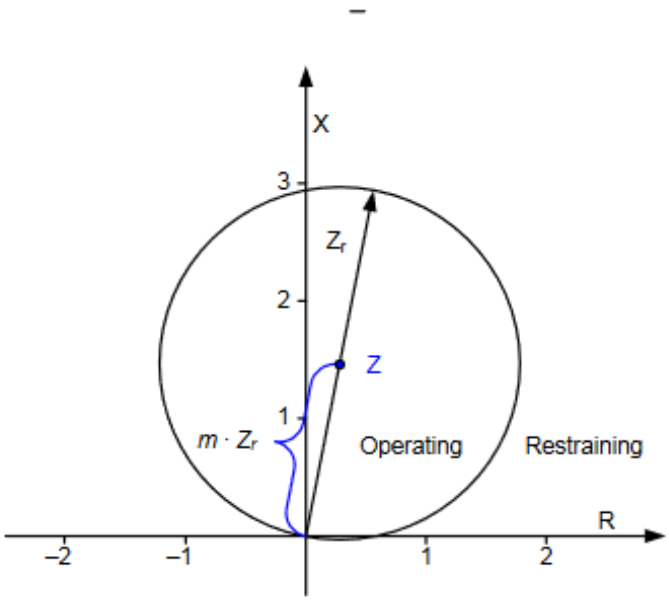

Figure 5: Self polarising mho [2]

Traditional distance protection techniques utilise a circular shape in the complex plane known as the mho, where if the measured relay impedance lies within this region the circuit is tripped to clear the fault. Such a mho is seen in figure 5 , where the diameter is determined by the reach, i.e the fraction of the transmission line impedance hence length we want the relay to protect. If a measured fault does not lie within this region then it lies in a region outside that controlled by the relay[2]. For a bolted fault, any measured fault impedance within the zone lies on the Z_r vector representing the impedance of the line. The shape has a circular form as this allows for the implementation of efficient phase angle comparisons to determine if a fault lies within the mho[2].

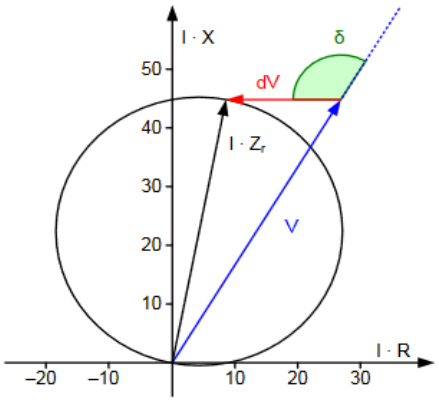

Figure 6: Phase angle measurement [2]

We see this in figure 6, where angle($\frac{V}{I \cdot Z_r}$) is $> 90°$ if the measured relay voltage, hence fault impedance, lies outside the mho and $< 90°$ if it lies within the mho due to the properties of a circle. Here the reach is defined as a voltage proportional to the reach impedance and V is the measured relay voltage proportional to the measured fault impedance.

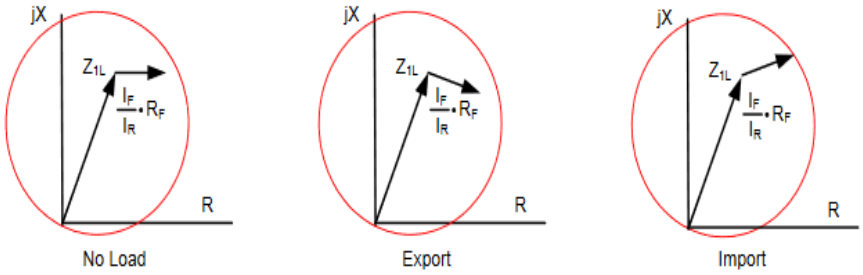

Figure 7: mho under fault resistance [1]

Figure 7 demonstrates the impact of fault resistance and grid currents on the detected fault impedance. Since the phase of the relay current heavily depends on the control mechanisms of the power converter, we see how for large $\frac{I_{fault}}{I_r}$ ratios or large fault resistances, traditional mhos can fail to accurately determine fault locations[1].

6.2 Advancements in mho characteristic shaping

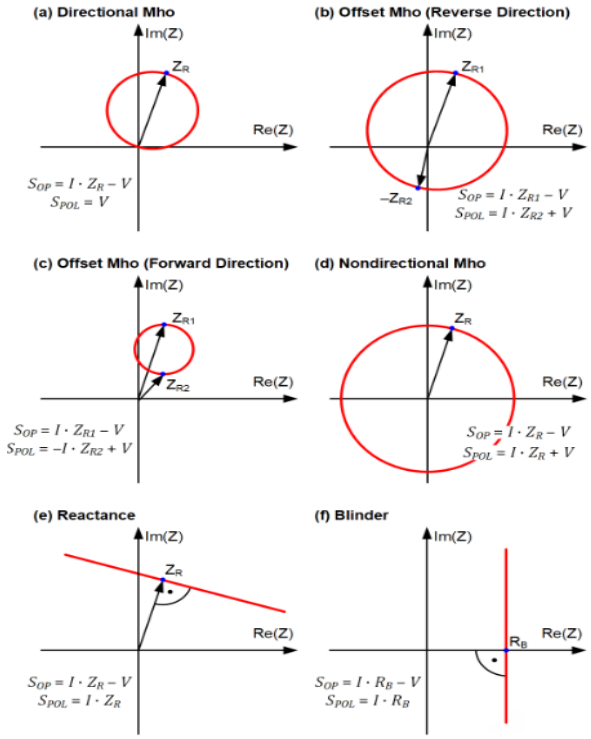

Figure 8: Different mho characteristics [3]

The advent of microprocessors and digital signal processing has allowed for the improved flexibility in shaping mho characteristics. Figure 8 shows the different polarising signals that can be used to shape

the mhos. This is achieved by comparing the phases of the polarising signal and operating signal dV, with the same angle criterion as in figure 6. An example of this is seen with Offset Mhos, which are often utilised in memory voltage systems. Here if the fault occurs close to the relay, utilising the relay voltage as a polarising signal may be inaccurate since it cannot be accurately measured. Utilising a pre-fault memorised positive sequence voltage as the polarising voltage allows for the mho to dynamically expand and provide additional resistive coverage to compensate for the lower measured relay voltage [2]. Memory polarisation faces many challenges when utilising power converters however. A power converter operates independently of its pre-fault conditions, unlike a synchronous generator where the terminal voltage does not change during the fault. This means that the pre-fault polarising voltage can be very different to the operating voltage, resulting in a distorted mho shape[3].

The reactance and binder mhos are utilised in microcontrollers to produce a quadrilateral mho as shown in figure 9.

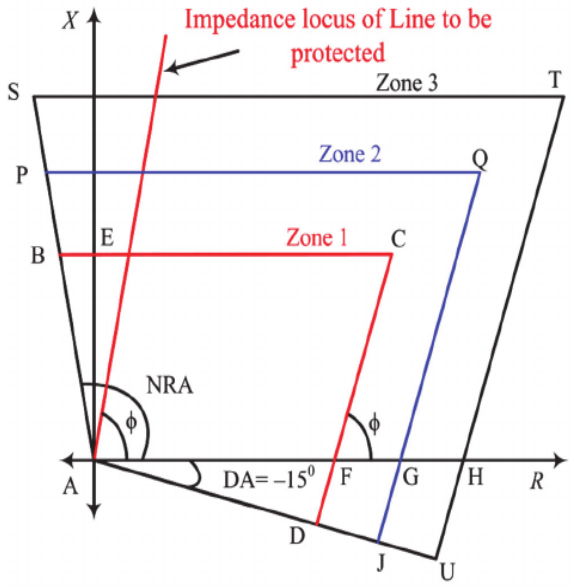

Figure 9: Different quadrilateral mho characteristics [4]

With microcontrollers the impedances can be directly calculated using phasor analysis through software and the settings of the quadrilateral mho dynamically adjusted. This is particularly useful with fault resistances, as the mho can be extended to further cover the right hand side of the complex plane [3].

6.3 Alternative techniques for impedance measurement in distance protection

Quadrilateral mhos with a microprocessor implementation can be used in wind and solar farms to provide adaptive distance protection [7], where the measured relay impedances can be corrected for by estimating the $\frac{I_{fault}}{I_r}$ ratio, and thus producing a more accurate mho. However, this can only be implemented near to the renewable generation site, requiring extensive computation to understand the behaviour of the fault currents for different environmental conditions. Many of the distance protection systems in the UK and globally still rely on traditional mho fault detection, with transformer based relays [3]. As penetration of renewables in the grid becomes more widespread, replacing electromechanical systems with computationally heavy microprocessing would become very costly.

This provides the motivation to evaluate alternative methods of fault detection that are still compatible with traditional mho characteristics or require quadrilateral mhos with less adaptability needed.

6.4 Communication between relays

Since most converter interface control schemes affect the positive sequence current, zero-sequence current can become a useful indicator in fault detection. In order to address the issues caused under line-line faults, where there is no zero sequence current, It has been proposed that if two relays at either end of a transmission line can communicate with one another, and the direction of the fault determined, the zoning of the fault can be determined. This is because we can ascertain more information about the network nodal voltages and thus calculate impedances to the fault more accurately. The fault direction is determined using a series of logic gates that measure current magnitudes relative to a fixed threshold, as well as utilising negative impedance measurements [10].
Relay communication however, presents many challenges in terms of system security and cost when applied at scale. Co-ordination between relays can become very complex and more prone to maintenance issues when used on a large scale.

6.5 Travelling wave distance protection

Travelling waves are created from sudden changes in voltage levels that produce a propagating electrical signal. Their relative arrival times and polarities help us to determine the distance to faults.

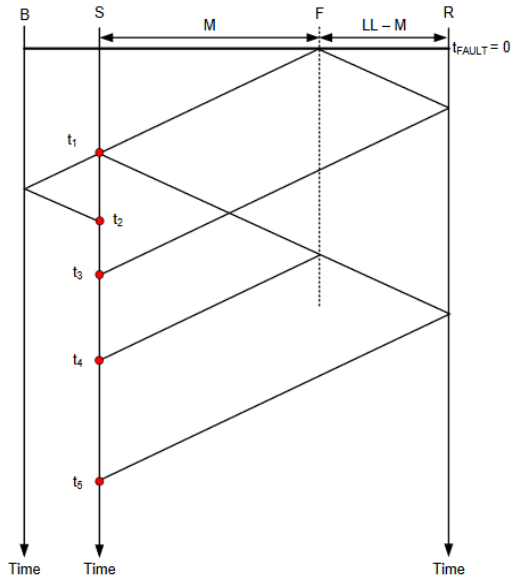

Figure 10: Bewley diagram to show time delay measurements [3]

Figure 10 shows a Bewley diagram demonstrating how long it takes for the wave to propagate to the fault back to terminal S. Since $2M = (t_4 - t_1)PS$, where PS is the propagation speed of the wave defined as the line length divided by the time taken for the wave to travel from one end of the line to the other. This allows us to directly measure the distance M using $\frac{LineLength}{2}\frac{t_4-t_1}{Timetaken}$. A reach setting can then be set based on a maximum time delay between t_4 and t_1 This allows for a direct measurement of the distance to fault without the need of voltage and current calculations.
However, many challenges still remain in identifying the true fault reflection. The relay algorithm must be able to accurately distinguish t_4 as the correct signal rather than t_2 or t_3. There are also challenges

concerning close in faults, since the close a fault is to the relay, the smaller the time differences between returning signals which becomes problematic due to finite sampling times [3].
Current voltage sensors in power systems are also not currently designed for travelling wave detection, making high fidelity voltage measurements with directionality more challenging [3].

6.6 Harmonic voltage injection

Currently proposed for use in microgrids, harmonic injection operates by injecting a voltage signal at an additional harmonic, i.e a multiple of the fundamental frequency, when a fault needs to be measured. Through the use of synthetic harmonic distance relays that are designed to measure these injected harmonics, the fault impedance can be measured at a harmonic separate to the fundamental harmonics of the grid [11][12]. The higher harmonic frequency also increases the X/R ratio of the line allowing for improved impedance relaying by enhancing the reach settings [11].
However, there are many potential issues if on a large scale, harmonics are injected into the grid. This is due to potential resonance in lines and signal distortion.

An alternative take on this idea to utilise the Fourier decomposition of the voltage drop that occurs across the relay whenever a fault happens. Through signal transformations such as wavelet transform the high frequency components of the voltage drop can be extracted and a high frequency equivalent model of the network can be derived, allowing for improved distance protection performance [13].
This however requires heavy computation and high noise tolerance, since a relay voltage drop is likely to be subject to distortion due to other transient properties of a transmission line. Scalability and cost thus become issues.

6.7 Converter fault current control

To address the problem of converter interfaced current being of different phase to the grid side current during a fault, various schemes have been proposed to ensure that the measured relay impedance shows no over or under-reaching, thus easing the design and adaptability needed by relays as the error becomes purely resistive [14]. A control circuit is proposed that mimics the behaviours of synchronous generators. It achieves this by utilising reference currents and control circuitry to regulate the power converter and generate currents that mimic the balanced positive sequence currents found in generators [14]. This allows the $\frac{I_{fault}}{I_r} Z_f$ term to become largely resistive, reducing the under-reach that was seen before.

Other techniques propose the use of sequence measurements from the relay [10] [15]. Zero-sequence current is supplied directly from the grid and so is not current limited giving a much more accurate relay voltage as the relay current closer matches the fault current. This also allows fault current angle to be estimated thus allowing for a current angle to be injected such that no over or under reach occurs [10].
Similarly, the negative sequence relay voltage measurement can be used to estimate information about the fault [15]. This is particularly useful for line to line faults where there is no zero-sequence current. The issues of low short circuit current magnitude however cannot be solved through control alone, since we are only making changes to the current angle. The current magnitude limitations still remain.

7 Thesis aims and objectives

This thesis aims to demonstrate in detail how and why current limited converters cause increased maloperation of distance protection relays, particularly so for line to line faults [10]. The objective is to demonstrate that synchronous generators show lower maloperation compared to converters for a variety of test factors. It is also to demonstrate the improvement that adding a non current limited zero sequence current to the relay current has on converter distance protection performance.
This thesis also aims to investigate and evaluate two solutions that improve converter interfaced distance protection. From evaluation of the background literature, harmonic current injection and converter current control through angle injection have been chosen. A key objective is to find a solution that provides secure distance protection with the use of traditional mho technology, thus presenting a cost effective solution. Relative simplicity of relay operation and the minimization of communication infrastructure has led to the above two solutions best meeting this objective. A further objective is to identify where each solution is best suited and best meets the key objective. This is addressed by comparing the advantages, dis-advantages and trade-offs of the two solutions.

While there are four types of line faults, this thesis will mainly investigate distance protection for line to line and line to ground faults. Much of the analysis for line to ground faults can be applied to three phase faults and line to line to ground fault detection often consists of a combination of line to line and line to ground fault detection [1]. Since three phase and line to line to ground faults contain a zero sequence current, the literature suggests that their distance protection performance will be less prone to maloperation compared to line to line faults for power converters [10]. Thus investigating line to ground and line to line faults is sufficient to study the main issues surrounding distance protection with converter interfacing.

8 Testing: Development of Matlab Script

In order to fully investigate the behaviour of distance protection for a variety of network parameters, a Matlab script representing the circuit equations for the grid interfacing network must be derived. This section will go through the key script equations and derivations using sequence analysis. The test circuit used to demonstrate distance protection performance consists of a generator connected to an electricity grid network, i.e the point where the generator connection meets with an interconnected network of other generators and load centers. It connects to the grid through a transformer and distributed transmission line.
All voltages, currents and impedances in this section are analysed in per-unit in the script.

8.1 Synchronous generator distance protection script equations

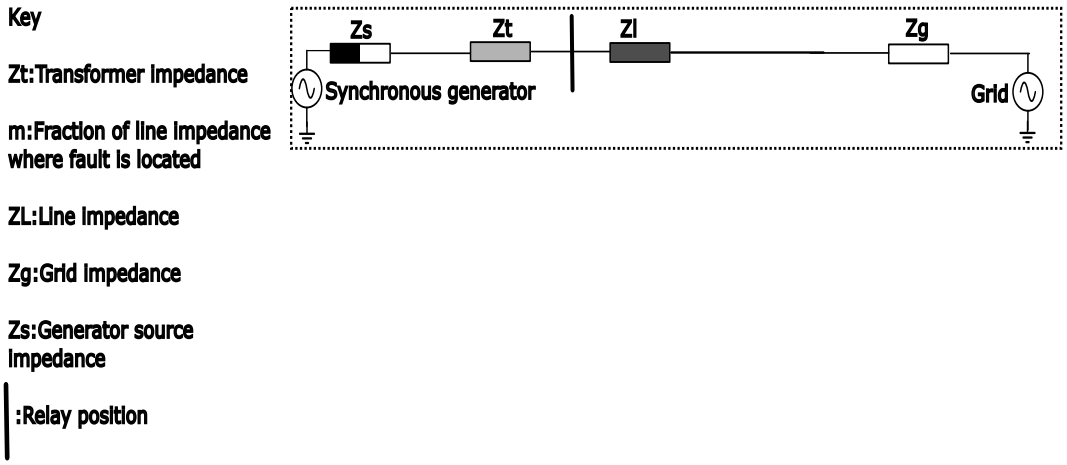

Figure 11: Circuit diagram of pre-fault synchronous generator network

Figure 11 shows the circuit diagram for the pre-fault synchronous generator interfaced with the grid, where the generator and grid are modelled as ideal voltage sources. This allows us to calculate the synchronous generator voltage when injecting current at one per unit. Therefore,

$$V_{gen} = I_{pu} \cdot (Z_s + Z_t + Z_l + Z_g) + V_{grid} \tag{17}$$

When a fault occurs we convert the circuit to its unbalanced sequence equivalent shown in figure 12 [16].
Note that the positive sequence line impedance is identical to the pre-fault line impedance since positive sequence denotes a balanced three phase sequence component. It is also assumed that all negative sequence impedances are identical to their positive sequence equivalents.
The circuit diagram above allows us to calculate the fault current and the sequence currents that flow through the relay. To find the fault current, since the positive sequence network is the only network with active components, the Thevenin equivalent network must be found. The Thevenin voltage is defined as the open circuit voltage at the fault location, i.e the voltage at the fault location before the fault is connected. Since the positive sequence network voltages and impedances are identical to their pre-fault values these are used to find Thevenin equivalent parameters. This gives the following circuit in figure 13.
The sequence equivalent fault current I_{a1} is equal to

$$\frac{V_{th}}{Z_{thev1} + Z_{thev2} + Z_{thev0} + 3R_{fault}} \tag{18}$$

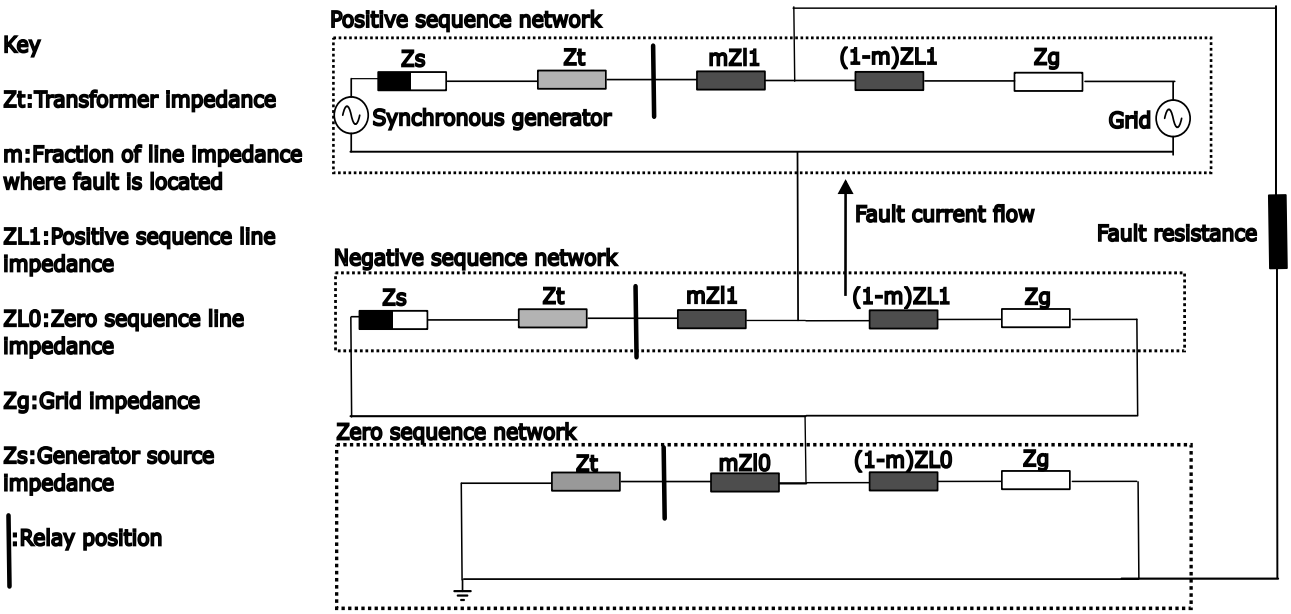

Figure 12: Sequence diagram of a line to ground fault for a synchronous generator

where Z_{thev} represents the equivalent impedance of a sequence network. This is multiplied by 3 to give the A phase fault current. This then allows the calculate of negative sequence and zero sequence relay currents through current divider equations with

$$I_{r2} = I_{a1} \cdot \frac{(1-m)Z_{L1} + Z_G}{Z_{L1} + Z_T + Z_S + Z_G} \tag{19}$$

and

$$I_{r0} = I_{a1} \cdot \frac{(1-m)Z_{L0} + Z_G}{Z_{L0} + Z_T + Z_G} \tag{20}$$

To find our positive sequence relay voltage, superposition is used. The pre-fault relay current was defined to be 1pu. We then add to this the positive sequence current due to the fault equal to

$$I_{a1} \cdot \frac{(1-m)Z_{L1} + Z_G}{Z_s + Z_T + Z_{L1} + Z_G}. \tag{21}$$

The sequence voltages at the relay can be calculated with

$$V_{r1} = I_{r1} \cdot (mZ_{L1}) + V_f \tag{22}$$

where $V_f = V_{th} - I_{a1} \cdot Z_{thev1}$, i.e the voltage at the fault location.

$$V_{r2} = I_{r2} \cdot (mZ_{L1}) - I_{a1} \cdot Z_{thev2} \tag{23}$$

and

$$V_{r0} = I_{r0} \cdot (mZ_{L0} - I_{a1} \cdot Z_{thev0}) \tag{24}$$

This then allows us to calculate the relay impedance using zero-sequence compensation. This is equal to $\frac{V_{AR}}{I_{AR} + K0 \cdot I_{r0}}$ as derived in equation 9, where V_{AR} is the A phase relay voltage equal to the sum of the relay voltage sequence components and I_{AR} is the A phase relay current equal to the sum of the current sequence components. K0 represents the zero-sequence compensation co-efficient equal to $\frac{Z_{L0}}{Z_{L1}} - 1$.

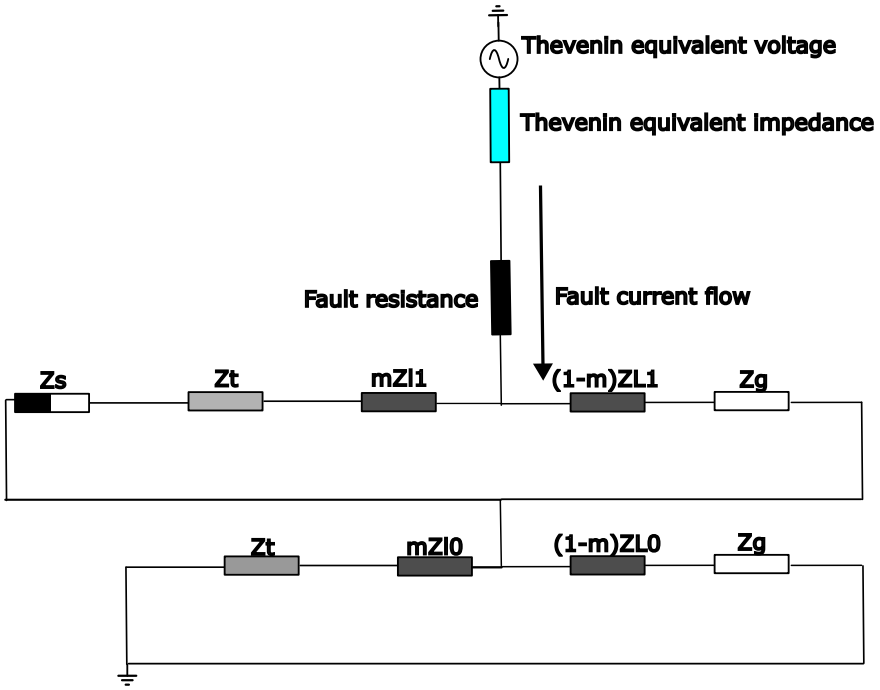

Figure 13: Sequence diagram of a synchronous generator line to ground fault with a Thevenin equivalent positive sequence network

Using figure 14 the same analysis for a line to ground fault is performed now without the zero-sequence component. Here our sequence equivalent fault current I_{a1} is equal to

$$\frac{V_{th}}{Z_{thev1} + Z_{thev2} + R_{fault}} \tag{25}$$

I_{r2} now has the opposite sign and V_{r2} is now equal to

$$I_{r2} \cdot (mZ_{L1}) + I_{a1} \cdot Z_{thev2} \tag{26}$$

since the positive and negative sequences form a complete circuit and so our fault current in the negative sequence is the opposite sign to that in the positive sequence. Our B-phase fault current now equal to $-i\sqrt{3} \cdot I_{a1}$. We then use $\frac{V_{r1} - V_{r2}}{I_{r1} - I_{r2}}$ to find our relay impedance.

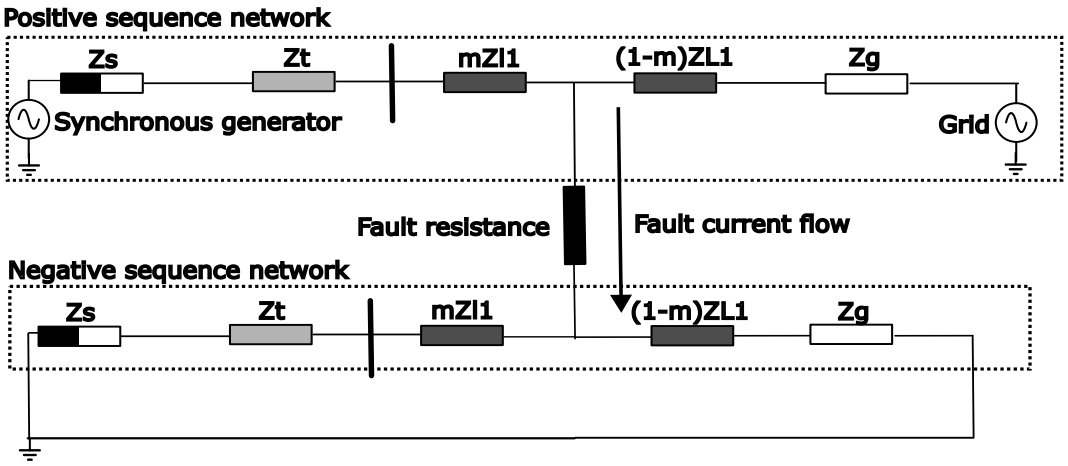

Figure 14: Sequence diagram of a synchronous generator line to line fault

8.2 Power converter distance protection script equations

To derive relevant equations for distance protection analysis the sequence equivalent circuit shown in figure 15 is obtained. Here the converter is modelled as a constant current source at its maximum rated output current of 1pu.

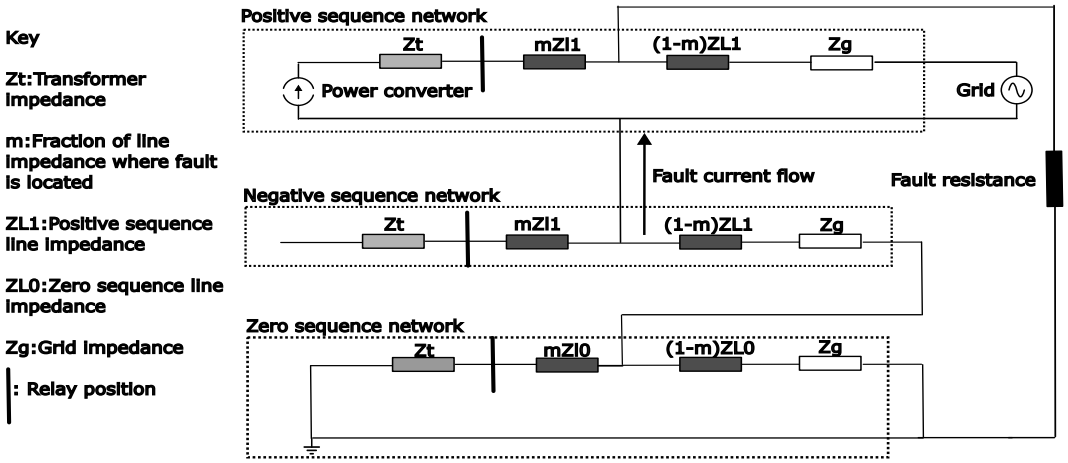

Figure 15: Sequence diagram of a converter interfaced line to ground fault

The key differences here are that the converter is an open circuit in the negative and zero sequence networks, since it is assumed that the converter only outputs a balanced three phase current. This means I_{r1} is now equal to the output of the power converter and I_{r2} is equal to 0. Our positive and negative sequence equivalent impedances have also changed and now only consist of the grid side line impedance and grid impedance $(1-m)Z_{L1} + Z_G$. The expressions for I_{a1}, V_{r1}, I_{r0} and V_{r0} remain unchanged compared to a synchronous generator with however $V_{r2} = -I_{a1} \cdot Z_{thev2}$, thus being proportional to the fault current.

Similar conclusions can be drawn for line to line faults shown in figure 16. Here the relay current is now solely composed of the converter current. Since the positive and negative sequence networks form a complete circuit our V_{r2} is now equal to

$$V_{r2} = I_{a1} \cdot Z_{thev2} \tag{27}$$

according to Kirchhoff's current laws.

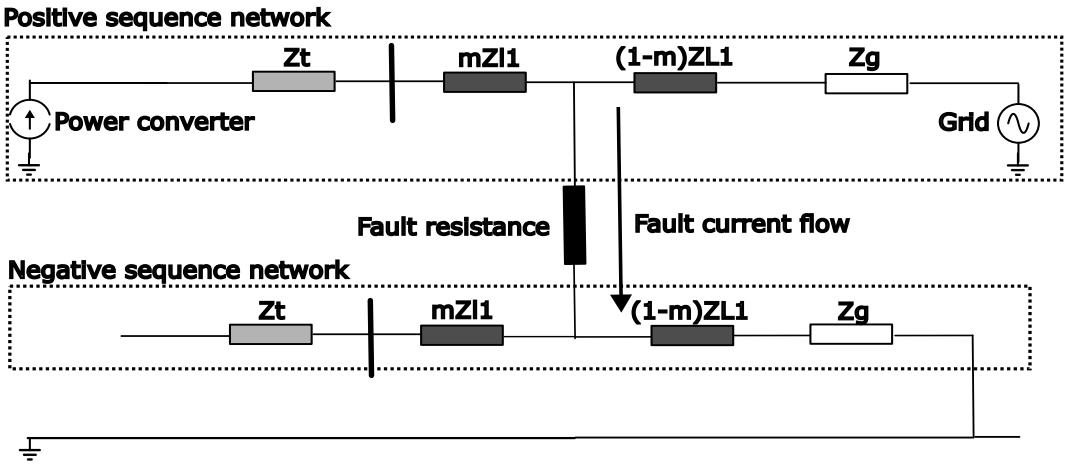

Figure 16: Sequence diagram of a converter interfaced line to line fault

9 Verification through Simulink

In order to verify the validity of our Matlab script, it is tested with an equivalent model in Simulink. Figures 17 and 18 show the Simulink models used for verification. For our converter three current sources 120° apart in phase are used. The resistances in parallel with the current sources are added for solver purposes to ensure the Simulink simulation can converge.

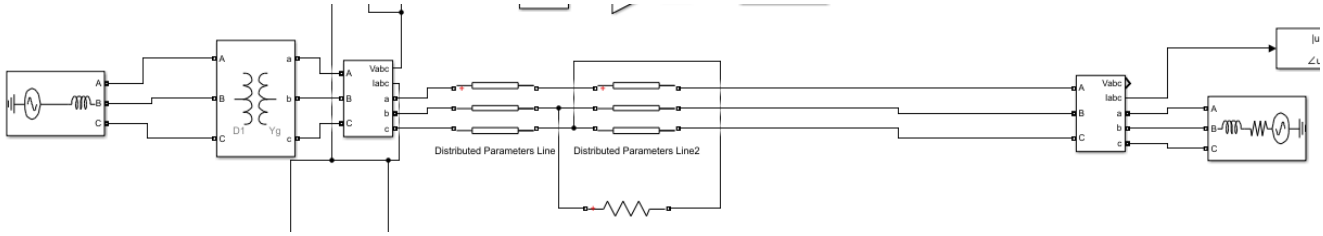

Figure 17: Simulink model of synchronous generator line to line fault

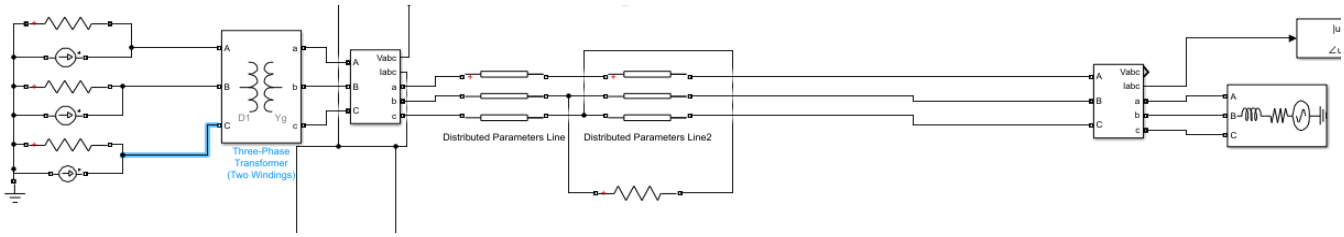

Figure 18: Simulink model of a converter interfaced line to line fault

9.1 Component base case parameters

The test circuit components are defined in per-unit values. This means the base values are chosen and all circuit parameters are divided by these. The model represents a 315KV r.m.s connection to the grid. As a result our base voltage is 315KV, making the grid voltage 1 per unit. It is also assumed that the generator has a rated apparent power of 300MVA thus this forms the base power. The base impedance is thus given by $\frac{V_{base}^2}{S}$ and equal to 330.75Ω, where S is our apparent rated power. Similarly the rated current is given by $\frac{S}{\sqrt{3}V_{base}}$, giving 550A r.m.s. For a power converter, its current limited rated output is equal to 1pu and its magnitude does not change. However, for a synchronous generator the pre-fault current is of magnitude of 1pu, which increases during the fault. This allows the calculation of the generator voltage using 13 where $V_{gen} = I_{pu} \cdot (Z_s + Z_t + Z_l + Z_g) + V_{grid}$. The base case operating frequency is 60 Hz.

Component name	$Z_{positive}$ **(pu)**	$Z_{positive}$ **(Ω)**	Z_{zero} **(pu)**	Z_{zero} **(Ω)**
Transformer	0.08i	26.46i	0.08i	26.46i
Synchronous generator	0.05i	16.5375i	0.05i	16.5375i
Distributed transmission line	0.0041 + 0.0573i	1.3681 +18.9541i	0.0389 + 0.2099i	12.8555 +69.4250i
Grid impedance	0.0060 + 0.0597i	1.9747 +19.7465i	0.0060 + 0.0597i	1.9747 +19.7465i

The table above shows our base case component parameters used in the Simulink model and in our Matlab script showing positive and zero sequence impedance parameters. The values given in ohms

are the absolute impedances which are inputted to the Simulink model. For the transformer and sub-transient generator impedance, the resistive components are assumed negligible and the inductances remain constant for the duration of the fault. The transformer is in a delta-star configuration and has a 1-1 turns ratio to simplify per unit to absolute value conversions. The grid impedance is defined based on a typical short-circuit power rating of 5000MVA with a resistance to reactance (X-R) ratio of 10. Short-circuit power and grid impedance will be further explained in section 10.3. The model is simplified by assuming the impedance to be a passive resistor and inductor in series.

Finally, the distributed line parameter represents a model of a transmission network which consists of infinitely small pi-transmission network models integrated over a distance to give a total impedance for the line. This consists of a resistor in series with an inductor with a shunt capacitor going to ground. Our per length line resistance, inductance and capacitance values are based on the default values given by the Simulink power line parameters tool. Here the values for a 315KV ACSR 1355 MCM conductor transmission cable adapted for three phases are given at 60 Hz[17]. Mutual inductance, resistance and capacitance terms have been neglected to simplify modelling for our script.
As a base case the transmission line length is set to 50km and the fault position set to be along 75% of the line length. Unless otherwise stated, the circuit can be assumed to use base case values.

9.2 Verification of Matlab script with Simulink:Synchronous generators

The results for impedances measured by the relay for both Matlab script and Simulink are shown. Results given by Simulink are assumed to be our accurate result to which we compare our script with.

The biggest discrepancy in results is expected to be due to the distributed parameters modelling. For our script a linear approximation of the distributed parameters is made in order to obtain an R-L series equivalent impedance model. This is done by measuring the input impedance of the network for a 1pu positive sequence and zero sequence voltage, shorting it at its output, in order to obtain positive and zero sequence impedances. In Simulink however, distributed parameters form a complex R-L-C network with higher order behaviours such as resonance and thus has no identical two terminal impedance equivalent. Despite this, the overall behaviour of the two models should remain the same as we vary other circuit parameters such as fault resistance.

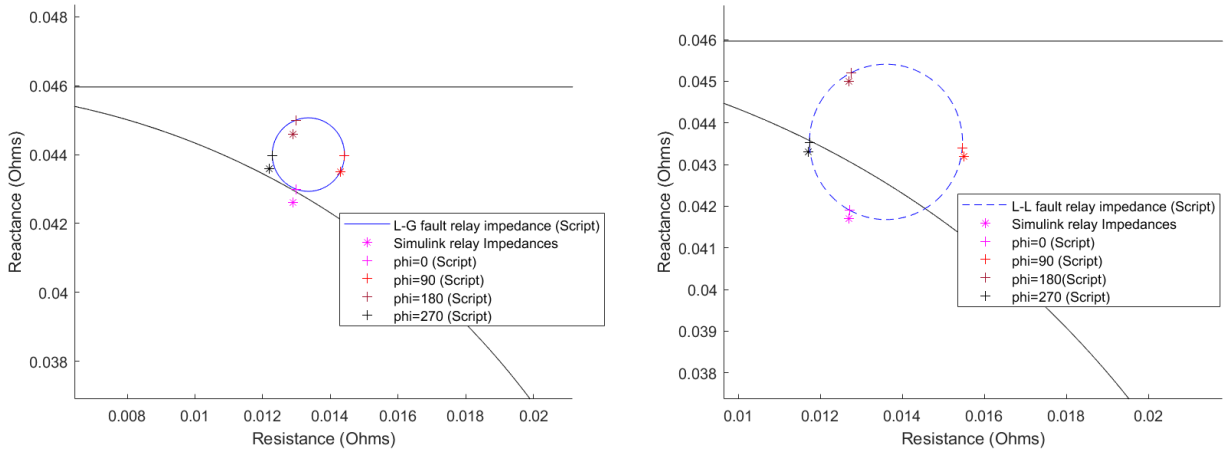

(a) Synchronous generator line to ground fault (b) Synchronous generator line to line fault

Figure 19: Verification of Matlab script and Simulink for pre-fault current angles 0 to 360° at 2Ω fault resistance

Figure 19a shows the plot for a synchronous generator at 2Ω fault resistance for a line to ground fault. Similarly figure 19b shows this for a line to line fault. The circle represents the relay impedances given by the Matlab script at pre-fault current angles ranging from 0 to 360°. The markers on the circle represent the script relay impedance at a specific injected current angle. The accompanying markers that lie close to the circle represent the relay impedance measurements given by our Simulink model. The marker colour indicates at what pre-fault current angle the Matlab script and Simulink generator were programmed to inject at.
There is close similarity between the Simulink and script relay impedances at all four current angles with a magnitude error of the order 10^{-4} for both fault types. While the true relay impedance is shifted further down, the overall shape remains similar.
We verify that the script and simulation agree at different fault resistances by simulating at 10Ω fault resistance in figures 20a and 20b.

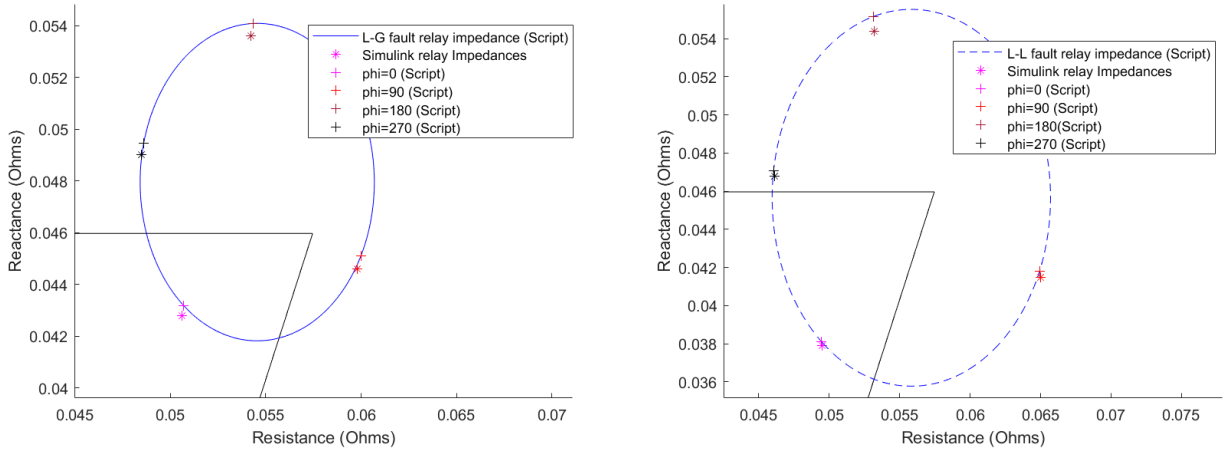

(a) Synchronous generator line to ground fault (b) Synchronous generator line to line fault

Figure 20: Verification of Matlab script and Simulink for pre-fault current angles 0 to 360° at 10Ω fault resistance

The Simulink simulation and Matlab script show similarly close agreement for both fault types. The true relay impedance values have shifted according to the fault resistance and pre-fault current in a very similar manner to our Matlab script, suggesting a constant magnitude error. Thus we can utilise our Matlab script for synchronous generators with confidence in its ability to capture network behaviours.

9.3 Verification of Matlab script with Simulink:Power converters

Now the power converter Matlab script is verified with the Simulink model using the same test conditions. Here the angle at which the converter injects current into the network is varied. We then compare relay impedance measurements from the script and those given by Simulink at four distinct current angles.

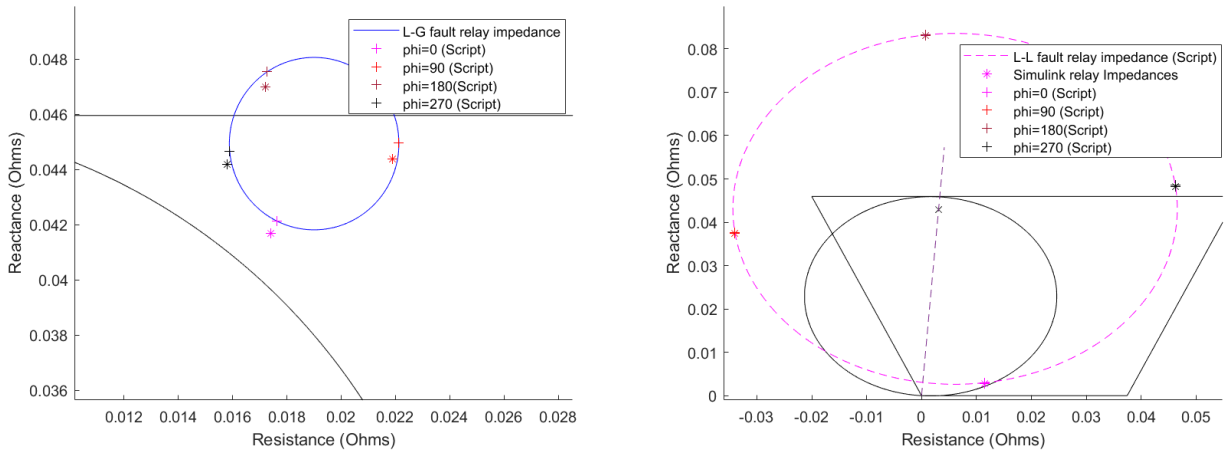

(a) Line to ground fault

(b) Line to line fault

Figure 21: Verification of Matlab script with Simulink for a power converter at 2Ω fault resistance for current angles 0 to 360°

The results are compared for a line to ground and line to line fault at 2Ω fault resistance as shown in figures 21a and 21b. They demonstrate discrepancies of similar order magnitude to figures 19a and 19b for the synchronous generator. The true relay impedance Simulink results lie slightly shifted to the left at lower reactance values, however the overall relationship of relay impedance with current angle remains in agreement.

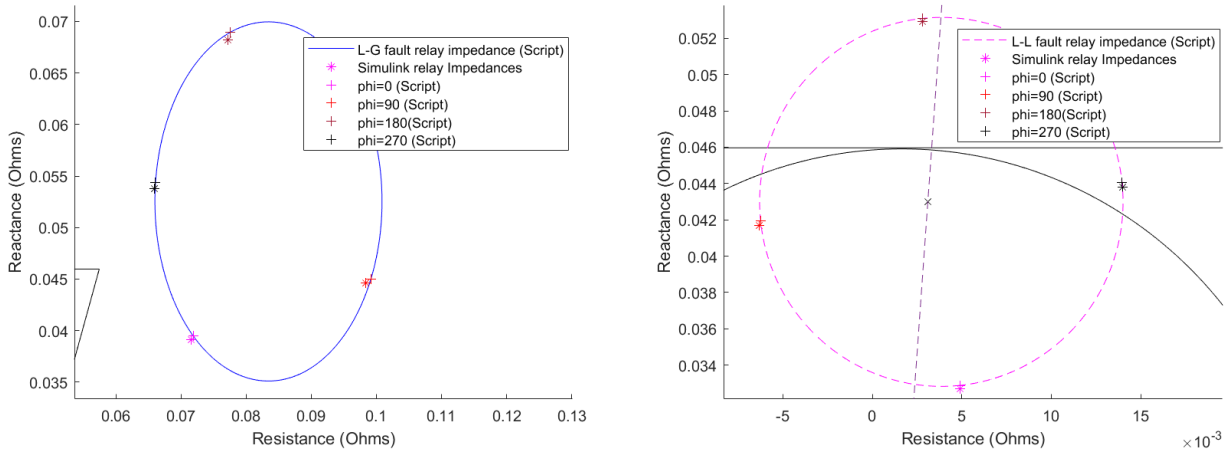

(a) Line to ground fault at 10Ω fault resistance

(b) Line to line fault at 0.5Ω fault resistance

Figure 22: Verification of Matlab script with Simulink for a power converter for varying fault resistance and current angle 0 to 360°

To ensure the script and Simulink results are in agreement for varying fault resistances the plot is repeated at 10Ω fault resistance for line to ground faults and 0.5Ω for line to line faults. Figures 22a and 22b are obtained. There is a similarly close agreement between Matlab and Simulink results for both fault types. Since line to line faults see much larger variation in relay impedance, the Simulink and Matlab values will appear closer together.

The table below shows the Simulink and script relay impedance values for line to ground faults for a synchronous generator. The magnitude of the error remains of order 10^{-4} for both fault resistances.

Current angle (°)	Z_{relay} **(script)**	Z_{relay} **(Simulink)**	$\|error\|10^{-4}$
R=2Ω			
0	0.013 + 0.043i	0.0129+0.0426i	4.0539
90	0.0144 + 0.044i	0.0143+0.0435i	4.7341
180	0.013 + 0.045i	0.0129+0.0446i	4.0784
270	0.0123 + 0.044i	0.0122+0.0436i	3.7648
R=10Ω			
0	0.0507 + 0.0432i	0.0506+0.0428i	3.9144
90	0.06 + 0.0451i	0.0598+0.0446i	5.3775
180	0.0543 + 0.0541i	0.0542+0.0536i	5.0374
270	0.0486 + 0.0494i	0.0485+0.049i	4.5857

The error table is repeated for the power converter line to ground fault relay impedance measurements below

Current angle (°)	Z_{relay} **(script)**	Z_{relay} **(Simulink)**	$\|error\|10^{-4}$
R=2Ω			
0	0.0176 + 0.0421i	0.0174+0.0417i	4.9522
90	0.0221 + 0.0445i	0.0219+0.0444i	6.0552
180	0.0173 + 0.0475i	0.0172+0.047i	5.5292
270	0.0159 + 0.0447i	0.0158+0.0442i	4.7614
R=10Ω			
0	0.07198 + 0.0395i	0.0716+0.0391i	4.6902
90	0.0992 + 0.045i	0.0984+0.0446i	8.5993
180	0.0775 + 0.0689i	0.0772+0.0682i	7.9960
270	0.0661 + 0.0543i	0.0659+0.0538i	5.7381

While the error magnitude has slightly increased at both fault resistances, the error magnitude remains within an order of 10^{-4}.

Other sources of difference include the transformer magnetising resistances and inductances which have been set to 10^6 and neglected in our script. The resistances added in parallel with the current sources are another source of error. These are equal to 1MΩ and so will have a minor effect on current flow. These resistances are not included in our script.
Thus it can be concluded that the Simulink and Matlab scripts show sufficient agreement such that the distance protection performance of the test circuit can be captured by the script.

10 Performance of synchronous generators in distance protection

To investigate and compare the performance of synchronous generators and renewable generation with converter interfacing, relay impedance measurements will be compared under different test conditions for a classical angle comparison based circular mho and a more adaptable quadrilateral mho. Detectability of a certain type of mho is defined in terms of the position of the fault along the line. If the fault position lies within the reach of the mho, i.e within the circle or trapezium, then the relay impedance is correctly detectable if it too lies within the mho. Similarly, if the position of the fault lies outside the mho reach then our mho correctly does not detect a fault if the relay impedance does not lie within it. This is distance protection without maloperation.
The key performance metric is how close the relay impedance measurement lies to its position along the transmission line, since this is what allows determination of fault distance. This closeness is defined both in terms of magnitude error (how far away the impedance is) and phase error (over and under-reaching). We refer to this as relay impedance accuracy. These relay detection technologies are chosen because quadrilateral mhos represent the most adaptable relay technology currently in use, while circular mhos use traditional angle based relay detection. This helps to qualify the detectability of a relay impedance measurement, since if it can be accurately detected by a basic circular mho, the measurement can be considered sufficiently close to the fault position. However, if a relay impedance inaccurately falls outside or within a quadrilateral mho it can be deduced that it has very poor accuracy.

10.1 Behaviour with varying fault resistance

Investigating relay measurements for varying fault resistances allows us to analyse the contribution of fault resistance towards the error.This can be quantified by identifying the fault resistance where the relay impedance first exceeds the classical mho i.e falls outside it, assuming the fault position lies within the mho reach. While the absolute value of this resistance is less useful, as this is heavily network dependant, it provides a useful metric to compare different technologies with.
Utilising an argand diagram where complex impedances can be plotted, figure 23 shows the quadrilateral and circular mho and the deviation of relay impedance from the true fault position along the line impedance for a fixed current angle. Here we increase the fault resistance from 0 to 10 Ω. It is noted that the line to ground fault exceeds the classical mho at 1.97Ω fault resistance, whereas for the line to line fault this is exceeded at 2.48Ω. However, our under-reaching is worse for a line to line fault.

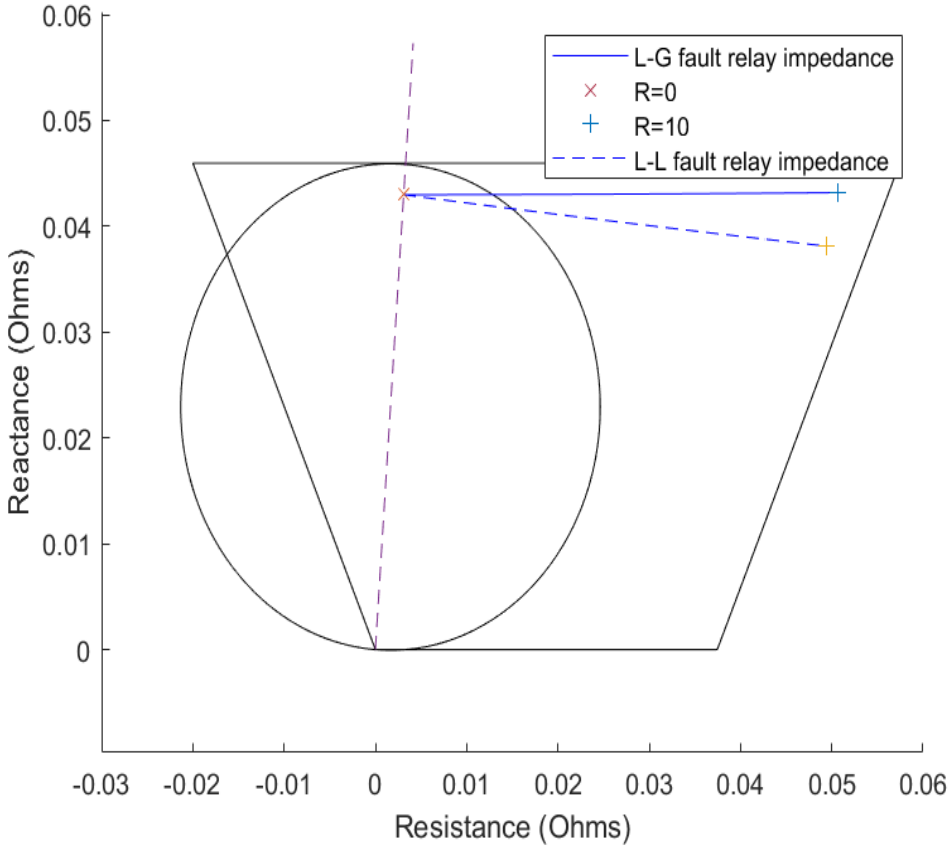

Figure 23: Measured relay impedances for increasing fault resistance from 0 to 10Ω for a synchronous generator at 0° pre-fault current

10.2 Behaviour with varying current angle injection

Relay current angle has a significant impact on the accuracy of the impedance measurement due to the angle differences between relay and grid current causing over-reaching and under-reaching of the measured relay impedance. For a synchronous generator, the relay impedances for generator pre-fault current at unity per unit magnitude and phase angles are investigated, ranging from phi=0 to 360° for a fixed 2Ω fault resistance. This is because a synchronous generator cannot change its emf during the short time duration that a fault occurs in. Once the current it supplies has changed from its pre-fault to during fault value, it remains constant during the fault.

The power factor angle at the grid end is typically within ±20° in order to maximise real power transfer which equals $\sqrt{3} \cdot V_{grid} \cdot I \cdot cos(phi)$, where the sign indicates the export or import of reactive power. While a generator would never import real power with phi=180 under normal operation, the impact of having a pre-fault current at all angles is studied in order to determine the robustness of the relay measurement to current angles.
Figure 24 shows plots of the impedance measured at the relay for line to ground and line to line faults. Here we vary the pre-fault generator current across 360°, with the markers indicating the relay impedance at a particular current phase angle.
The fault resistance acts to amplify the magnitude error as well as worsen the under-reach as we see in figure 25. The line to line fault shows increased variation in relay impedance compared to line to

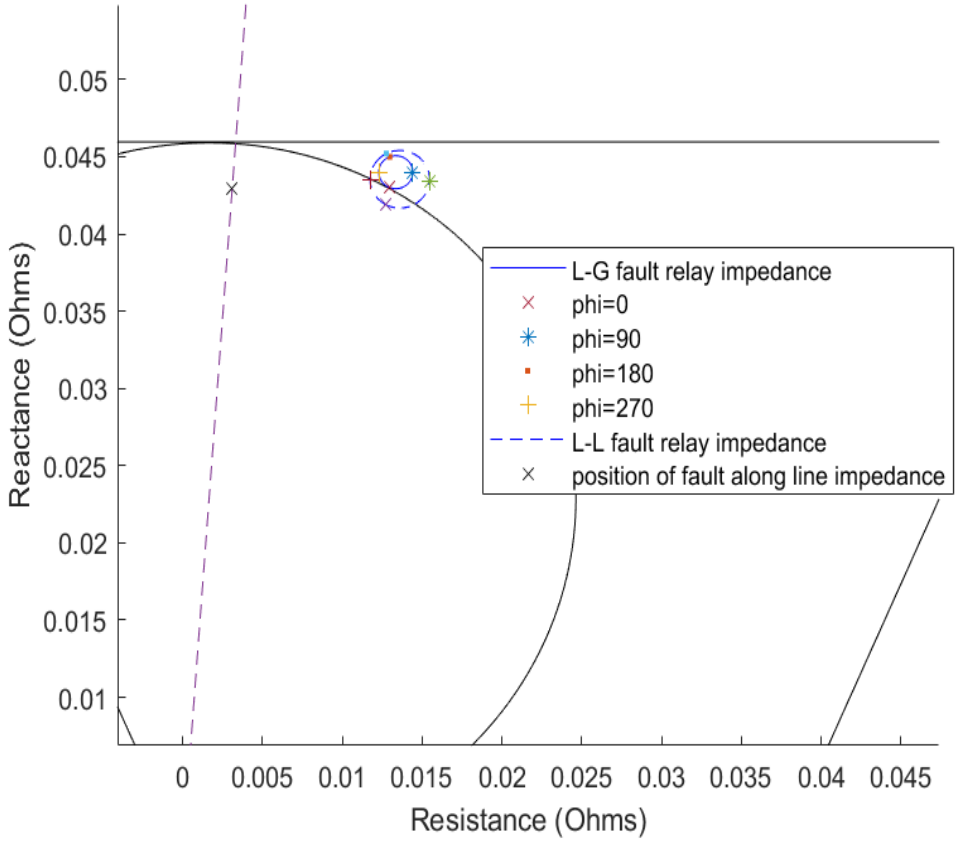

Figure 24: Measured relay impedances for varying pre-fault current angles at 2Ω fault resistance for a synchronous generator

ground faults. This can be attributed to the absence of a zero-sequence current. Equations from figures 12 and 14 in section 8 show that the negative and zero-sequence relay currents depend on the fault current, which in turn depends on the Thevenin equivalent voltage of the positive sequence network. $V_{Thevenin} = I_{pre-fault} \cdot ((1-m)Z_{L1} + Z_G) + V_{grid}$ as shown in figure 13. Since the $(1-m)Z_{ZL1} + Z_G$ term is equal to $0.007 + 0.074i$ we can approximate this as largely inductive. It is also noted that its magnitude is 0.074, less than 10% 1 per unit. This implies that the Thevenin voltage has an angle very close to the grid voltage, which deviates little with current angle injection. This is illustrated in figure 26 where we see due to the small magnitude of the I*X term, which is assumed purely reactive, the Thevenin voltage shows little angle variation from the grid voltage, which is at 0 degrees, as the current angle changes.

As a result, the larger our negative and zero sequence terms are, the less I_{AR} varies with current angle. Our relay current equals $I_{r1} - I_{r2}$ in a line to line fault, noting that I_{r2} has a negative fault current sign so the two terms add. I_{r1}, is a sum of the pre-fault current plus positive sequence fault current flowing through the relay and so changes more with pre-fault current angle. In the absence of a zero sequence current as well as a scaling $K0$ compensation factor our positive sequence current dominates more of the relay current. Thus our $\frac{I_{fault}}{I_{relay}}$ term varies more with pre-fault current angle.

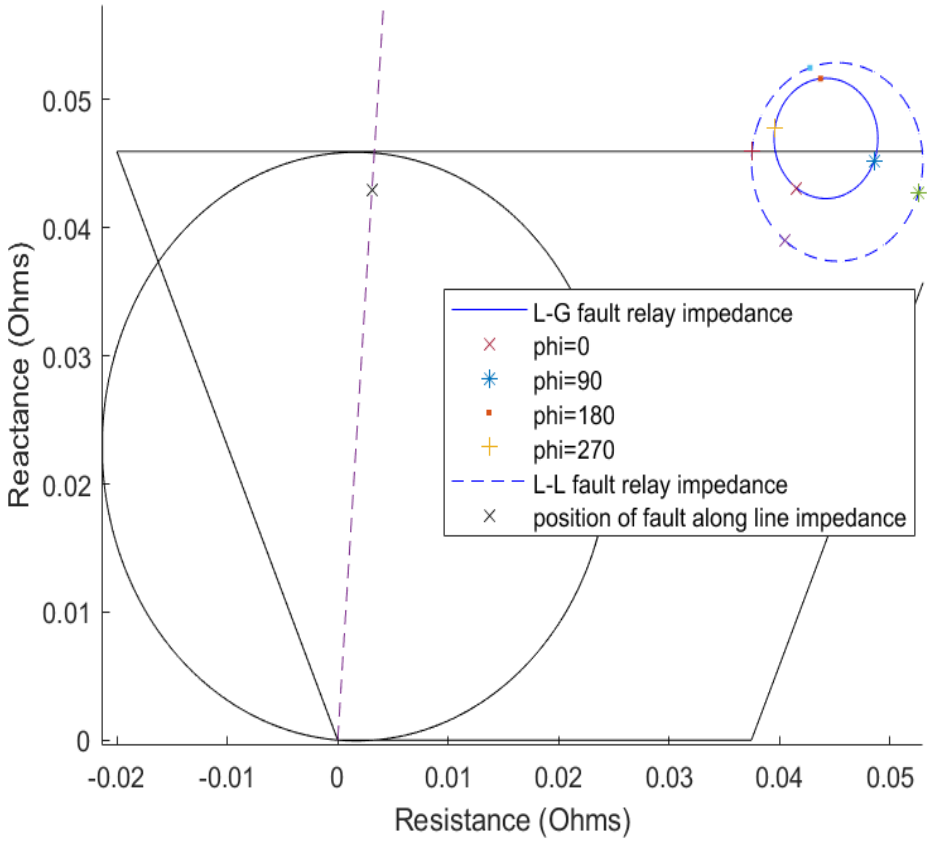

Figure 25: Measured relay impedances for varying pre-fault current angles at 8Ω fault resistance for a synchronous generator

10.3 Behaviour with different grid impedances

The transmission grid is a dynamic and complex network of loads, transmission and distribution lines and generators. In a grid network that increasingly uses power converters and renewable energy, lowering short circuit level has become a particular focus in network design and fault protection. In order to analyse the contribution that various grid configurations make to distance fault protection, we analyse how relay impedance is affected by grid short circuit level [6].

Grid impedance is often defined as a Short-Circuit Level which defines the amount of current that flows from the grid during a fault with zero resistance at the grid terminal or point of connection. Similarly a Short-Circuit Apparent Power can be defined in MVA at rated voltage giving the apparent power the grid supplies during a fault. We also assume an X/R ratio of ten, indicating the reactive impedance is ten times the resistive impedance. Since absolute impedance is given by $\frac{Vb^2}{Power_{SC}}$. $Z_{abs} = \sqrt{X^2 + R^2}$. Since $X = 10R$, this gives $R = \frac{Z_{abs}}{\sqrt{1+10^2}}$. As a result, a higher Short circuit power implies a higher short circuit current level and lower grid impedance.

In figure 27 for a higher grid short circuit level the relay impedance error increases and suffers increased variation with pre-fault current angle, especially for line to line faults. This leads us to conclude that a lower short circuit level improves the performance of distance protection. Referring back to figures 12 and 14 this is consistent with the analysis. A lowering grid impedance means the positive sequence current that the grid supplies would increase, as it sees a lower impedance to the fault and maintains a constant 1pu voltage pre and during fault, as well as the overall fault current increasing due to lower

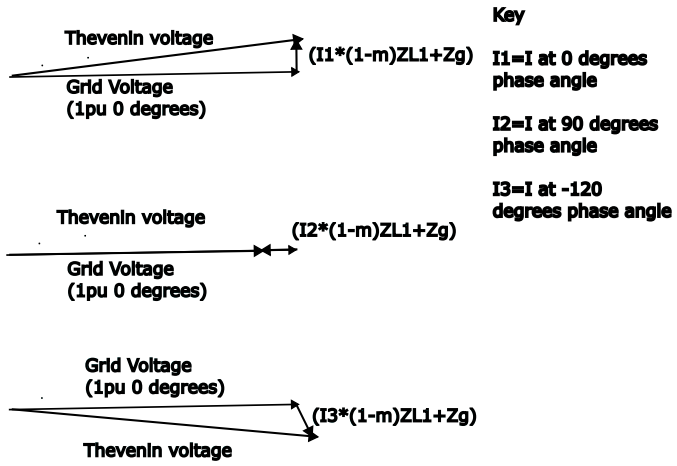

Figure 26: Vector diagram illustrating the small deviation of Thevenin voltage from grid voltage at all current angles

sequence equivalent impedances. We also see that an increasingly lower proportion of the fault current flows through the relay side for all three sequences as the impedance Z_G on the grid side decreases. This worsens our error term $1 + \frac{I_{grid}}{I_{relay}}$ as I_{grid} becomes larger.

As the negative and zero-sequence currents decrease and our positive sequence relay current falls closer to its pre-fault value, our relay current becomes more dependent on the pre-fault current angle. This explains why a line to line fault shows increased current angle variation, since the relay current only composes of the negative and positive sequence currents thus is more heavily influenced by the positive sequence current. Reductions in negative sequence current are more greatly felt. It is however worth noting that the grid side current is still limited by the grid side line impedance $(1 - m)Z_L$. This explains why we see the circular variations in relay impedance with angle become closer together as short circuit power increases.

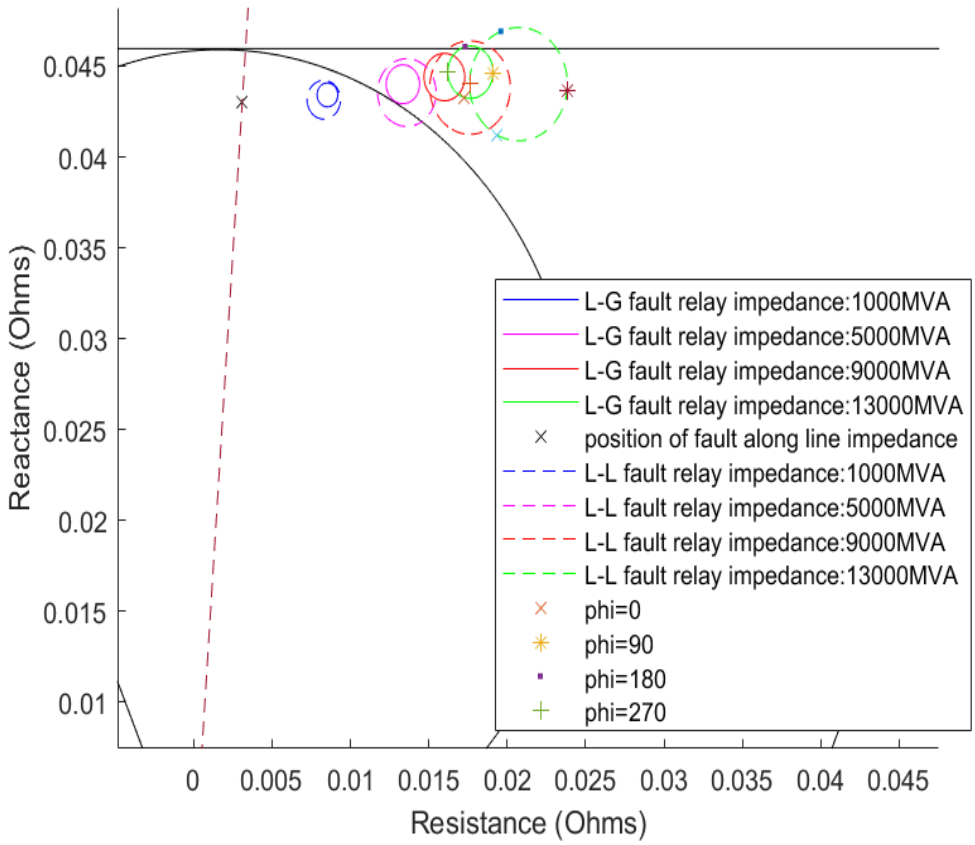

Figure 27: Measured relay impedances for varying grid short circuit powers at 2Ω fault impedance for a synchronous generator

10.4 Behaviour with varying line length

Transmission line length is a widely varying parameter in network design, depending on cable voltage ratings, geographic distance between generation and load and thermal capacity of lines. It is thus important to investigate how distance protection for various technologies performs with varying line length.

Figure 28 shows relay impedance measurements for both fault types from 10 to 100km, accompanied by the respective fault position along the line. Since the impedance of a transmission line is known when setting mho detection parameters we scale our circular and quadrilateral mhos for each line length. We see that our relay impedance falls closer to the fault position as we increase our line length, since the relay impedance increasingly falls within both the circular and quadrilateral mhos. At 10km and 40km our relay impedances lie outside the circular mhos despite their fault positions being within the reach. Line to ground faults suffer particularly more so as we see at 10km it lies almost completely outside the quadrilateral mho thus being very difficult to detect. This shows that our relay impedance measurements become more sensitive to fault resistance and pre-fault current angle at shorter line lengths thus distance protection becomes simpler and cheaper for higher line impedances and longer lengths.

A higher line length increases the line impedance and thus reduces the fault current that the grid supplies, since it sees an increased impedance towards the fault node and maintains a constant 1pu voltage pre and during fault. As a result the positive sequence current flowing through the grid reduces

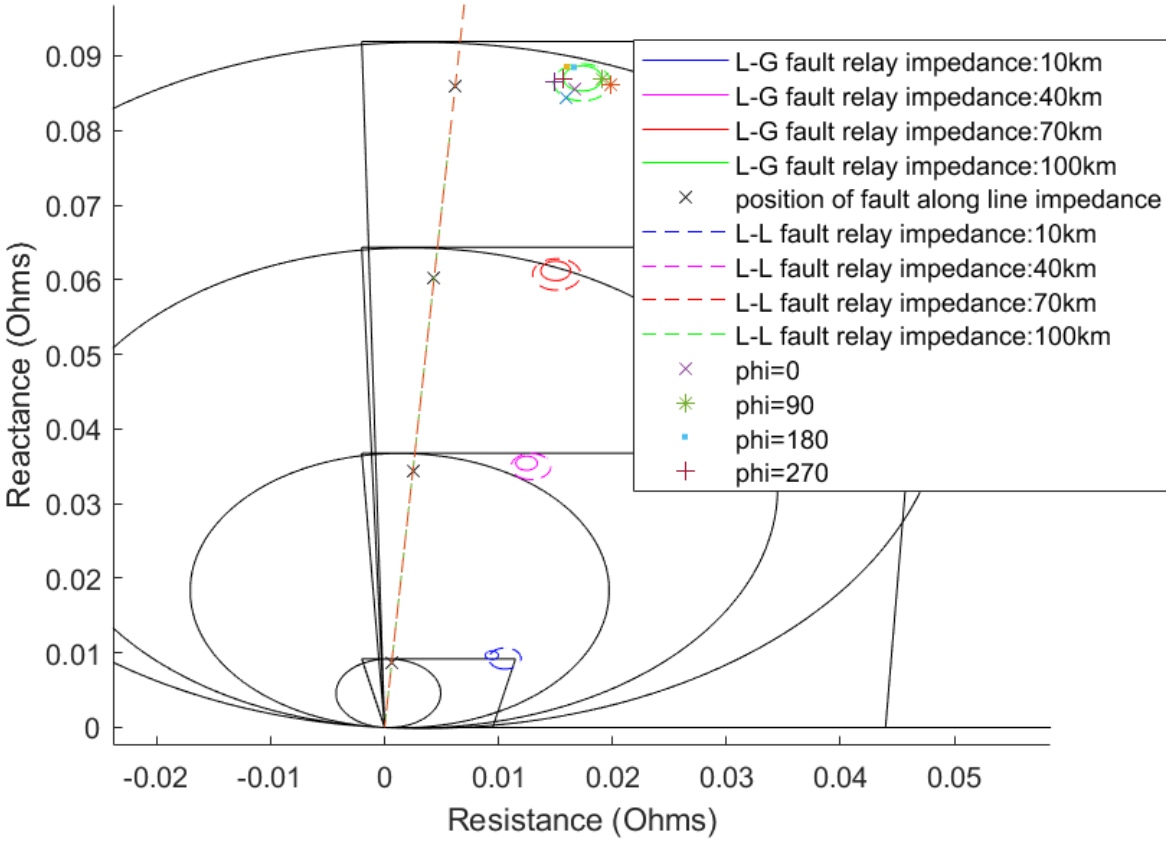

Figure 28: Measured relay impedances for varying transmission line length at 2Ω fault impedance for a synchronous generator

and a higher proportion of the fault current now flows through the positive sequence relay. As a result the magnitude of our $\frac{I_{grid}}{I_{relay}}$ error term reduces and so both fault types fall closer within the mho. We see a further shift towards the fault position with line to line faults as line distance increases. This is because the positive sequence current plays a more influential role due to the absence of zero sequence current in the total relay current. Since a larger line impedance mainly affects the positive sequence network, where the grid is an active voltage source supplying current, the improvements are more heavily felt.

10.5 Behaviour with varying fault position

Establishing behaviour at different fault positions along a line is very important for tolerance setting and determining which detection technologies to use. Figure 29 shows us line to line and line to ground fault relay impedances for different fault positions along the line. The relay measurements move further from the fault position as it moves further toward the grid end of the transmission line. Looking at figures 12 and 14 this is because the $(1-m)Z_L$ impedance decreases as the fault moves towards it. As a result the grid sees a reduced impedance towards the fault location and thus, keeping its voltage fixed at 1pu, provides a larger contribution to fault current. The sequence currents the relay sees reduces as the fault current increasingly flows through the path of lowering resistance on the grid side, thus it sees a reducing negative and zero-sequence current and a positive sequence current that reduces closer to its pre-fault value. The presence of zero-sequence current worsens this as we see

from the line to ground fault moving further away from the fault position as it moves closer to the grid. This occurs because the line impedance on the grid side becomes smaller than that on the generator side making I_{g0} much larger than I_{r0}. Thus the total grid current becomes even larger compared to the total relay current with the addition of an extra sequence term. This results in a larger magnitude $\frac{I_{grid}}{I_{relay}}$ error, as well as increasing variation with pre-fault current angle and power factor as we see from the circles becoming larger.
Note: This does not account for relay measurement tolerances, where if the fault is too close to the relay the relay voltage becomes too small and a measurement cannot be made.

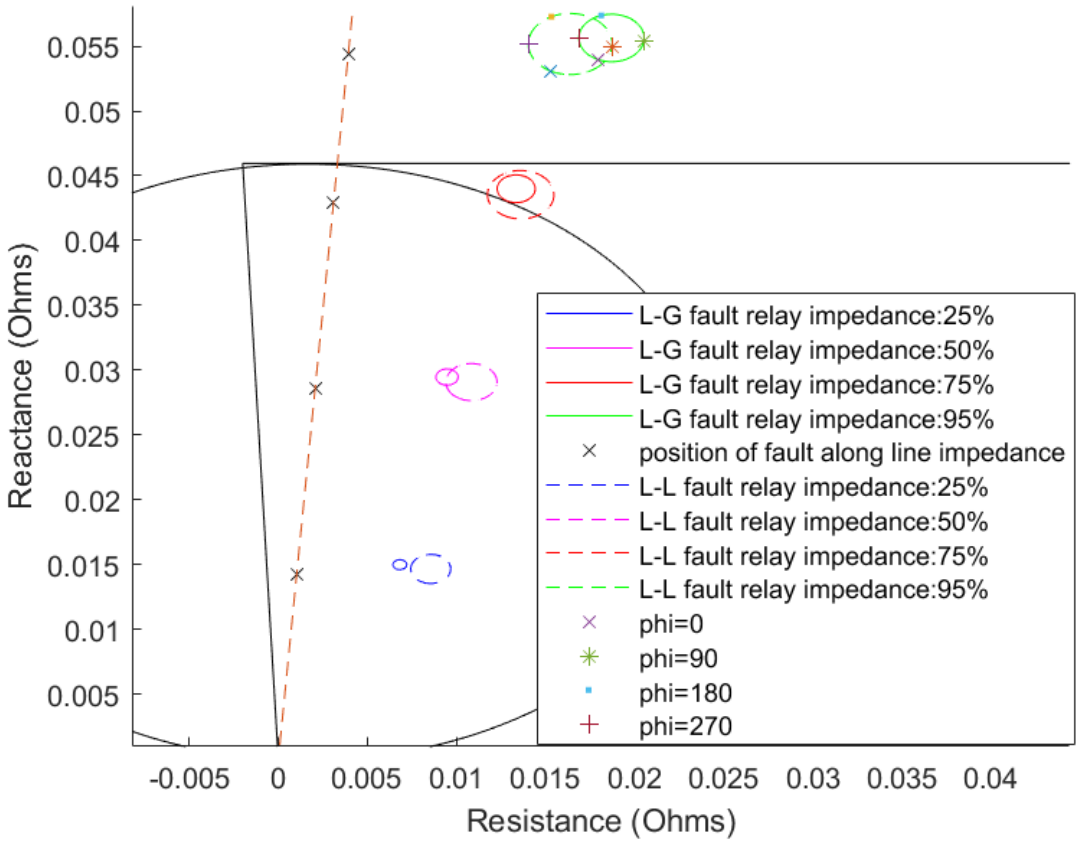

Figure 29: Measured relay impedances for varying fault position along the transmission line at 2Ω fault impedance for a synchronous generator

11 Performance of power converters in distance protection

The same series of tests for a current limited converter are now performed to ascertain the differences in performance due to technology.

11.1 Behaviour with varying fault resistance

We first perform an investigation with fault resistance increasing from 0-10Ω and current injected at a fixed zero degrees relative to the grid.

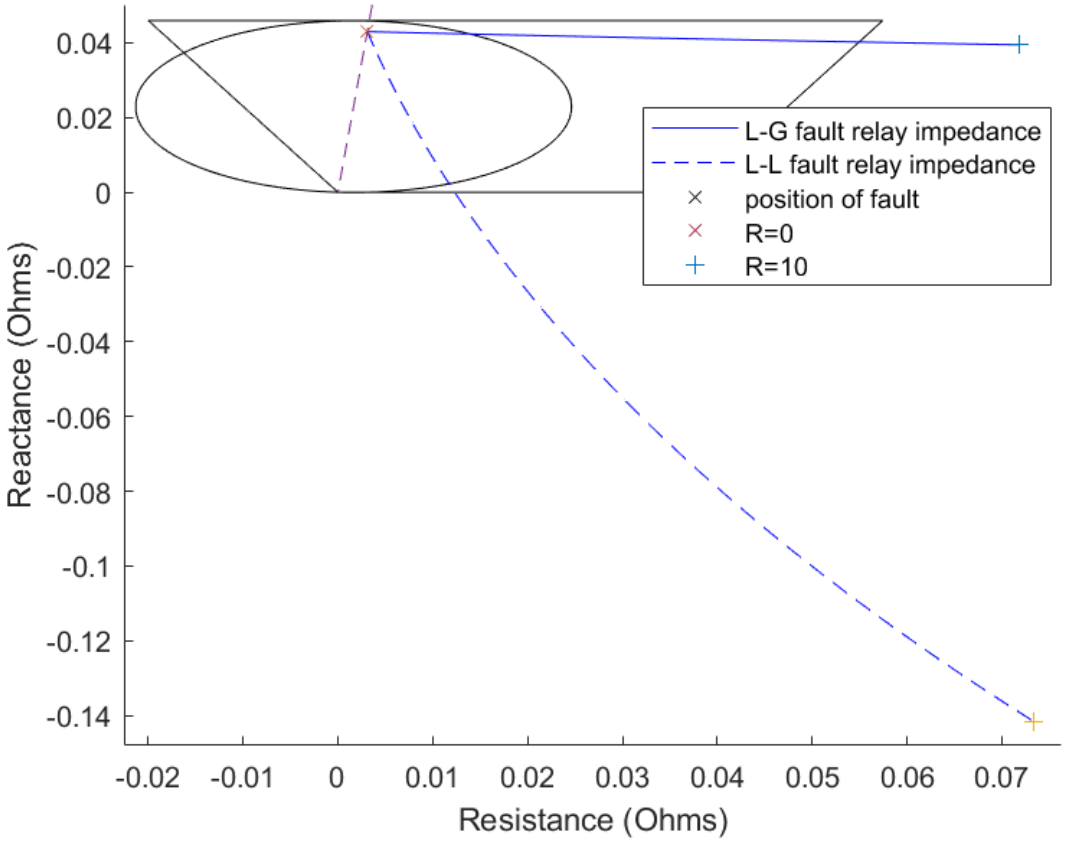

Figure 30: Measured relay impedances for fault impedance increasing from 0 to 10Ω for a power converter injecting current at 0° phase

In figure 30 we see a larger deviation with fault resistance compared to figure 23 for the synchronous generator as the line to ground fault has a relay impedance which has fallen out of the quadrilateral mho before 10Ω fault resistance, despite the fault position being within the reach. It falls outside the circular mho at 1.49Ω demonstrating a higher sensitivity to fault resistance.
However, the biggest difference is seen with line to line faults where significant under-reach is occurring, exceeding the circular mho at 2.042Ω fault resistance. The error magnitude is also significantly larger as at 10Ω fault resistance, the relay impedance lies well outside both mhos. Such under-reach is a major problem as it can mean faults at shorter distances along the line are not detected as the relay impedance falls outside the mho. Similarly fault positions that lie outside the reach of a mho can have relay measurements that fall inside, resulting in incorrect breakers being activated.

11.2 Behaviour with varying current angle injections

A grid interfaced power converter behaves differently to a synchronous generator. The generator emf does not change during a fault due to the very short time scales (micro to milliseconds) that they occur in. A power converter can however change its current, specifically the angle at which it injects at, within the time frame of a fault. As a result, the current angle does not have to depend on pre-fault conditions and can be specifically chosen for distance protection. This makes it more important to investigate how distance protection performs at all possible current angle injections.

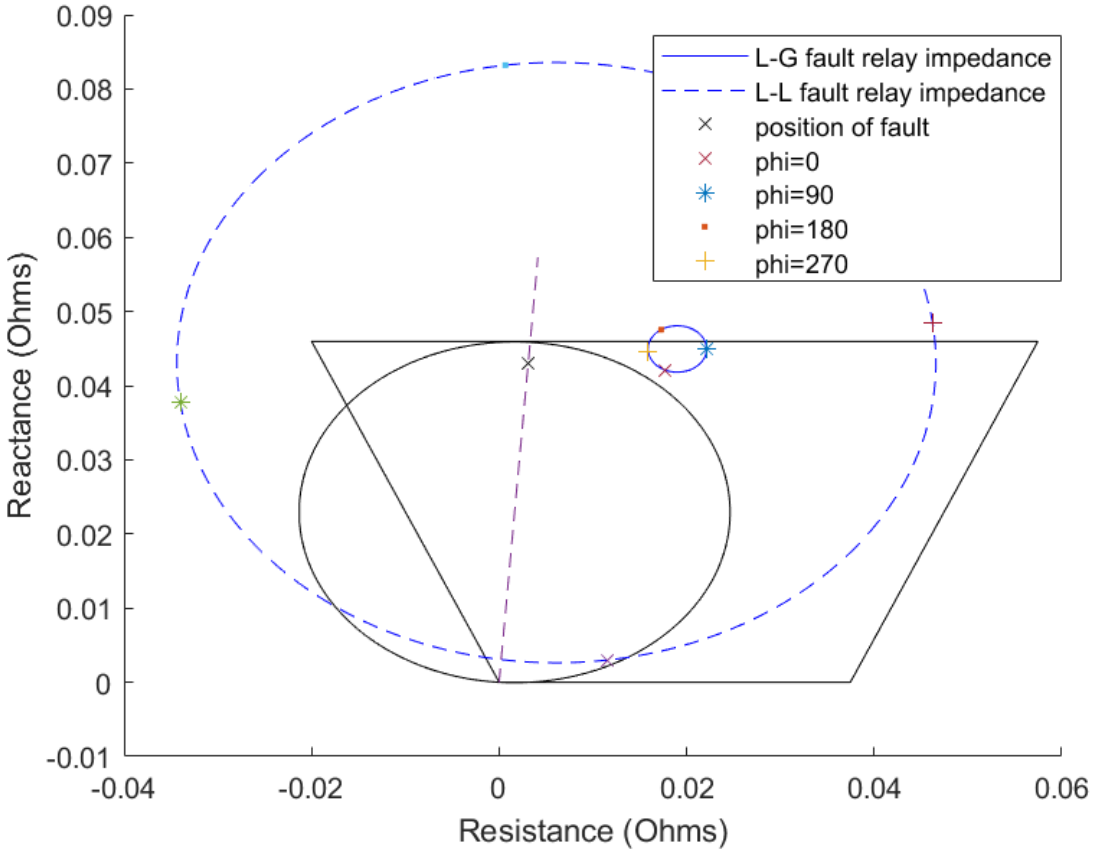

Figure 31: Measured relay impedances for varying current angle injections at 2Ω fault resistance for a power converter

Figure 31 confirms that both fault types perform worse than synchronous generators for all injected current angles at the same fault resistance. While line to ground faults see increased relay error and variation with current angle, line to line faults fall completely outside of both circular and quadrilateral mhos when injected at ±90°. Our angle dependence is also significantly worse. This highlights the heightened importance of zero-sequence current in converter interfaced distance protection.
Fig 32 demonstrates how fault resistance further acts to amplify our magnitude and over-reach errors to a greater extent than compared to synchronous generators, particularly for line to line faults.

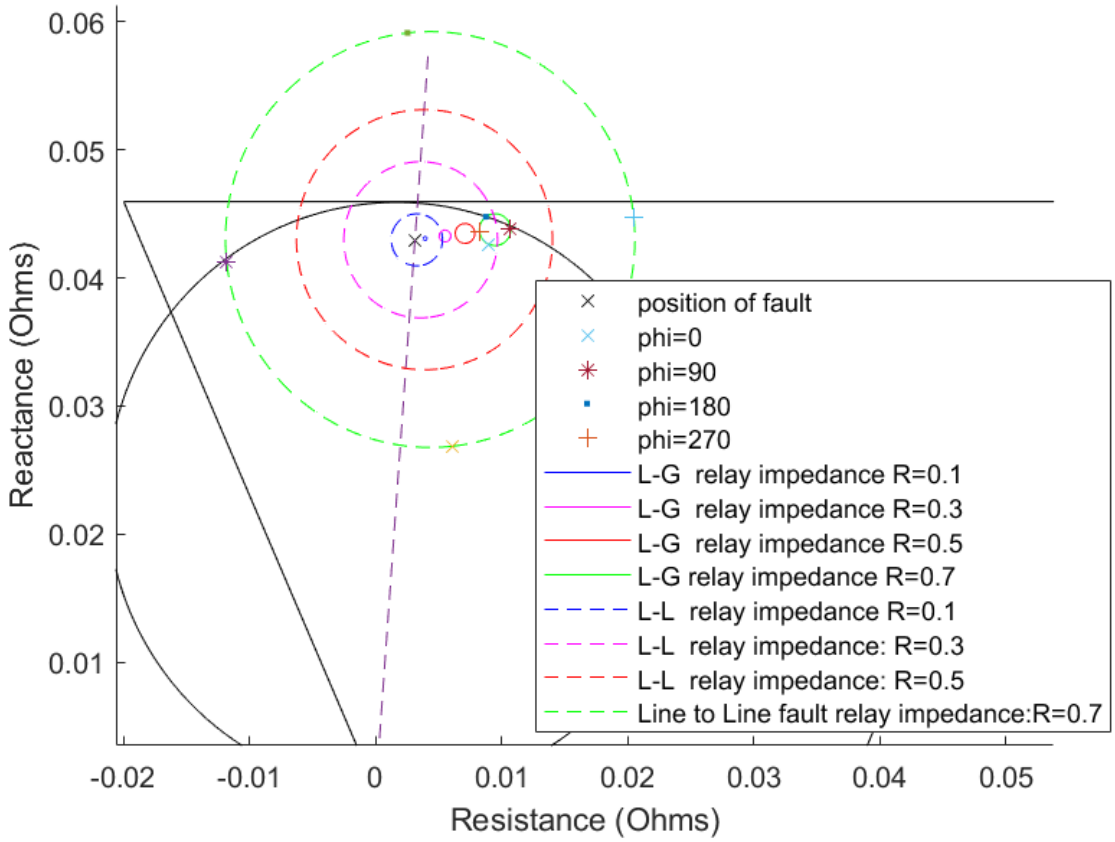

Figure 32: Measured relay impedances for varying current angle injections at varying fault resistances for a power converter

11.3 Behaviour with different grid impedances

As expected, figure 33 shows both fault types suffer from increased error as grid short-circuit level increases. Comparing with figure 27, we see our line to ground faults are generally further away from the fault position compared to a synchronous generator. At 5000MVA for a synchronous generator our line to ground fault relay impedance lay on the boundary of the circular mho, whereas for a converter the circular mho could not detect it. However, our line to line faults show the biggest differences. At 5000MVA our relay impedance measurements are significantly further away from the fault position at all current angles compared to figure 27 for a synchronous generator. At 9000MVA figure 27 shows our relay impedances for line to line faults were still detectable using a quadrilateral mho at almost all pre-fault current angles. However figure 33 shows a relay impedance that falls completely outside both mhos, being undetectable despite the fault position being within our mho reach. This demonstrates how current limited converters show worsened susceptibility to grid side in-feed current and the subsequent difference between relay impedance and fault position it introduces.

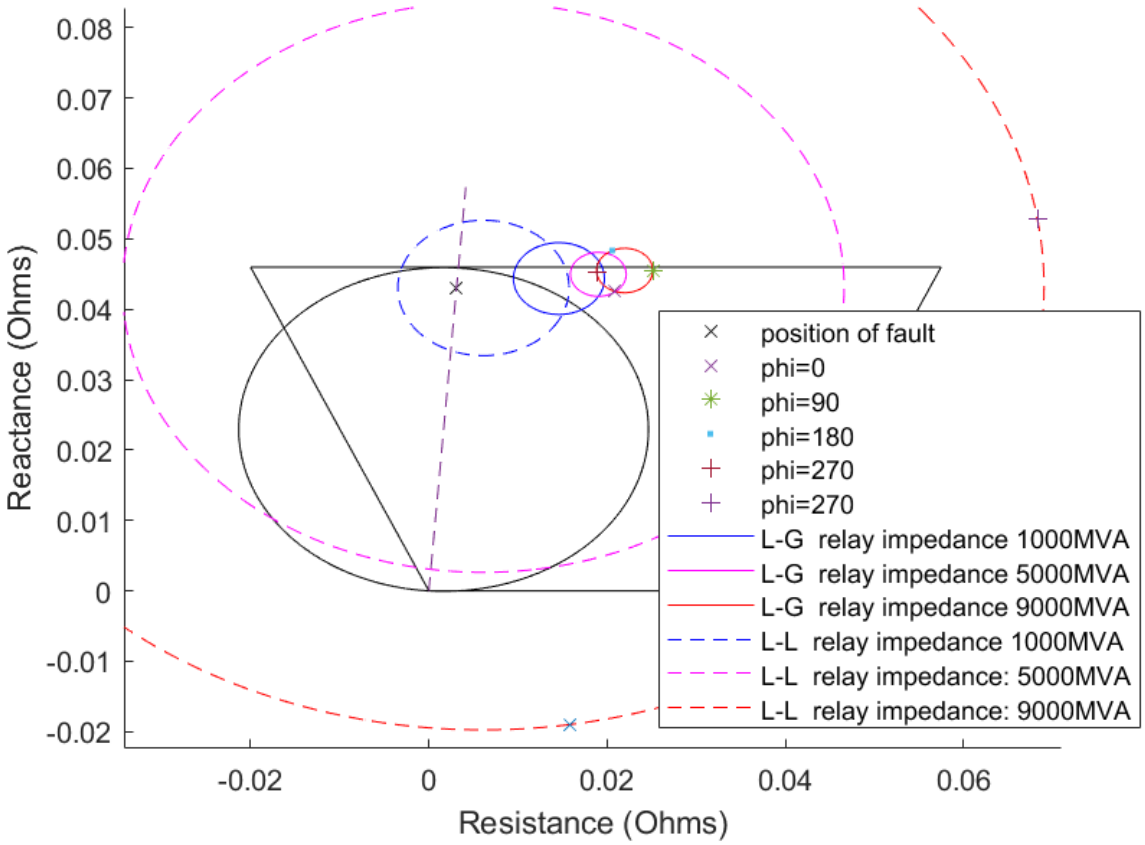

Figure 33: Measured relay impedances for varying short-circuit grid powers at 2Ω fault impedance for a power converter

11.4 Behaviour with varying line lengths

Figure 34 echos the trends seen in figure 28. Higher line impedances reduce the in-feed current the grid supplies and bring our relay measurements closer to the fault position. Here however our line to ground measurements always perform more accurately compared to our line to line measurements. Since there is no negative sequence current outputted by the converter our line to line relay current is always equal to the positive sequence current flowing from the current source. This means it will always have an increased variation with current phase angle compared to line to ground faults, where zero sequence current is included in the relay current measurement.

We see how for 10km the line to line and line to ground relay impedances fall completely outside both the classical and quadrilateral mhos. In figure 28 for synchronous generators a quadrilateral mho could still detect line to line faults at current angles close to 0. This demonstrates another extreme case where higher fault current and higher grid in-feed current can result in undetectable faults. Similarly at 40km for the synchronous generator in figure 28 a quadrilateral mho could detect both fault types for almost all current angles, whereas figure 34 shows for line to line faults the relay impedance lies almost entirely outside the quadrilateral mho except for a small range of current angles.

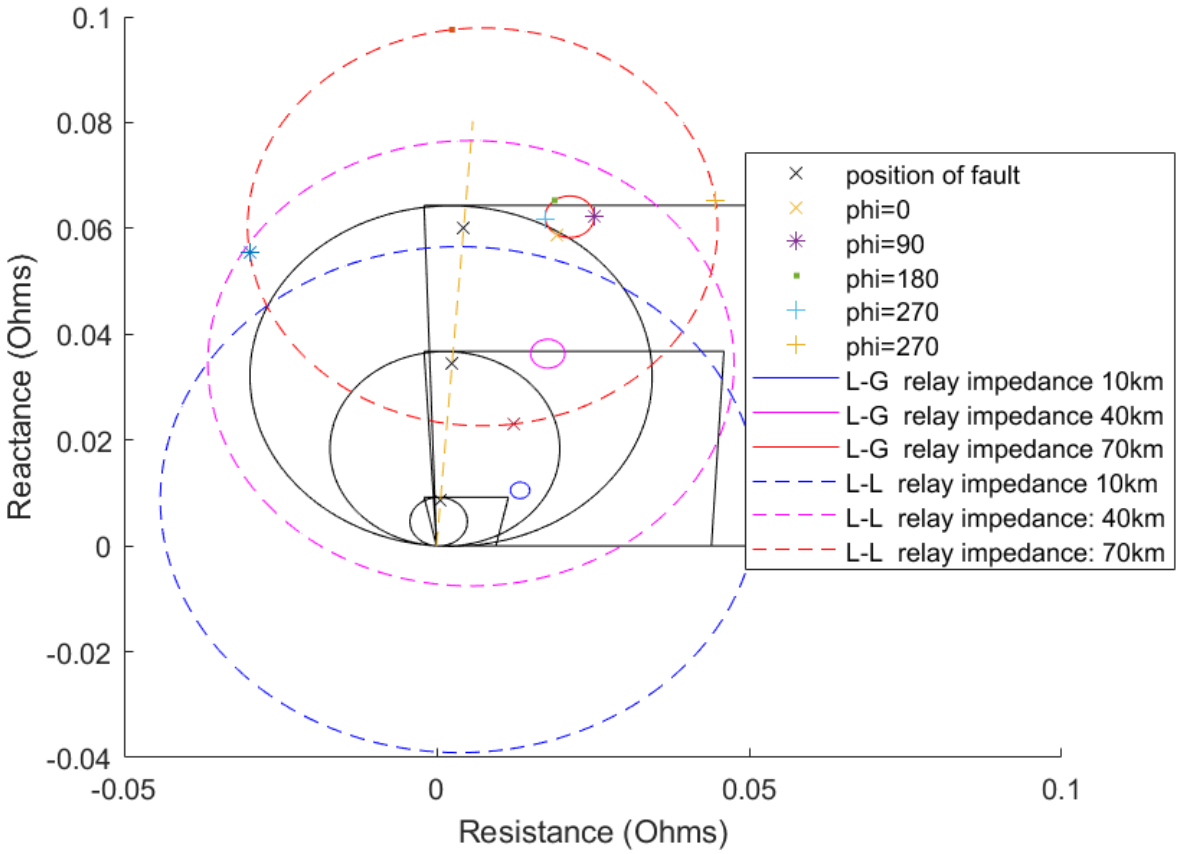

Figure 34: Measured relay impedances for varying line lengths at 2Ω fault impedance for a power converter

11.5 Behaviour for varying fault position

Investigating the impact of fault position gives figure 35. We see for line to ground faults a similar trend as in figure 29 where as the fault moves closer towards the grid our error and dependence on current angle worsens due to increased in-feed from the grid. Our line to line fault relay measurement however only sees the current generated by the current limited converter. As a result, it benefits less from faults being closer to the generator side, thus providing larger inaccuracies at all three positions compared to synchronous generators. We also see the problems that large under and over-reaching can cause as at 95% line impedance even though the fault position lies outside the mho, the relays would incorrectly trip for line to line faults with current angles close to 0.

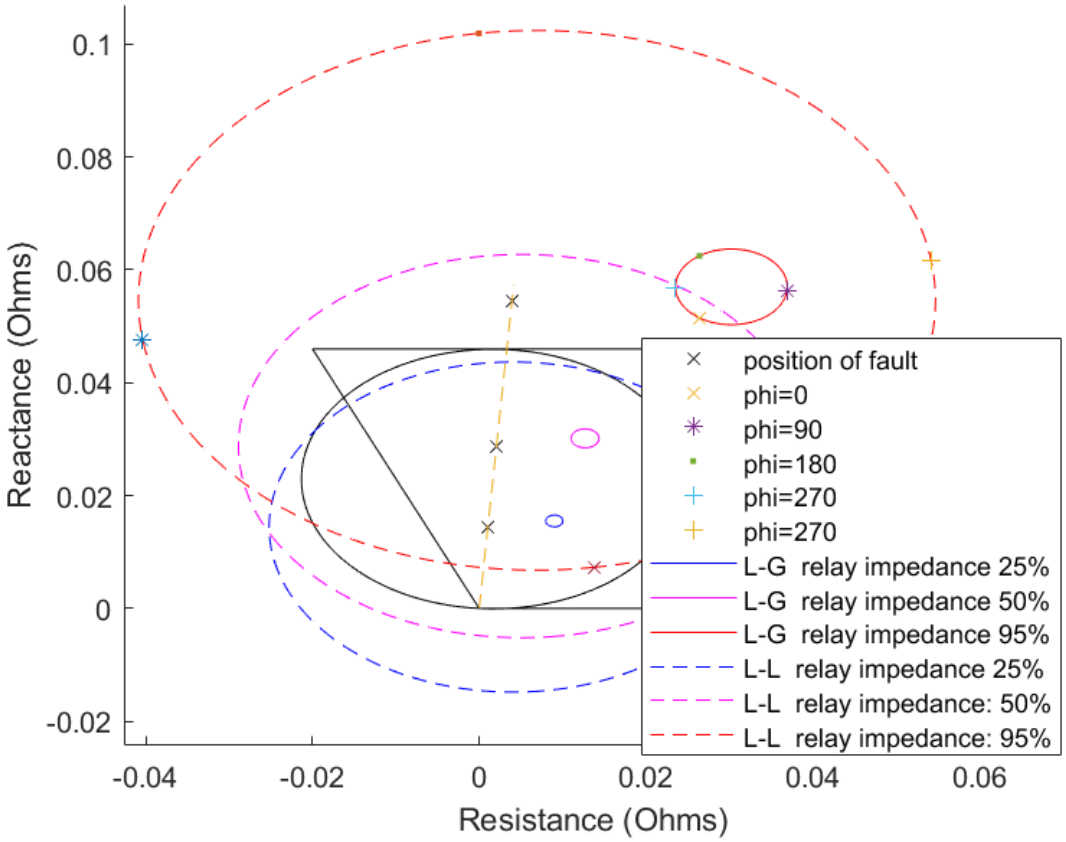

Figure 35: Measured relay impedances for varying fault positions at 2Ω fault impedance for a power converter

12 Comparison and evaluation of distance protection performance between technologies

Through the analysis in the previous two sections we have demonstrated the overall worse performance of the current limited power converter compared to a synchronous generator with a significantly higher fault current level. The key differences being due to the 1pu current limitation on the power converter, which a synchronous generator does not have, as well as the inability of the converter to generate a negative sequence current only dependent on pre-fault conditions.

12.1 The importance of zero sequence current

We have shown that for converters line to ground faults give relay impedance measurements that are closer to the position of the fault along the line. They are also less dependent on the angle of the injected current for both technologies. This is largely because zero sequence current is only dependent on the fault current for a given fault position and network configuration as we saw in section 8. Since the fault current is equal to $\frac{3V_{th}}{Z1_{th}+Z2_{th}+Z0_{th}+3R_{fault}}$ for line to ground faults and $-\sqrt{3}\frac{V_{th}}{Z1_{th}+Z2_{th}+R_{fault}}$ for line to line faults, the Thevenin voltage is the only term dependent on generator voltage and current conditions. The Thevenin voltage is very close to the grid voltage in magnitude and angle for all injected current angles.

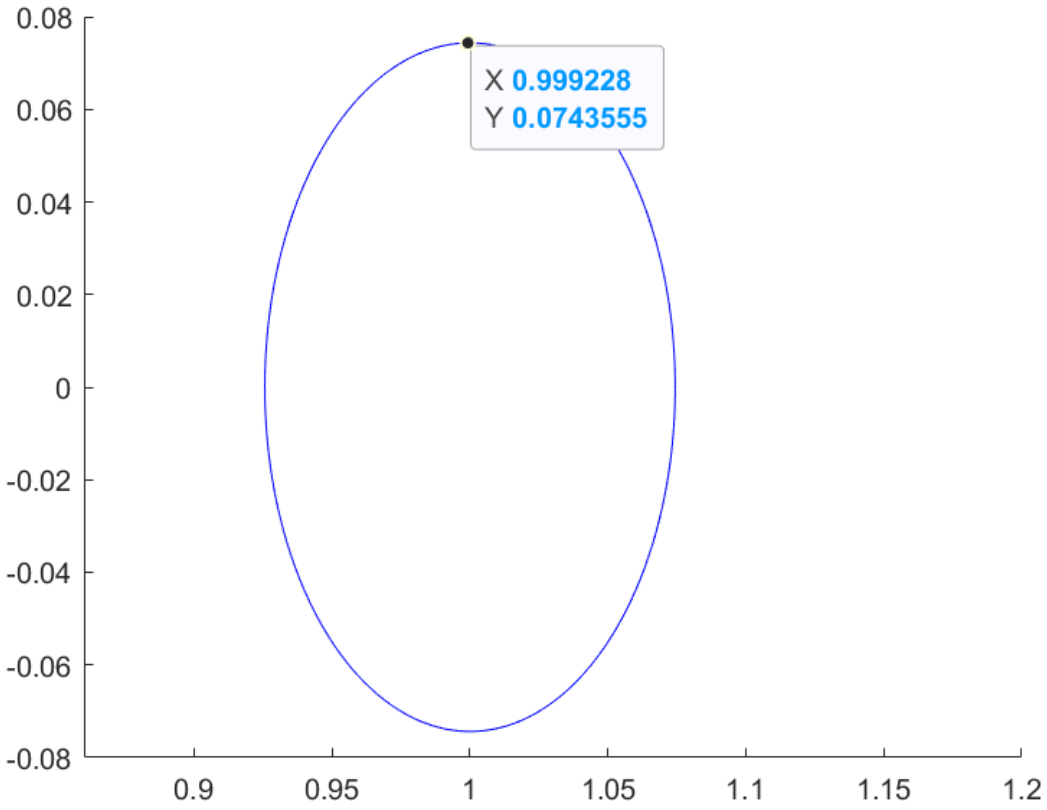

Figure 36: Variation of Thevenin voltage with current angle

Figure 36 demonstrates this as we see the Thevenin voltage has a maximum angle variation of ±4.3° from our grid angle, which we have defined at 0°, and a maximum magnitude deviation of ±0.08 from the grid voltage which we have defined as 1pu. Since the pre-fault and positive sequence currents from the generator are identical for synchronous generators and power converters respectively, this is true for both technologies. As a result the inclusion of zero sequence current in the relay current reduces the influence of positive sequence current and thus the influence of current angle.
Importantly for converter interfacing however, the zero sequence current does not flow through the converter and can still flow through the relay due to the delta star transformer configuration as we see in figure 15. As a result, in-feed current supplied by the grid, which is therefore not current limited, can still flow to the zero-sequence relay. This results in a reduced magnitude difference between fault position and relay impedance as our relay current in our $\frac{I_{grid}}{I_{relay}}$ error term can become much larger. This helps to explain why line to line faults, which do not contain zero-sequence components, perform significantly worse when compared to line to ground for converters, particularly when grid side in-feed current and fault current increase.

12.2 Lack of negative sequence current

We saw for synchronous generators that the negative sequence relay current also only depends on the fault current and pre-fault Thevenin voltage conditions, thus provides reduced relay current dependence on current angle. We also saw the difference between line to line faults and line to ground faults in terms of closeness to fault position along the transmission line was not as extreme as we saw for

power converters, with line to line faults also having much less variation with current angle. This is because the negative sequence current injected by the generator is not limited and so can directly flow from the generator to the negative sequence relay current as we saw in figure 12. As a result our relay current term $I_{r1} - I_{r2}$ can become much larger compared to the fault current and the in-feed from the grid.
In the modelling of our power converter we have assumed it only injects a balanced three phase current. While it could inject a negative sequence current this would still be current limited, since the total output current must be within the rating. It must also be injected at a particular chosen angle, not an angle determined by the fault current and sequence network as we saw for the synchronous generator. As a result, the converter relay current effectively relies entirely on positive and zero sequence currents for line to ground faults, and only the positive sequence current in line to line faults. Since the negative sequence network is open circuit at the generator end, all the fault current now flows through the grid side in the negative sequence network, as we saw in figure 15 and figure 16. This further helps to explain why our grid side fault current contribution is higher and why line to ground and particularly line to line faults show worsened relay impedance measurements.

12.3 Effect of limitation on generator current

The main driving force in the error is the limitation on positive sequence current supplied from the power converter. We saw how for a synchronous generator, the relay current was a combined sum of positive, negative and zero sequences, where the relay negative and zero sequences depended on fault current, and the positive sequence current was a sum of the pre-fault and fault currents. This is because the synchronous generator does not have a current limitation in our model and thus can be modelled as an ideal voltage source. A power converter is always limited by its current rating and as a result the relay current is smaller in magnitude, since only the zero sequence current can freely flow. Similarly, all the negative sequence current now flows through the grid, since in the negative sequence equivalent network the generator is now an open circuit and so no current can flow through the relay. This is especially problematic in converter line to line faults, where the relay current is now purely dependent on the current limited positive sequence, allowing the $\frac{I_{grid}}{I_{relay}}$ term to grow much larger with increased in-feed from the grid. The phase angle of our denominator term is also purely dependent on the angle of the injected converter current thus our relay impedance robustness to phase angle is severely diminished. This is evidenced by the large difference in accuracy a grid generated zero sequence relay current, which is not subject to current limits, makes as we see when comparing line to ground and line to line faults.

13 Investigation of solutions: Current angle injection-Resistive relay impedance errors

In the previous section we confirmed the analysis given in our background and introduction through Matlab simulations. Converter interfaced grid networks suffer from worsened distance protection performance due to the limited current output of the power converter relative to the grid supplied fault current.
In this section we will focus on analysing and evaluating techniques that can improve distance protection performance for converter interfaced grids. Such techniques play an important role in facilitating increased use of renewables and power converters in a decarbonised electricity network. We begin by investigating the role that current angle injection can play in reducing detection inaccuracies. We saw in the previous section that relay impedance measurements vary significantly with current angle, particularly for line to line faults. However, at a particular current angle we saw that the relay impedance did not suffer from any under or over-reaching, producing a purely resistive relay measurement error[14].

13.1 Motivation

The major advantage of this is that faults which occur at line positions outside the reach of the mho will never under-reach and fall into the mho, causing relays to falsely trip. Similarly faults within the mho will not produce relay impedances that under or over-reach and fall outside, causing relays to incorrectly not trip. Quadrilateral mhos are very well suited to detect resistive impedance errors since their resistive reach can be easily modified through resistive and reactive binder settings. There is much less of a requirement for adaptability if reaching can be eliminated, thus quadrilateral mhos can deployed more cheaply [3]. It is also easier to implement angle injection algorithms for most power converters especially when compared to synchronous generators, due to faster response times, increased flexibility and converter operation being decoupled from generation for example in a converter interfaced type 4 wind turbine.

13.2 Utilising sequence relay measurements-Line to Ground faults

For the following analysis and simulations it is assumed that the converter injects the same current pre-fault and when the fault first occurs. This current is at 1pu magnitude and has a phase of zero degrees relative to the grid. We then calculate the angle we need to inject converter current at for a purely resistive relay impedance error term. This represents a worst case scenario where our converter terminal voltage angle deviates the most from the grid voltage angle as shown in figure 13. It is also assumed that our positive sequence equivalent Thevenin voltage, thus our fault current, does not change with positive sequence current angle. This assumption for estimating current angle is justified based on figure 36 where the angle deviation for the Thevenin equivalent voltage is 4.3° at most when the positive sequence current angle varies.

The angle where a purely resistive deviation from fault position for our relay measurement can be calculated through sequence analysis of our model. Here the aim is for the relay current angle to equal the fault current angle. This means the error term $\frac{I_{fault}}{I_{relay}}$ as derived in equation14 becomes purely resistive and the phase angles cancel. For a line to ground fault, figure 15 shows that the zero sequence current measurement allows accurate information about our fault to be obtained, since it equals $I_{a1} \cdot \frac{(1-m) \cdot Z_{L0} + Z_G}{Z_{L0} + Z_T + Z_G}$ as derived in equation 20 [10]. There are several variables here we would not know however. We would not know the position of the fault along the line since this is

what we are trying to determine. We would also not be able to calculate our total impedance since in reality obtaining data on real time grid impedance is difficult and complex. We can however assume the numerator and denominator terms to have a similar phase angle making the term approximately resistive, since they are both predominantly reactive and have similar magnitude resistances due to sharing the grid impedance term. This means we can approximate the fault phase angle to be the phase of our zero-sequence current. This approximation depends purely on the reactance to resistance ratios of the grid and line.
The relay current measurement consists of the A phase relay current plus our zero-sequence compensated term $K0 \cdot I_{relay0}$ as shown in equation 9. We can re-write this as

$$I_{relay1} + [(K0 + 1) \cdot I_{relay0}] \tag{28}$$

in terms of our positive and zero-sequence relay currents. For a current limited converter the positive sequence relay current I_{relay1} is equal to the output of the power converter and so this is the angle we can vary to ensure no under or over-reaching of our relay impedance. It is assumed that the zero sequence current remains constant for all positive sequence current angles injected. The aim is for the phase angle of the $I_{relay1} + [(K0 + 1) \cdot I_{relay0}]$ relay current to equal the phase angle of the fault current. Since the equation is a complex number, we can find its phase angle by splitting the equation into its real and imaginary parts. Because I_{relay1} is also a complex number we can express it in the form

$$|Magnitude| \cdot [cos(\phi) + isin(\phi)] \tag{29}$$

where ϕ is the phase angle of the positive sequence relay current. This means the positive sequence relay current, equal to the output of the converter, can be expressed as $cos(\theta) + isin(\theta)$ where the current magnitude is 1pu and θ represents the during fault current angle injected to make the error resistive (No over or under-reaching). The phase angle of any complex number is determined by finding the arctan of the imaginary component divided by the real component. Hence,

$$Angle(I_{fault}) = arctan(\frac{imag((K0 + 1) \cdot I_{relay0}) + sin(\theta)}{real((K0 + 1) \cdot I_{relay0}) + cos(\theta)}) \tag{30}$$

To show the accuracy of this technique it is first assumed that we know all circuit parameters. If the fault resistance is 4Ω, we can obtain the zero-sequence relay current from our script which is measured as $0.412 - 1.3455i$. The impedance term

$$\frac{(1 - m) \cdot Z_{L0} + Z_G}{Z_{L0} + Z_T + Z_G} \tag{31}$$

is equal to $0.2823 - 0.0007i$. From our I_{r0} equation this gives a sequence equivalent fault current I_{a1} equal to $1.47125 - 4.7626i$. Thus the fault current has a phase of -72.833°. This is the phase the relay current must now be equal to. I_{r0} is multiplied by $(K0 + 1)$, which would depend on known line parameters Z_{L0} and Z_{L1}, to obtain $0.96737 - 5.1379i$. The equation

$$-72.833 = arctan(\frac{-5.1379 + sin(\theta)}{0.96737 + cos(\theta)}) \tag{32}$$

for θ is then solved. This gives the equation $3.237cos(\theta) + sin(\theta) = 2.0064$ which can then be solved numerically to obtain $\theta = 70°$
Figure 37 shows the resulting relay impedance measurement when injecting current at 70° when the fault resistance equals 4Ω. We see this is close to giving a purely resistive error with the fault position, with no under or over-reaching. There is however a slight under-reach as the fault current angle changes with the injected current angle. This change is negligible however due to the zero sequence compensated term in the denominator which will always be similar to the fault current phase angle and is larger than the positive sequence current.

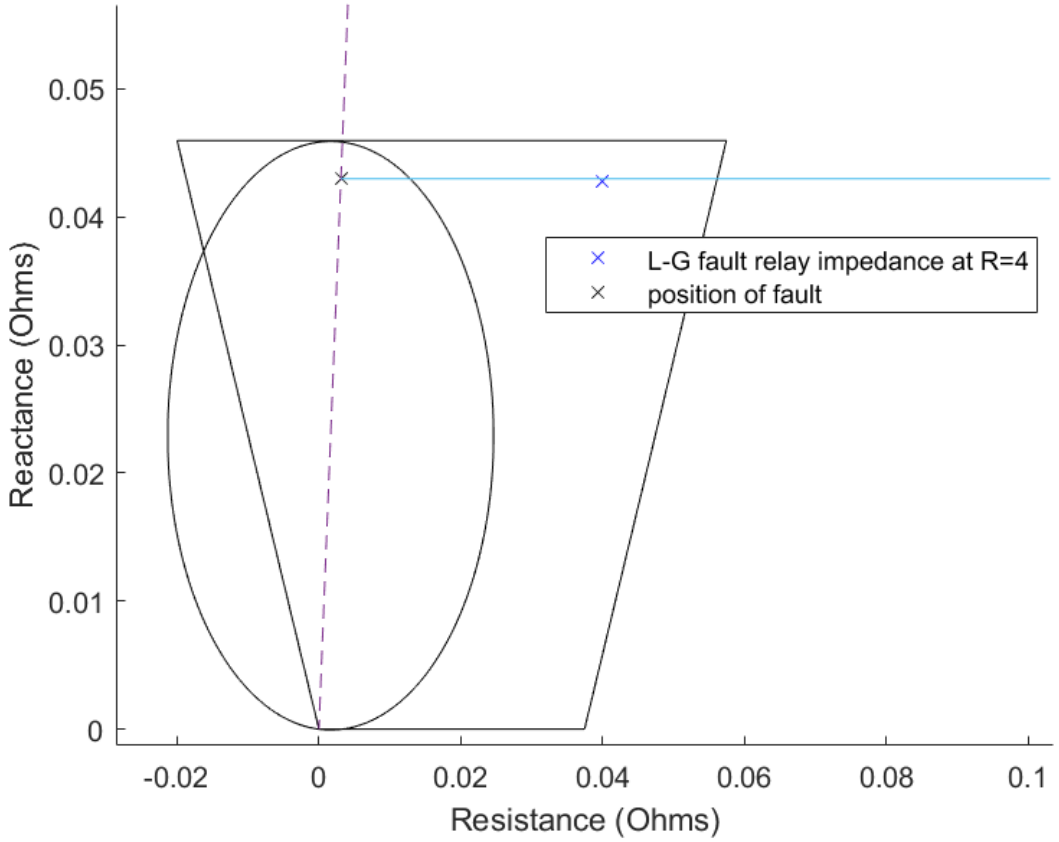

Figure 37: Perfectly resistive relay impedance at 70° current angle injection at 4Ω fault impedance

In figure 38a the above algorithm is applied but now assuming the $\frac{(1-m)\cdot Z_{L0}+Z_G}{Z_{L0}+Z_T+Z_G}$ term is purely resistive and the fault current angle equals the zero sequence relay current angle, since in reality this term is not known. This is applied at ten fault resistances ranging from 1-7Ω. There is very close agreement with the perfectly resistive impedance error plot, particularly for small fault resistances. However, the small differences in angle introduced from our assumptions result in increased deviation from a purely resistive relay error as the fault resistance increases. This results in worsening accuracy and increased over-reach.
Comparing figure 38a with 38b, which was our original zero degrees current injection base case seen in figure 30, we see significantly improved resistivity at all fault resistances. This is because relay measurements are used to dynamically improve accuracy. This does however introduce additional complexity in terms of computation and monitoring relay measurements. In section 11 for power converters we saw line to ground faults perform much better than line to line faults in terms of over-reach and magnitude difference from fault position without any corrective measures. As a cost-benefit trade off it might not be worth the additional cost and complexity in angle injection since the room for improvement for line to ground faults is smaller, especially compared to the errors seen for uncorrected line to line faults in converter interfacing.

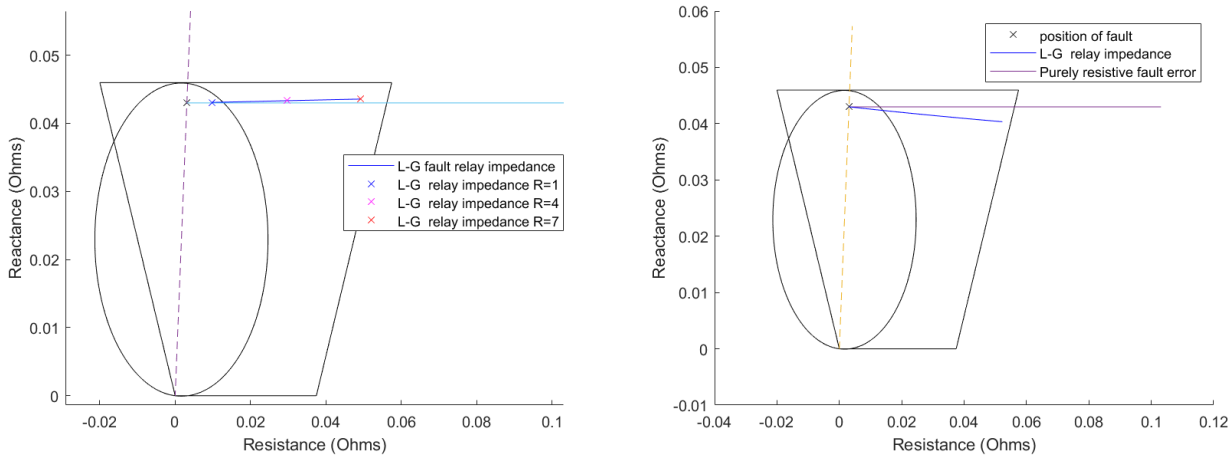

(a) Measured relay impedance for fault impedances ranging from 1 to 7Ω

(b) Measured relay impedance at unchanged 0° current angle injection with increasing fault resistance 0-7Ω

Figure 38: Improvement using zero-sequence current for line to ground fault angle injection

13.3 Utilising sequence relay measurements-Line to Line faults

For line to line faults the analysis is simpler since our relay current term $I_{relay1} - I_{relay2}$ is equal to our power converter current since the negative sequence relay current is zero. To achieve a purely resistive relay impedance error we simply need our converter current angle to match the fault current angle, which is given by $\frac{V_{th}}{Z_{thev1} + Z_{thev2} + R_{fault}}$ as derived in equation 25. The simplest approach for this is to assume our Thevenin equivalent voltage approximately equals the grid voltage in magnitude and the pre-fault relay voltage in phase angle. Our pre-fault relay voltage angle on the A phase is 6.6° while figure 36 shows our Thevenin voltage has a maximum angle deviation of 4.4° relative to the grid. This shows that voltages across the line show relatively small differences in phase angle from each other. We can similarly approximate the equivalent impedances of our positive and negative sequence networks to be purely reactive and so have a phase angle of 90°, since both grid impedance and line impedances have high X:R ratios of 10-15. This gives us an angle injection of $-83.4°$.
Figure 39a demonstrates what happens if we inject at this fixed angle when a fault is detected. The measurement performs very well up to a fault resistance of 1Ω. Past this however, the over-reach worsens at an increasing rate with fault resistance. This shows how the reactive approximation worsens with fault resistance as our denominator resistive term in our $\frac{V_{th}}{Z_{thev1} + Z_{thev2} + R_{fault}}$ fault expression becomes larger, reducing its phase angle. We have however eliminated the significant under-reach seen in figure 30 with little complexity involved. This technique only utilises pre-fault relay voltage data and so the angle can be changed instantly when the fault occurs, unlike previously where we needed to obtain during fault relay measurements. As a result, it could be useful for small fault resistances less than 1Ω or very long and inductive line lengths, where less accuracy but a faster response time may be needed. Figure 39b shows a nearly perfectly resistive error term when the grid in-feed is low for example.

There is not a sequence current dependent on the fault for line to line faults. As a result it will be more challenging for the relay current phase angle to match the fault current angle, since the fault current angle will change as we change the angle of converter current injection. The lack of zero sequence current in our relay means angle differences between the positive sequence relay current and

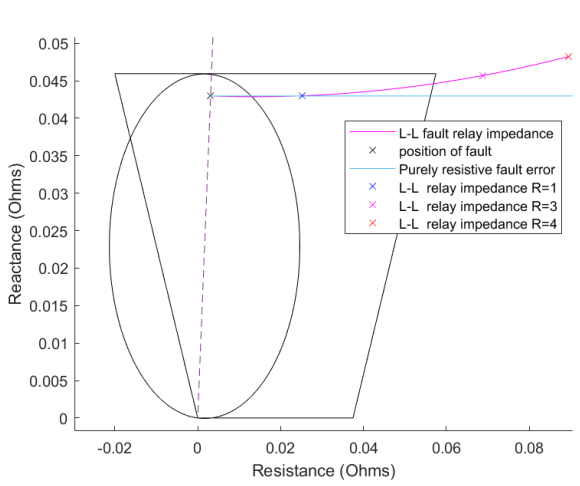

(a) Relay impedance at -83.4° current angle injection

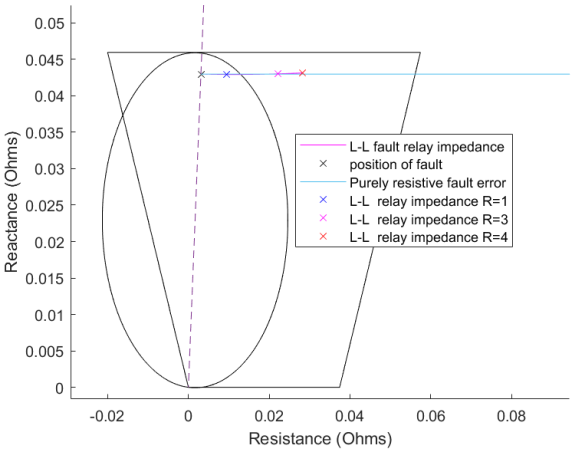

(b) Relay impedance at -83.4° curretn angle with grid SCP 1000MVA

Figure 39: Measured relay impedances for increasing fault resistance from 0 to 4Ω

fault current result in more over and under-reaching.

It is possible however to utilise the negative sequence relay voltage instead as this is proportional to the fault current as shown in equation 27 [15]. Here $V_{relay2} = I_{a1} \cdot Z_{thev2}$, where I_{a1} is the sequence equivalent fault current whose angle we wish to match. To investigate if injecting at this angle will produce a purely resistive fault, we inject current at an angle equal to the phase of $\frac{V_{relay2}}{Z_{thev2}}$ for increasing fault resistance. V_{relay2} is the negative sequence relay voltage when injecting current at 1pu and 0° relative to the grid before applying current angle correction.

Figure 40 demonstrates that our relay impedance measurements show under-reaching. Our assumption that the fault current does not change with converter current angle becomes less valid for line to line faults.

Since in reality it is not possible to know Z_{thev2} as it is dependent on the grid side line impedance and grid impedance, both of which are unknown, we must apply approximations to the negative sequence Thevenin impedance term. We can begin by approximating the term to be purely reactive. This means we inject at an angle equal to the V_{relay2} angle minus 90°.

Figure 41a demonstrates that by over-estimating the phase angle of Z_{thev2} the relay impedance error term has become more resistive compared to figure 39a and 40, no longer suffering from the curved variation with fault resistance. To improve the relay measurement even further it is attempted to utilise the line impedance phase angle in order to closer reach the true phase angle of Z_{thev2} [15]. For our configuration the line has a positive sequence phase angle of 85.876°. If we assume the grid has a similar impedance phase angle we obtain the plot in figure 41b

This suffers from a slightly worse reach error compared to figure 41a. As figure 40 demonstrates, obtaining a more accurate estimation of the fault angle at 0° does not translate to a more resistive relay eror as the fault current will change with the positive sequence current. Figure 26 shows at a zero degree current angle the Thevenin equivalent voltage sees a maximum angle deviation from the grid. This means any changes to the converter current angle will result in a decrease of the Thevenin equivalent voltage phase angle, thus a decrease in the fault current angle. By overestimating the phase angle of Z_{thev2} to be purely reactive, the phase angle of $\frac{V_{r2}}{Z_{thev2}}$ becomes smaller. This means the positive sequence relay current we inject is also reduced. By reducing I_{relay1} further than an ideal calculation, such as in figure 40, would suggest we mitigate the reduction in fault current angle that any change in converter current angle brings. The advantage of injecting current at 0° when the fault

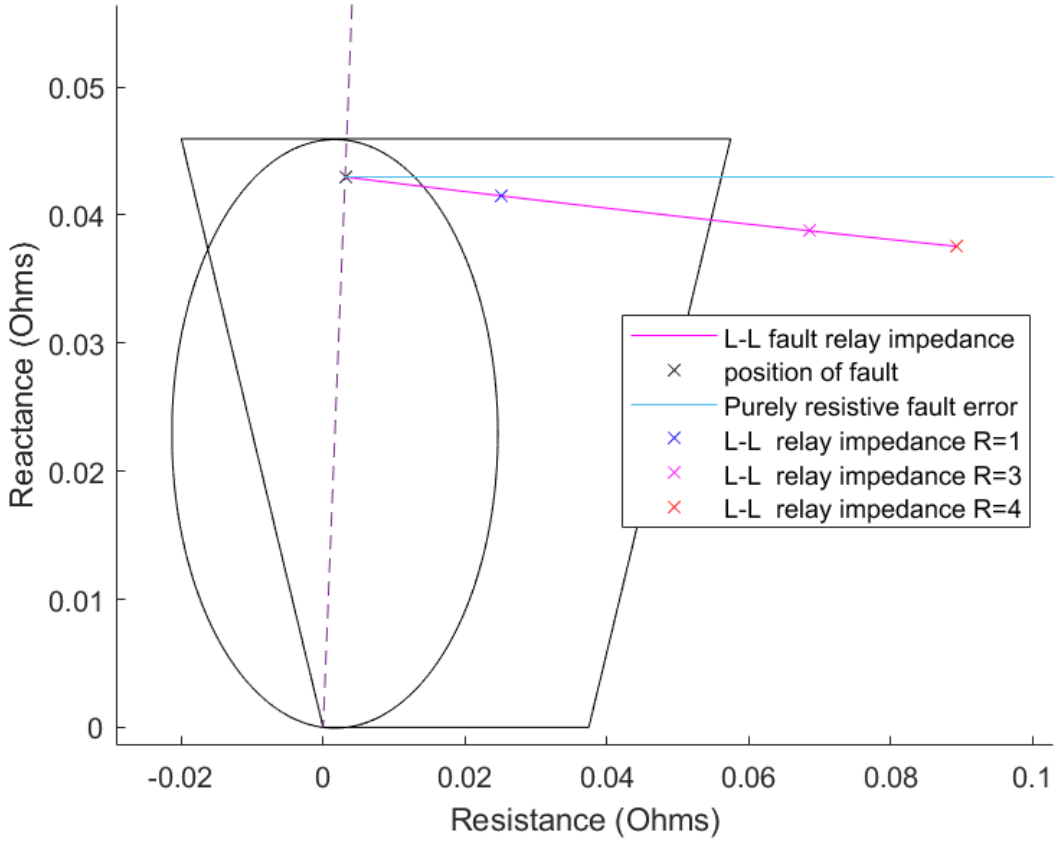

Figure 40: Relay impedance error assuming all parameters known for increasing fault resistance from 0 to 7Ω

first occurs is that we can obtain a more resistive error term while having less information about the network.

Figure 42a shows how, if we utilise the line impedance phase instead of assuming Z_{thev2} is purely reactive, the relay impedance measurement varies with fault resistance for different grid impedance X-R ratios. At lower X-R ratios using the line impedance phase results in an over-estimation of the fault current phase angle. This helps to mitigate the reduction in fault current phase angle as the converter current angle changes, hence we see the best performance when the X-R ratio is 5.

This demonstrates that current angle injection can be simple to implement without the knowledge of during fault specific network parameters, such as the line impedance on the grid side of the fault. However, the accuracy of angle estimation techniques depends on network properties as this determines how the fault current angle will change with positive sequence current. Figure 42b demonstrates this as the technique used in figure 41a now performs worse, as the Thevenin voltage changes less with current angle due to the lower grid impedance. While this is less important for line to ground faults, line to line faults are more affected by angle differences between fault and relay current. Knowledge of pre-fault network values and estimations of how the fault current angle changes with angle injection will help determine the optimal current angle estimation technique.

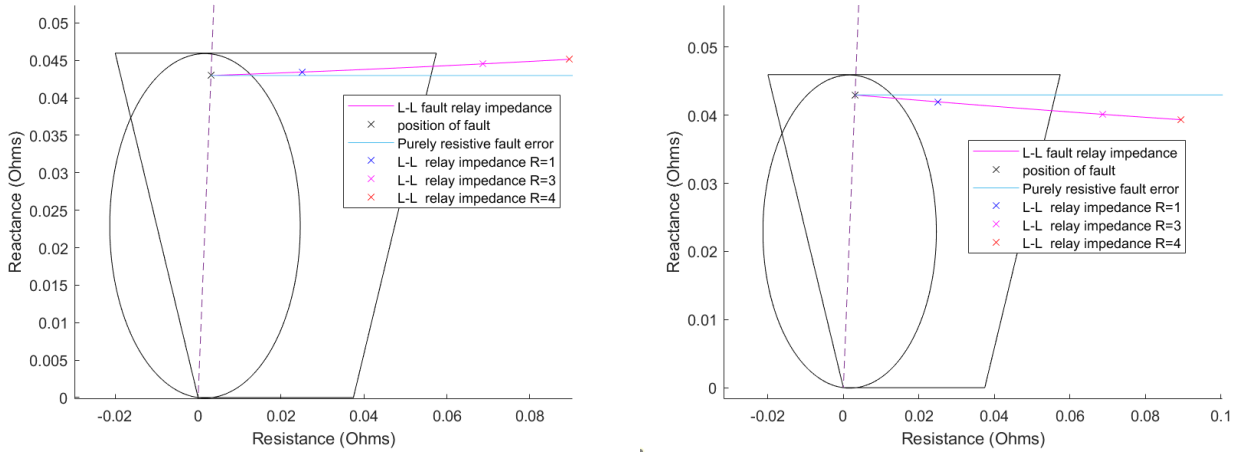

(a) Measured relay impedance for fault resistance increasing from 0 to 4Ω

(b) Measured relay impedance using line impedance phase for increasing fault resistances from 0 to 4Ω

Figure 41: Relay impedance measurements using negative sequence voltage for current angle injection

13.4 Mimicking synchronous generators

Section 10 showed that synchronous generators gave overall more accurate relay impedance measurements, showing reduced under and over-reach for both fault types at all injected angles. While this was largely due to their increased fault current limit, we can still mimic the behaviour of an ideal voltage source that synchronous generators are modelled as in terms of current angle. This can be useful as the grid behaves as a constant voltage source that sees a reactance dominated impedance towards the fault. As a result this can provide an approximate way of matching the grid current angle for the positive sequence relay current[14].

This is achieved by measuring the pre-fault voltage at the terminals of the current source, equal to

$$I_{conv} \cdot (Z_{L0} + Z_T + Z_G) + V_{grid} \tag{33}$$

which is close in magnitude to the grid voltage due to the low per unit line impedance values relative to the grid voltage. A synchronous generator does not change its emf voltage over the duration of a fault while its terminal voltage drops with the fault occurrence. A simple phasor model of a synchronous generator consists of its emf voltage connected to the terminal via a source inductor. We can emulate this model by replacing the generator emf with our pre-fault voltage at the terminal of the converter, the source inductance with our transformer and the terminal voltage with our relay voltage. If we assume that the terminal voltage of the converter does not change from its pre-fault, we obtain the current that would be injected equal to

$$\frac{Vconv_{pre-fault} - V_{relay1}}{Xj} \tag{34}$$

where V_{relay1} is the during fault positive sequence relay voltage and Xj is the equivalent synchronising reactance. Here V_{relay1} acts as an approximation of the voltage at the fault node and $Vconv_{pre-fault}$ is typically close to the grid voltage and angle due to the low grid impedance relative to the grid voltage as shown in figure 13. Thus $Vconv_{pre-fault} - V_{relay1}$ is an approximation of the voltage drop between the grid and the fault node. To imitate this current angle, the current is injected at the angle of the $Vconv_{pre-fault} - V_{relay1}$ term minus 90° due to the denominator reactance term.

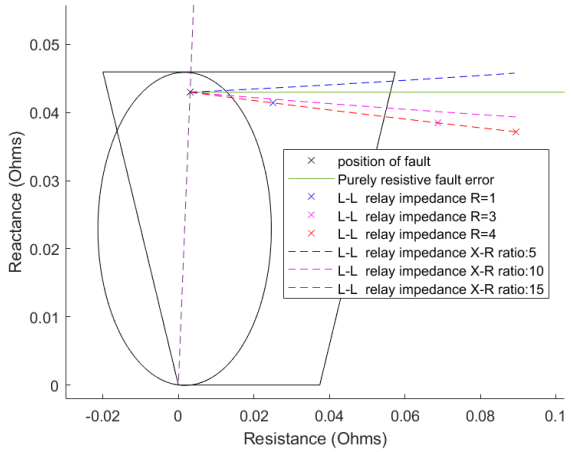

(a) Relay impedance using line impedance phase for fault resistances 0-4Ω and varying X-R ratio

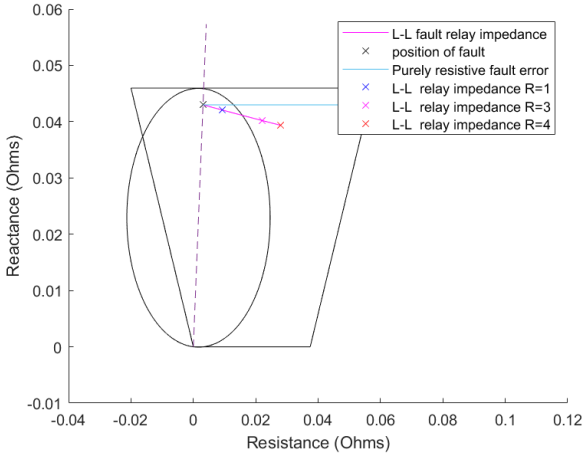

(b) Relay Impedance using purely reactive Z_{thev2} for SCP 1000MVA

Figure 42: Relay impedances for varying line parameters when using negative sequence voltage to estimate fault current angle

Figure 43 shows the results of this. For line to ground faults there is no significant improvement in measurement angle from figure 38b, where we undertook a purely passive approach with no change in angle injection. Since line to ground faults generally suffer from lower over and under-reach the benefits of this method are limited. As a result, mimicking the positive sequence behaviour of a voltage source is not enough to match the fault current phase angle, as our zero-sequence current angle must also be taken into account.
However, for line to line faults the under-reach is improved compared to 30 for the base case 0 degree angle injection with no correction applied. It is however worse than figure 39a and figure 41a. This is largely because this method of angle estimation cannot take into account variation of current angle with converter angle. However, if an approximation of the Z_{thev2} angle cannot be made, and the over-reach from 39a must be avoided, then this technique provides a simpler alternative where only pre-fault terminal voltages and during fault relay voltages need to be known. An additional advantage is that memory polarized mhos, such as the offset mho shown in figure 8, can now be utilised to expand the circular mho reach. This is because the current angle is mimicking that of a synchronous

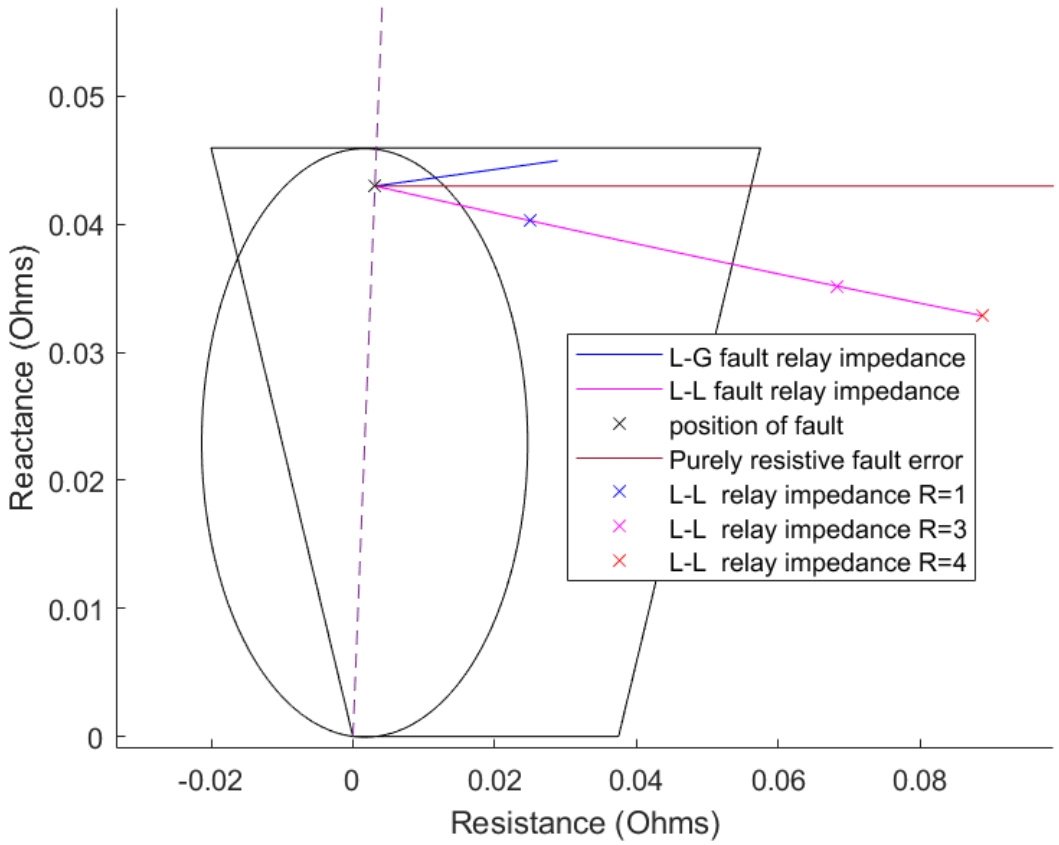

Figure 43: Measured relay impedance using synchronous generator imitation for fault current with increasing fault resistance from 0 to 4Ω

generator so the pre-fault relay voltage acts to further expand the mho size.

13.5 General disadvantages of resistive relay measurement errors

It has been shown how angle estimation techniques depend on the network conditions such as grid short circuit level. This is because estimating how the fault current angle, hence its equivalent Thevenin voltage angle, changes with positive sequence current is important in understanding the optimal technique to use. If the fault current angle change is more than 4°, then injecting initially at zero degree current and over-estimating Thevenin impedance phase angles can result in reduced reach errors without the knowledge of during-fault network parameters. If the fault current remains relatively constant with converter current angle, then obtaining accurate fault current angle estimations becomes more important. However, the biggest disadvantage with current angle methods is that the error magnitude is not improved, with only the over and under-reaching targeted. This means that classical mhos, which cannot change their resistive reach, are still unable to detect many faults particularly for line to line faults where the error magnitude is much larger. While quadrilateral mhos are more adaptive and can detect a wider range of resistive faults they too are limited by load encroachment[3]. This is when the pre-fault relay impedance measurement falls within the quadrilateral mho. This poses increased limitations on quadrilateral mho reach especially for heavily loaded lines.
The majority of the angle estimations required during-fault relay measurements to be taken in order to find a current angle that matches the fault current angle. This introduces additional delays in relay responses lasting at least one additional cycle. If sufficiently fast acting power converters are unavailable then angle injection may be unsuitable if fault clearance must occur within a very limited number of cycles.

14 Investigation of solutions: Harmonic frequency injection

In this section we will investigate the improvement in relay impedance measurement performance when we temporarily inject current at higher order harmonics, i.e at frequencies n times our base 60 Hz frequency, and use this current to measure relay impedance and determine the fault location [11][12].

14.1 Motivation

When injecting at a higher order harmonic frequency, we use superposition of frequency components to analyse the circuit. This means 60 Hz voltage sources are considered short-circuited at the injected harmonic frequency. We obtain the sequence diagrams in figure 45 for a line to ground fault and 46 for a line to line fault. We now have a current source feeding two impedances, Z_G and the equivalent negative and zero sequence network impedances in series with the fault resistance, in parallel.
The key benefits of this method are that at 120 Hz the grid behaves as a short circuit, since we assume it to be purely 60 Hz. This means the grid is now purely passive and does not supply real power to the network and so our positive sequence grid current flows in the opposite direction, opposing the fault current. The reactive impedances are also higher since they equal $j\omega L$ and are proportional to frequency. This means our sequence Thevenin equivalent impedances are also larger. As a result of these changes, the fault current and grid side in-feed current magnitude are now lower as they now see larger impedances to the fault. Improved accuracy of relay measurements to fault locations means traditional and cheaper circular mho technology can still be used for fault detection despite current limited converter interfacing. This simplifies distance protection as older angle based measurement relays do not need major upgrading and thus our cost-effectiveness can be improved.

14.2 Injecting current at 120 Hz to measure relay impedance

For the following simulations we assume that rated current from the converter flows entirely at 120 Hz frequency, switching from 60 Hz in order to detect a fault.

Figure 44, where we show relay impedance measurements for both fault types as the fault resistance increases from 0-10Ω demonstrates the benefits of injecting a higher second order harmonic frequency for relay impedance measurement. We see significantly reduced deviation from the fault position compared to both figure 23 for a synchronous generator and figure 30 for a 60 Hz power converter. Here the mho is exceeded at 8Ω fault resistance for line to ground faults, compared to 1.97Ω for synchronous generators and 1.48Ω for 60 Hz power inverters.
The over-reach happening at larger fault resistances is because the equivalent impedance the relay sees increases in angle as fault resistance increases. If two R-L impedances are in parallel and one becomes increasingly more resistive than the other then the equivalent impedance falls closer to the less resistive R-L impedance, which has a higher current angle. Line to line faults now produce relay impedance measurements much closer to the fault location, performing better than line to ground faults by showing a lower over-reach at the same fault resistances. Figures 45 and 46 show that the power converter is the only active circuit element. Since this is now feeding a passive impedance network, relay measurements do not change with injected current angle and only depend on the load network. This is why line to ground and line to line faults show similar over-reaching as fault resistance increases. The total current flowing through $Z_G + (1-m)Z_{L1}$ in the positive sequence network and the equivalent impedances of the other sequence components must now be equal to the converter current. This means the presence of the zero-sequence network only serves to add an additional current term to the total in-feed grid current. Since the impedance on the grid side is lower than that on the generator side, the zero sequence current adds more to the grid current than the relay current. We see in figure 46 that for a line to line fault the current flowing through $(1-m)Z_{L1} + Z_G$ in the positive

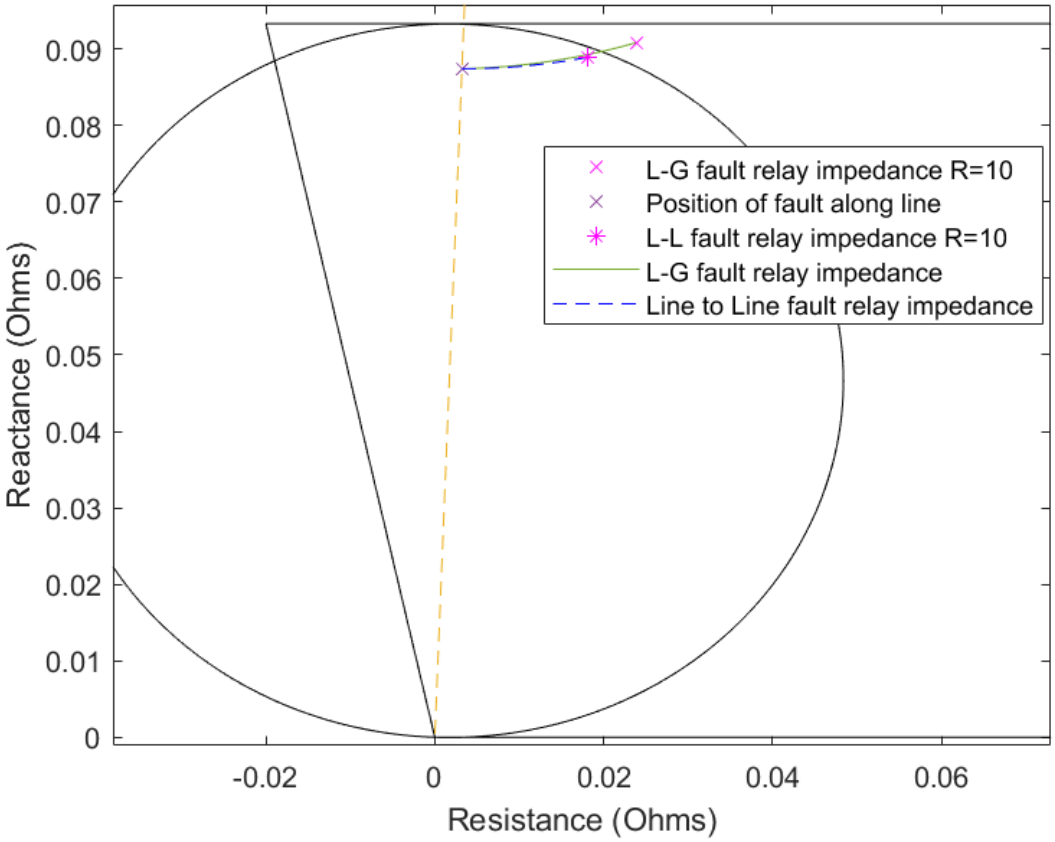

Figure 44: Measured relay impedance for 120 Hz injected current for increasing fault resistance from 0 to 10Ω

sequence network and the equivalent impedance of the negative sequence network must similarly equal the converter current. However, we do not have a zero-sequence current term adding to the total grid in-feed current resulting in a smaller $\frac{I_{grid}}{I_{relay}}$ ratio.

Figure 47 shows the performance when changing our grid short circuit power level. At a fault resistance of 2Ω there is significantly lower error compared to both figure 33 for our 60 Hz converter and 27 for our synchronous generator. The line to line fault relay impedance has especially improved showing reduced error and over-reach. There is however a worsening over-reach and increased error as short circuit power increases. A lowering grid impedance increases the influence of our fault resistance which results in the network impedance angle and magnitude error increasing more for the same fault impedances. While the grid is not supplying real power at 120 Hz, as its grid impedance lowers the proportion of fault current flows increasingly through the grid side of the fault and less through the relay side for line to ground faults in the zero-sequence network. Thus this adds a larger additional zero-sequence term to the total grid in-feed current increasing our $\frac{I_{grid}}{I_{relay}}$ error ratio. Unlike with a converter and synchronous generator however, this over-reach cannot be corrected through angle injection, since our converter is now feeding a passive network. The angle difference between the grid and relay currents is now purely dependent on the impedance of the grid and the resultant network impedances. For line to line faults, the lack of zero sequence network means our error terms are improved as our $\frac{I_{grid}}{I_{relay}}$ ratio is lower.

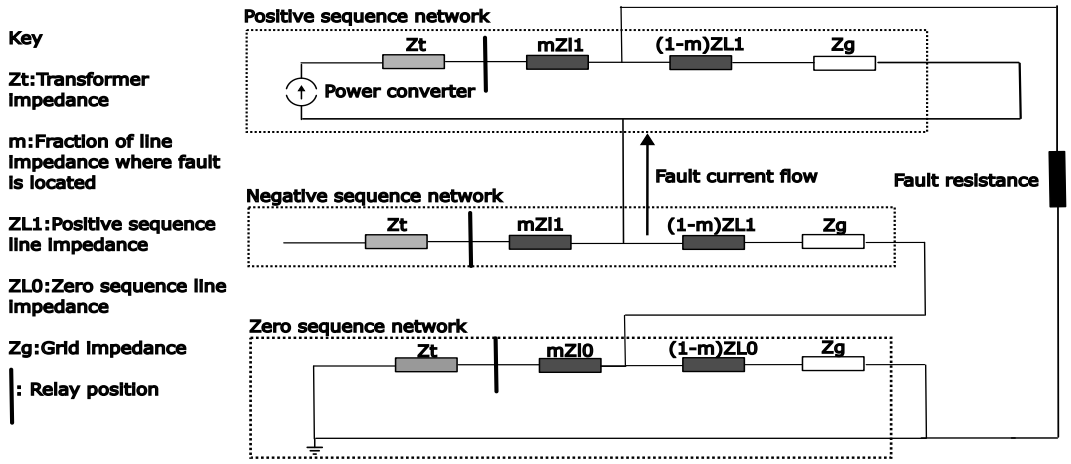

Figure 45: Sequence diagram for a line to ground fault at 120 Hz injected harmonic current

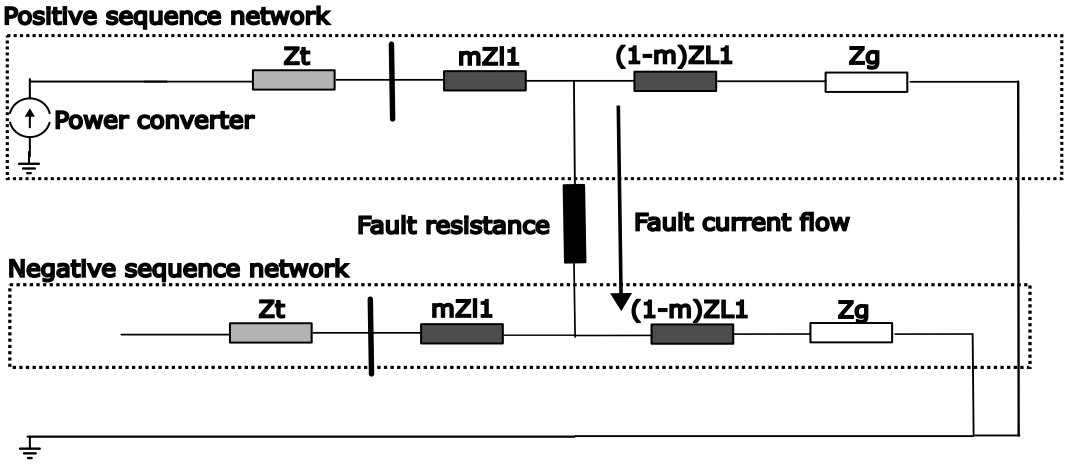

Figure 46: Sequence diagram for a line to line fault at 120 Hz injected harmonic current

Figure 48a demonstrates the relay impedance performance for different line lengths, where the black x represents the relay impedance at 2Ω fault resistance. Again compared to figure 34 for our 60 Hz power converter and 28 for our synchronous generator, there is a significantly reduced error as at 2Ω fault resistance the relay impedance falls within the circular mho for almost all line distances, being borderline at 10km. This is again especially useful for line to line faults, where our 60 Hz power converter saw significant over and under-reaching as well as the error being so large as to fall completely outside the circular and quadrilateral mhos, despite the fault position being within the mho.

Finally, figure 48b demonstrates an improved performance for varying fault positions, with less variation in accuracy as fault position changes. We see at 95% line length no under-reaching occurs and at 2Ω fault resistance the error magnitudes are much lower and more resistive compared to 35 for our 60 Hz converter and 29 for our synchronous generator for both fault types. Once again, line to line fault relay impedance measurements are especially improved due to the absence of the zero-sequence network, with measurements for all fault positions within the reach falling within the classical and the quadrilateral mhos for up to 10Ω fault resistance. We note that at a fault resistance of 10Ω, the difference in line to line and line to ground fault relay impedance becomes worse as the fault moves closer to the grid. This confirms the analysis of the zero sequence network worsening our relay measurement.

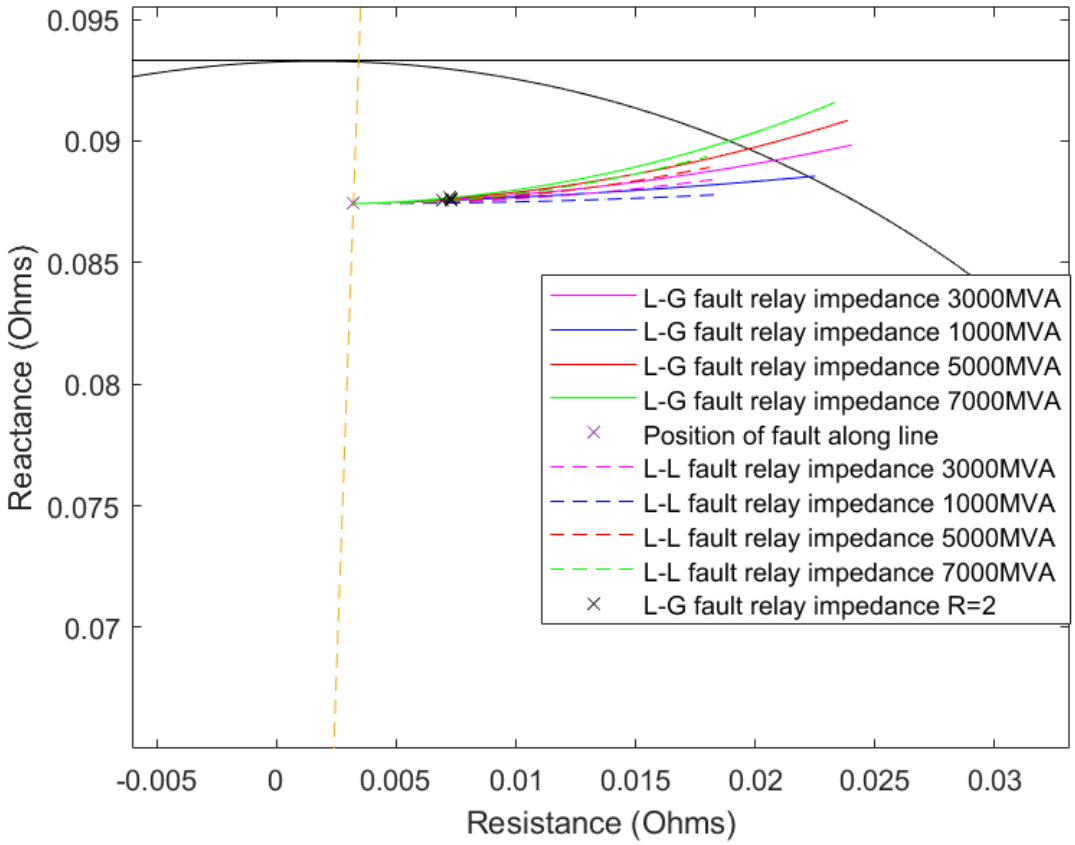

Figure 47: Measured relay impedance for 120 Hz injected current at increasing grid short circuit power for increasing fault resistance from 0 to 10Ω

14.3 Optimising frequency injection performance

It is expected that our relay measurement performance improve even further if a higher order harmonic is utilised, as this further increases our reactive impedances thus reduces our over-reach and our error as the impact of fault resistance becomes more negligible. We also want to utilise a higher order harmonic to ease the design of our filters that isolate the fault measurement harmonic from our base 60 Hz current. However, this is limited by the voltage rating of our cables.

Using a time domain simulation in Simulink, figure 49 demonstrates for a line to ground fault, a maximum instantaneous voltage of 315KV at a second order harmonic supplying rated current. However, if we inject at a fourth order harmonic, we obtain figure 50, where our peak voltage has now reached 430KV.

To mitigate this, we can inject our harmonic at a lower magnitude current. This presents a more practical harmonic injection since we do not want to radically alter the 60 Hz rated power output of our converter every time a fault is suspected. In theory this does not impact the performance of our relay impedance measurements, since at higher harmonics the converter is the only active circuit element that supplies both the relay and fault current. As a result our $\frac{I_{relay}}{I_{grid}}$ term does not worsen as the converter is supplying a passive network. We also reduce the I^2R power losses when performing a harmonic injection. However, in reality this is limited by relay and filter tolerances and attenuation. Figure 51 demonstrates that if we inject 75% of the 1pu rated converter current at 60 Hz and 25% at 240 Hz, we remain within our voltage rating while utilising a higher fourth order harmonic.

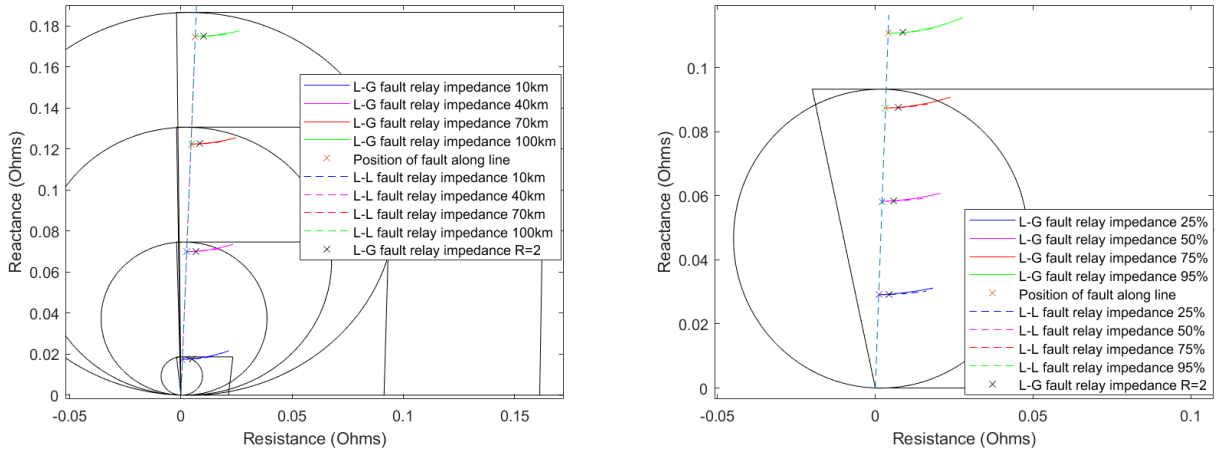

(a) Varying line lengths from 10 to 100km (b) Varying fault position from 25 to 95% line length

Figure 48: Measured relay impedance for 120hz injected current for increasing fault resistance from 0 to 10Ω

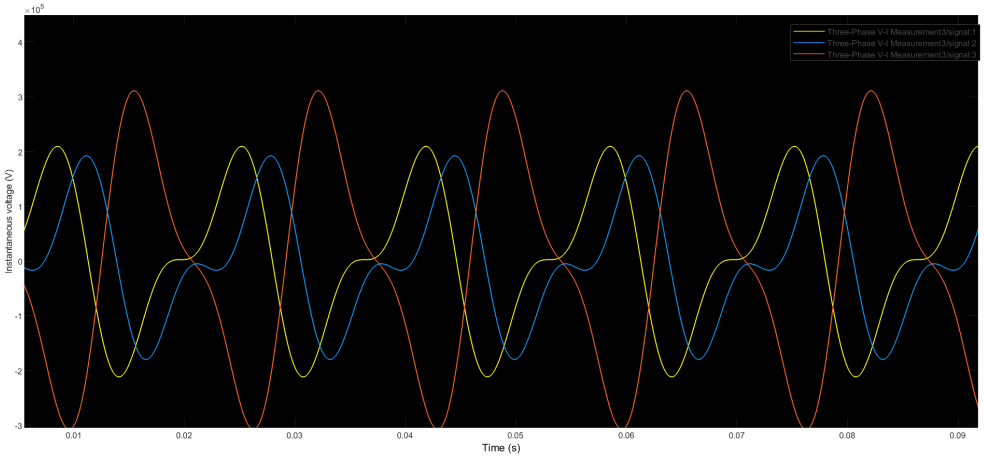

Figure 49: Voltage at converter terminal when injecting current at 120 Hz

Figure 52 shows the relay measurements at 240 Hz for fault resistances varying from 0-10Ω. Here both the relay impedance measurements for line to ground and line to line faults lie within the circular mho. We also see a reduced over-reach and thus an overall significantly improved performance.

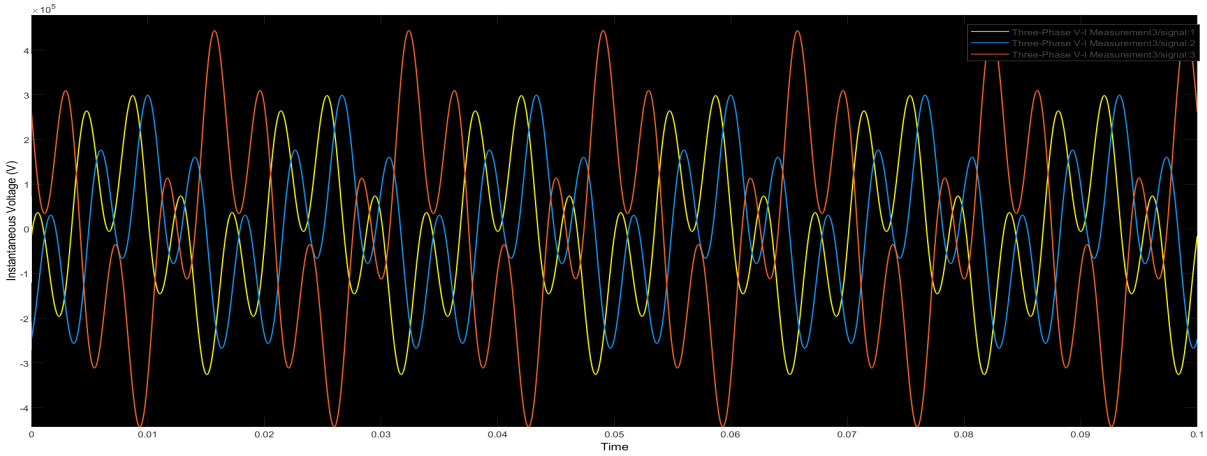

Figure 50: Voltage at converter terminal when injecting current at 240 Hz

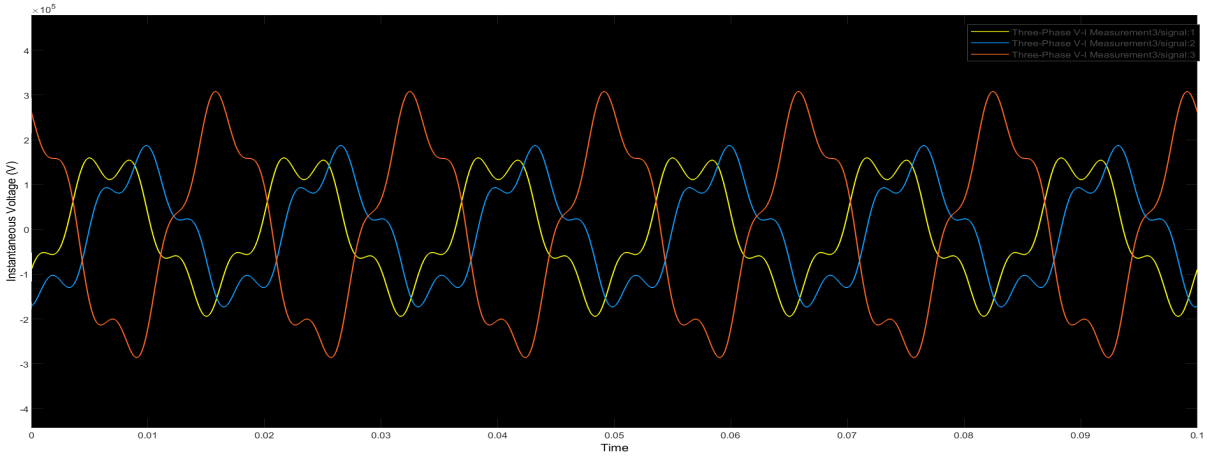

Figure 51: Voltage at converter terminal when injecting 25% rated current at 240 Hz and 75% at 60 Hz

14.4 Verification of harmonic relay impedances

Similar to section 9 we use Simulink to verify our sequence model when injecting at higher order harmonics.

Figure 53a shows us our relay impedance values given by the script (indicated along the Green line) and our Simulink values which do not lie on our green curve. We see our error is larger when compared to figure 21a for a 60 Hz converter. This is because of the higher order effects of our distributed parameter. This includes resonance, where the distributed parameters attenuate the input voltage through a frequency dependent gain factor that increases with frequency until a resonant frequency is reached. However, the shape of our curve, i.e how relay impedance changes with fault resistance, is similar between the script and the Simulink model. Thus our script has captured the behaviour of the higher harmonic circuit.
We see figure 53b showing similar agreement for line to line faults. The error is largely reactive suggesting frequency dependent errors.

To further show the worsening of our discrepancy between script and Simulink with frequency, we show our script and Simulink plots when we inject at 240 Hz at 25% per unit current magnitude.

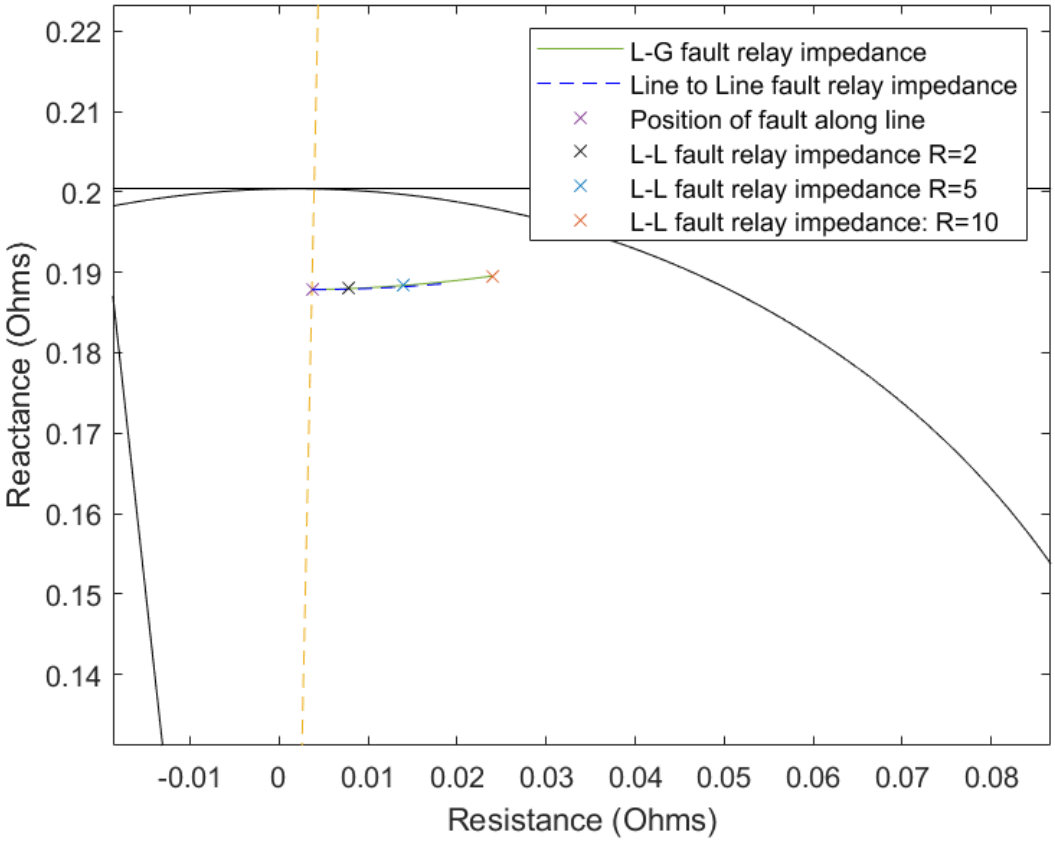

Figure 52: Measured relay impedance for current injected at 240 Hz for increasing fault resistance from 0 to 10Ω

Figure 54 demonstrates the worsening difference as resonant gain becomes increasingly dominant at higher frequencies. This however largely manifests as a constant error in the reactance term and the overall relationship between relay impedance and fault resistance remains captured by the script, since we are using superposition to analyse isolated frequencies that we assume constant for the duration of the fault analysis.

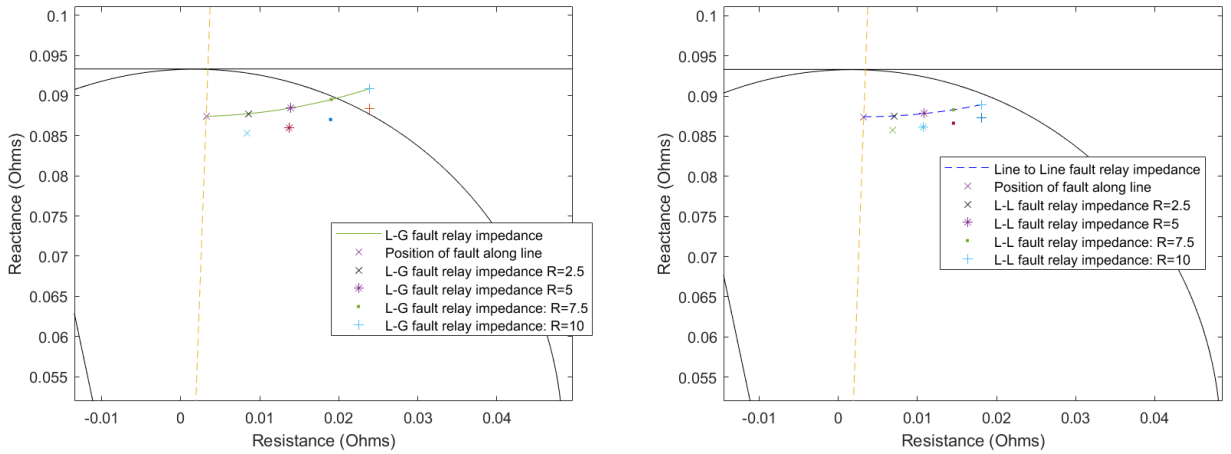

(a) Line to ground fault (b) Line to line fault

Figure 53: Verification of Matlab script with Simulink for 120hz current injection with fault resistance increasing from 0 to 10Ω

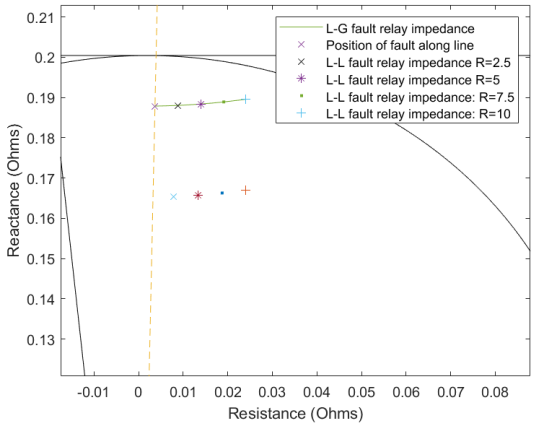

Figure 54: Verification of Matlab script and Simulink when injecting current at 240 Hz for a line to ground fault with increasing fault resistance from 0 to 10Ω

14.5 Limitations

While injecting harmonics at higher frequencies was shown to provide an improved performance, our modelling has not taken into account higher order transmission line effects such as resonance which become more prominent as the frequency increases. In a more realistic grid interfacing model, the converter and transmission line form an electronic resonance circuit, the effects of which would alter the accuracy of our sequence analysis which assumes a linear model.

We have also neglected the impact of injecting higher order harmonics into a large scale electricity grid in terms of adhering to grid codes and ensuring power factor and voltage specifications are met. If only one converter is injecting higher harmonics into the grid we can neglect this. However this technique faces challenges in scalability. If multiple power converters in a grid utilise frequency injection for fault identification they must all inject at unique frequencies sufficiently spaced apart from each other. This would lead to potential resonance in the grid network and harmonic distortion of our 60 Hz outputs. Most grids are not designed for such large scale multi-frequency injection.

We have also made simplified assumptions towards the design of the relays, assuming ideal bandpass

filters that can isolate the harmonic and mho reaches that accurately map the line impedance. In reality determining line impedances at higher order harmonics may be challenging since the line forms a complex distributed network of resistances, capacitances and inductances. Filter design also introduces additional cost and complexity and so while the fundamental technology does not change, relays would still require modifications, thus incurring additional cost and complexity.

15 Final conclusions

This thesis aimed to demonstrate the problems that occur in distance protection with increasing use of current limited converter interfacing. Simulation results and sequence analysis in the above sections has shown the worse performance of power converters compared to a typical spinning synchronous generator for a range of different varying parameters, highlighting the fault detection challenges particularly associated with converter interfaced line to line faults and the lack of zero sequence current.

The thesis also set out to investigate potential solutions to the worsening performance of power converters. The ideal aim was to find a solution such that traditional distance protection technologies would not require replacing with more complex relay schemes that require extensive use of microprocessors or communication infrastructure. To this end harmonic current injection and current angle injection methods were investigated. While harmonic injection was shown to give relay impedances that were closer to the fault location both in terms of error magnitude and reaching, both solutions presented pros and cons that limit their applicabilities.

Harmonic frequency injection was shown to pose serious challenges in their large scale use due to problems of resonance with transmission lines, as well as large scale injection of multi-frequency harmonics potentially causing major disturbances to grid operation. Current angle injection successfully managed to reduce excessive reaching, although this was heavily dependent on fault current characteristics. As more information about the network was known, a more optimal angle injection technique could be used, thus over-reach was better reduced. Angle injection is much better suited to power converters, since these already utilise control algorithms that modify phase angle for stability purposes as well as other ancillary functions. It also has significantly improved scalability, since there are fewer consequences for the grid when injecting current at different phase angles compared to different frequencies. Current phase angle variation is also simpler, more power efficient and cheaper to implement compared to the use of inverters for frequency up-scaling.

Despite this however, angle injection was unable to correct magnitude differences between relay measurement and fault position in all cases, since it could only correct for over and under-reaching. By managing to isolate out the grid frequency, harmonic injection was shown to provide overall better performance in terms of closeness to fault position while also minimizing over and under-reaching. Harmonic injection also did not require any during-fault relay measurements to operate and so could be deployed much faster whenever a fault is suspected. In most instances angle injection required the monitoring of during-fault relay measurements in order to find an angle to inject at, thus introducing further delays to relay operation.
In terms of simplicity of relay design, we found that both solutions brought their own complexities. Since angle injection does not correct for error magnitudes we found many instances, particularly for line to line faults, where a traditional mho could not detect a fault that lay within the mho reach due to the relay impedance falling outside the mho at all injected current angles. This meant that the use of more adaptable quadrilateral mhos, with detection criteria that are more complex, was needed in order to have an extended resistive reach. The reduction of over-reaching however helped to simplify the quadrilateral mho design as less adaptability was now needed. While traditional mho relays

were shown to work well with harmonic frequency injection, additional modifications were needed, including the use of filters as well as changes to the relay reach to reflect the different line impedances found at different frequencies. If injecting a frequency into a transmission line that is not designed to operate above 60 Hz, determining an accurate impedance might become difficult due to additional line resonance and distortion.

As a result, both solutions do not fully meet the ideal objective. However, in circumstances where harmonic injection can occur in isolation such as in a micro-grid, without other frequencies interfering, harmonic injection was shown to be a powerful solution to grid in-feed relay impedance errors. If however, a more widely applicable solution is needed, where the effect on rated converter output and grid must be minimal, current angle injection methods were shown to significantly improve under and over-reaching and ease the burden on quadrilateral mhos to adaptively detect relay impedances.

16 Recommendations for future work

So far the grid has only been modelled as an ideal voltage source. This does not allow us to see how the relay would be influenced by other generators in the grid, particularly if they are injecting at different current angles or have adopted other distance protection techniques. Similarly, it cannot be investigated how the relay would perform when it sees faults occurring at different points within a grid network. As a result, it is recommended that the test circuit be expanded to include a more complex grid representation. The impact of different grid configurations with different fault current levels can then be further investigated.
Since Simulink allows the modelling of higher order transmission line and grid properties, future work would involve further time domain simulations of faults as well as the use of more detailed converter and synchronous generator models. This allows for the further study of how the presented solutions behave under fault transients and what effect resonance and harmonic distortion have on distance protection operation.

17 Bibliography

References

[1] B. Kasztenny and D. Finney, "Fundamentals of distance protection," *2008 61st Annual Conference for Protective Relay Engineers : Texas A M University*, 2008.

[2] D. D. Fentie, "Understanding the dynamic mho distance characteristic," *2016 69th Annual Conference for Protective Relay Engineers (CPRE)*, 2016.

[3] E. O. Schweitzer and B. Kasztenny, "Distance protection: Why have we started with a circle, does it matter, and what else is out there?" *2018 71st Annual Conference for Protective Relay Engineers (CPRE)*, 2018.

[4] U. J. Patel, N. G. Chothani, and P. J. Bhatt, "Adaptive quadrilateral distance relaying scheme for fault impedance compensation," *Electrical, Control and Communication Engineering*, vol. 14, no. 1, pp. 58–70, 2018.

[5] GOV.UK, "Plans unveiled to decarbonise uk power system by 2035," https://www.gov.uk/government/news/plans-unveiled-to-decarbonise-uk-power-system-by-2035, 2022.

[6] "Provision of short circuit level data," National grid, 2022.

[7] V. Telukunta, J. Pradhan, A. Agrawal, M. Singh, and S. G. Srivani, "Protection challenges under bulk penetration of renewable energy resources in power systems: A review," *CSEE Journal of Power and Energy Systems*, vol. 3, no. 4, pp. 365–379, 2017.

[8] B. J. Cory, N. Jenkins, J. Ekanayake, G. Strbac, and B. M. Weedy, *Electric power systems*. Wiley, 2013.

[9] A. Hooshyar, M. A. Azzouz, and E. F. El-Saadany, "Distance protection of lines emanating from full-scale converter-interfaced renewable energy power plants—part i: Problem statement," *IEEE Transactions on Power Delivery*, vol. 30, no. 4, pp. 1770–1780, 2015.

[10] ——, "Distance protection of lines emanating from full-scale converter-interfaced renewable energy power plants—part ii: Solution description and evaluation," *IEEE Transactions on Power Delivery*, vol. 30, no. 4, pp. 1781–1791, 2015.

[11] K. A. Saleh and M. A. Allam, "Synthetic harmonic distance relaying for inverter-based islanded microgrids," *IEEE Open Access Journal of Power and Energy*, vol. 8, pp. 258–267, 2021.

[12] Z. Yang, Q. Zhang, W. Liao, C. L. Bak, and Z. Chen, "Harmonic injection based distance protection for line with converter-interfaced sources," *IEEE Transactions on Industrial Electronics*, pp. 1–1, 2022.

[13] Z. Yang, K. Jia, Y. Fang, Z. Zhu, B. Yang, and T. Bi, "High-frequency fault component-based distance protection for large renewable power plants," *IEEE Transactions on Power Electronics*, vol. 35, no. 10, pp. 10 352–10 362, 2020.

[14] A. Banaiemoqadam, A. Hooshyar, and M. A. Azzouz, "A control-based solution for distance protection of lines connected to converter-interfaced sources during asymmetrical faults," *IEEE Transactions on Power Delivery*, vol. 35, no. 3, pp. 1455–1466, 2020.

[15] S. Yang, Y. Li, Y. Zhu, W. Xiang, H. Zhang, J. Wen, and T. Green, "An enhanced distance protection scheme benefiting from negative-sequence fault current behaviors of ibrs under asymmetric faults(unpublished)."

[16] U. of Waterloo, "Ele b7 power system engineering: Unbalanced fault analysis," https://ece.uwaterloo.ca/~raelshat/COURSES_dr/eleb7.old/Unbalanced%20Fault.pdf.

[17] "315kv transmission line parameters (power systems toolbox line parameters)," Matlab.

18 Appendix

18.1 Matlab script code for synchronous generators

```
%% SImulink outputs
% v_simu=out.relay_voltage;
% i_simu=out.relay_current_a;
% seq_simu=out.relay_voltage_a;
% true_imp_ll=(v_simu(1)-v_simu(2))/(seq_simu(1)-seq_simu(2))
% true_imp_lg=v_simu(1)/(i_simu(1)+K0*seq_simu(3))
% fault=i_simu-curr_grid
%% Base parameters
Vb = 315e3;
Sb = 300e6;
Zb = Vb^2/Sb;
Ib = Sb/(sqrt(3)*Vb);
freq=60;
w = 2*pi*freq;

%% Fault Params
m=0.75;
Rf = 10;
Fault_Type = 1; % LG = 1, LL = 2;



     % Line Parameters Model

    leng = 50; %km
%     R10 = [0.03441    0.29318];
%     L10 = [0.00148    0.00374];
%     C10 = [7.84869e-09 5.67336e-09];
    R10 = [ 0.02715    0.25155];
    L10 = [0.00100    0.00364];
    C10 = [ 1.16622e-08  6.99588e-09];

    ZL1 = (2.7362 + 1i*37.90822)*leng/100;
    ZL2 = ZL1;
    ZL0 = (25.711 + 1i*138.85)*leng/100;
    ZL = [ZL1; ZL2; ZL0];
    K0 = (ZL0/ZL1-1);



% Grid Impedance

Psc = 5000e6; % Short Circuit level
Zs_abs = Vb^2/Psc;
XR_ratio = 10;
Rs = Zs_abs/sqrt(1+XR_ratio^2);
```

```
47 Ls = (Rs*XR_ratio)/w;
48 Zs = Rs + 1i*Ls*w;
49
50 % Transformer Winding Impedance
51 Lt_pu = 0.04;
52 Zt = 2*(1i*Lt_pu)*Zb; % 2 x because of two windings
53
54 % Mho Setting
55 reach = 0.8;
56
57 % Source Impedance
58
59 Lg=0.05*Zb/(w);
60 Zg=(1i*w*Lg);
61
62
63 %% Theory
64 limit_LG=0;
65 limit_LL=0;
66
67 V2 = 1;
68 Rfault = Rf/Zb;
69 Transformer_imp=Zt/Zb;
70 line_impedance1=ZL1/Zb;
71 line_impedance0=ZL0/Zb;
72 S2=Zs/Zb;
73 S1=Zg/Zb;
74
75
76
77
78 %phase
79
80 for phi=1:361
81 % phi=131;
82 current_injection=1*exp(1i*(phi-1)*pi/180);
83 V1=current_injection*(Transformer_imp + S1+S2 + line_impedance1)+V2;
84
85 %% Magnitude and angle for Simulink
86 % V1_test=1*exp(1i*(271-1)*pi/180)*(Transformer_imp + S1+S2 +
      line_impedance1)+V2;
87 % V1_simu=abs(V1_test);
88 % PhaseA=-30+(angle(V1_test)*180/pi);
89 % PhaseB=210+(angle(V1_test)*180/pi);
90 % PhaseC=90+(angle(V1_test)*180/pi);
91
92 V_th=((V1-V2)/(Transformer_imp + S1+S2 + line_impedance1))*((1-m)*
      line_impedance1+S2)+V2;
93
```

```
94  Z_1_thev=1/(1/(Transformer_imp+S1+m*line_impedance1)+1/(S2+(1-m)*
       line_impedance1));
95  Z_2_thev=Z_1_thev;
96  Z_0_thev=1/(1/(Transformer_imp+m*line_impedance0)+1/(S2+(1-m)*
       line_impedance0));
97
98  %% line to ground fault
99  if Fault_Type==1
100 I_fault=V_th/(Z_1_thev+Z_2_thev+Z_0_thev+3*Rfault);
101
102
103 I_r1=I_fault*(((1-m)*line_impedance1+S2)/(S1+S2+Transformer_imp+
       line_impedance1))+((V1-V2)/(Transformer_imp + S2 +S1+
       line_impedance1));
104 I_r2=I_fault*(((1-m)*line_impedance1+S2)/(S1+S2+Transformer_imp+
       line_impedance1));
105 I_r0=I_fault*(((1-m)*line_impedance0+S2)/(S2+Transformer_imp+
       line_impedance0));
106
107 V_r1=I_r1*(m*line_impedance1) + (V_th-I_fault*(Z_1_thev));
108 V_r2=I_r2*(m*line_impedance1) -I_fault*(Z_2_thev);
109 V_r0= -I_fault*(Z_0_thev)+I_r0*(m*line_impedance0);
110
111
112 I_AR=I_r1+I_r2+I_r0;
113 V_AR=V_r1+V_r2+V_r0;
114
115 Apparent_Impedance1(phi)=V_AR/(I_AR+K0*I_r0);
116
117 %% if statement to allow plotting of multiple outputs
118 % if p==1
119 %     temp1(phi)=Apparent_Impedance1(phi);
120 % elseif p==2
121 %     temp2(phi)=Apparent_Impedance1(phi);
122 % elseif p==3
123 %     temp3(phi)=Apparent_Impedance1(phi);
124 % elseif p==4
125 %     temp4(phi)=Apparent_Impedance1(phi);
126 %
127 % end
128
129 %% Code that allows detection of fault resistance where relay
       impedance falls outside mho
130 % error=(abs(Apparent_Impedance1)-abs(true_imp))*100/(abs(true_imp))
131 % if angle(reach*line_impedance1-Apparent_Impedance1(phi))-angle(
       Apparent_Impedance1(phi))>=(pi/2) && limit_LG==0
132 % limit_LG=Apparent_Impedance1(phi)
133 % limit_Rf=Rfault*Zb
134 % end
```

```
135
136 end
137
138
139 %% line to line fault
140 if Fault_Type==2
141 I_a1=V_th/(Z_1_thev+Z_2_thev+Rfault);
142 I_r1=I_a1*(((1-m)*line_impedance1+S2)/(S1+S2+Transformer_imp+
       line_impedance1))+((V1-V2)/(Transformer_imp + S1+S2 +
       line_impedance1));
143 I_r2=-I_a1*(((1-m)*line_impedance1+S2)/(S1+S2+Transformer_imp+
       line_impedance1));
144
145 I_fault=-i*sqrt(3)*I_a1;
146 I_AR=I_r1+I_r2;
147
148 V_r1=I_r1*m*line_impedance1+I_a1*(Rfault+Z_2_thev);
149
150 V_r2=I_r2*m*line_impedance1+(I_a1*(Rfault+Z_2_thev)-I_a1*Rfault);
151
152 V_AR=V_r1+V_r2;
153
154 Apparent_Impedance2(phi)=(V_r1-V_r2)/(I_r1-I_r2);
155
156 % if p==1
157 %     temp1l(phi)=Apparent_Impedance2(phi);
158 % elseif p==2
159 %     temp2l(phi)=Apparent_Impedance2(phi);
160 % elseif p==3
161 %     temp3l(phi)=Apparent_Impedance2(phi);
162 % elseif p==4
163 %     temp4l(phi)=Apparent_Impedance2(phi);
164 %
165 % end
166 end
167
168 % if angle(reach*line_impedance1-Apparent_Impedance2(phi))-angle(
       Apparent_Impedance2(phi))>=(pi/2) && limit_LL==0
169 % limit_LL=Apparent_Impedance2(phi)
170 % R_limit=Rfault*Zb
171 % end
172 % end
173
174
175 end
176 hold on
177 true=plot(m*line_impedance1,'x','DisplayName','position of fault along
       line impedance','Color','black');
178
```

```
179 %% Plotting classical mho
180 theta=-2*pi:0.00001:2*pi;
181 x=(reach/2)*(abs(line_impedance1))*(exp(1i*(theta))+exp(1i*angle(
        line_impedance1)));
182 % y=(reach/4)*(abs(line_impedance1))*(exp(1i*(theta))+exp(1i*angle(
        line_impedance1)));
183 %% Plotting the apparent impedances where 1 is the line to ground
        impedance and 2 is the line to line impedance
184
185
186 plot(x,'Color','black')
187
188
189 %% Plotting quadrilateral mho
190 plot([0, i*reach*abs(line_impedance1)-0.02,i*reach*abs(line_impedance1
        )+abs(line_impedance1),abs(line_impedance1)-0.02,0],'black');
191
192
193 test=[0,line_impedance1];
194 plot(test,'--')
195
196 imp1=plot(Apparent_Impedance1,'DisplayName','L-G fault relay impedance
        ','Color','blue');
197
198 %% Relay impedance values obtained from SImulink for verification
        purposes
199 %% R=2 l-g
200 % plot(0.0129+0.0426i,'x');
201 % plot(0.0143+0.0435i,'*');
202 % plot(0.0129+0.0446i,'.');
203 % plot(0.0122+0.0436i,'+');
204 %% R=10 l-g
205 % plot(0.0506+0.0428i,'x');
206 % plot(0.0598+0.0446i,'*');
207 % plot(0.0542+0.0536i,'.');
208 % plot(0.0485+0.049i,'+');
209 %% R=2 l-l
210 % plot(0.0127+0.0417i,'x');
211 % plot(0.0155+0.0432i,'*');
212 % plot(0.0127+0.045i,'.');
213 % plot(0.0117+0.0433i,'+');
214
215 %R=10
216 % plot(0.0495+0.0379i,'x');
217 % plot(0.065+0.0415i,'*');
218 % plot(0.0532+0.0544i,'.');
219 % plot(0.0461+0.0468i,'+');
220
```

```
221 %% Code to show relay impedance plots at all injected angles for
    different network parameters
222 % imp2=plot(Apparent_Impedance2,'--','DisplayName','L-L fault relay
    impedance (Script)','Color','blue');
223 % impMV1=plot(temp1,'DisplayName','L-G fault relay impedance:25%','
    Color','blue');
224 % impMV2=plot(temp2,'DisplayName','L-G fault relay impedance:50%','
    Color','magenta');
225 % impMV3=plot(temp3,'DisplayName','L-G fault relay impedance:75%','
    Color','red');
226 % impMV4=plot(temp4,'DisplayName','L-G fault relay impedance:95%','
    Color','green');
227 % %
228 % impMV1l=plot(temp1l,'--','DisplayName','L-L fault relay impedance
    :25%','Color','blue');
229 % impMV2l=plot(temp2l,'--','DisplayName','L-L fault relay impedance
    :50%','Color','magenta');
230 % impMV3l=plot(temp3l,'--','DisplayName','L-L fault relay impedance
    :75%','Color','red');
231 % impMV4l=plot(temp4l,'--','DisplayName','L-L fault relay impedance
    :95%','Color','green');
232 % plot(true_imp,'x');
233
234 %%Code to plot relay impedance values at a specific current angle
235 % imp0g=plot(Apparent_Impedance1(1),'x','DisplayName','phi=0');
236 % imp1g=plot(Apparent_Impedance1(91),'*','DisplayName','phi=90');
237 % imp2g=plot(Apparent_Impedance1(181),'.','DisplayName','phi=180');
238 % imp3g=plot(Apparent_Impedance1(271),'+','DisplayName','phi=270');
239 % plot(imp,'x');
240 % imp0l=plot(Apparent_Impedance2(1),'x','DisplayName','phi=0');
241 % imp1l=plot(Apparent_Impedance2(91),'*','DisplayName','phi=90');
242 % imp2l=plot(Apparent_Impedance2(181),'.','DisplayName','phi=180');
243 % imp3l=plot(Apparent_Impedance2(271),'+','DisplayName','phi=270');
244 % legend([impMV1 impMV2 impMV3 impMV4 true impMV1l impMV2l impMV3l
    impMV4l imp0g imp1g imp2g imp3g])
245
246 %%Code to calculate absolute magnitude differences between SImulink
    and script relay impedances
247
248 %%lg R=2
249 % error1=abs(0.0129+0.0426i-Apparent_Impedance1(1))
250 % error2=abs(0.0143+0.0435i-Apparent_Impedance1(91))
251 % error3=abs(0.0129+0.0446i-Apparent_Impedance1(181))
252 % error4=abs(0.0122+0.0436i-Apparent_Impedance1(271))
253 %%l R=10
254 % error1=abs(0.0506+0.0428i-Apparent_Impedance1(1))
255 % error2=abs(0.0598+0.0446i-Apparent_Impedance1(91))
256 % error3=abs(0.0542+0.0536i-Apparent_Impedance1(181))
257 % error4=abs(0.0485+0.049i-Apparent_Impedance1(271))
```

```
258
259 legend([imp2 imp0l imp1l imp2l imp3l])
260 hold off
```

18.2 Matlab script code for a power converter

```
1  %% SImulink outputs
2  % v_simu=out.relay_voltage
3  % seq_simu=out.relay_voltage_a
4  % i_simu=out.relay_current_a
5  % i_grid=out.current_grid
6  % imp=(v_simu(1)-v_simu(2))/i_simu(1)
7
8
9  %
10 % fl=i_simu-i_grid
11 %% Base parameters
12 Vb = 315e3;
13 Sb = 300e6;
14 Zb = Vb^2/Sb;
15 Ib = Sb/(sqrt(3)*Vb);
16 freq=60;
17 w = 2*pi*freq;
18 %% Fault Params
19 m=0.75;
20 Rf = 1;
21 Fault_Type = 2; % LG = 1, LL = 2;
22
23      % Line Parameters Model
24     leng = 50; %km
25
26     R10 = [ 0.02715     0.25155];
27     L10 = [0.00100     0.00364];
28     C10 = [ 1.16622e-08   6.99588e-09];
29
30     ZL1 = (2.7362 + 1i*37.90822)*leng/100;
31     ZL2 = ZL1;
32     ZL0 = (25.711 + 1i*138.85)*leng/100;
33     ZL = [ZL1; ZL2; ZL0];
34     K0 = (ZL0/ZL1-1);
35
36
37
38
39
40 % Grid Impedance
41 Psc = 5000e6; % Short Circuit level
42 Zs_abs = Vb^2/Psc;
43 XR_ratio = 10;
```

```
Rs = Zs_abs/sqrt(1+XR_ratio^2);
Ls = (Rs*XR_ratio)/w;
Zs = Rs + 1i*Ls*w;

% Transformer Winding Impedance
Rt_pu = 0;
Lt_pu = 0.04;
Zt = 2*(1i*Lt_pu)*Zb;

% Mho Setting
reach = 0.8;


%phase

limit_LG=0;
limit_LL=0;
V2=1;
% for z=1:361
% q=-83.4;
%% Phase terms for simulink model
q=-79.3;
PhaseA=-30 + q-1;
PhaseB=210 + q-1;
PhaseC=90 + q-1;

%% Theory
for z=1:361
curr = 1*exp(1i*(z-1)*pi/180);
% This term is used in angle injection to distinguish injected current
    before a resistive current angle is found: curr_th=1;
% curr_th;
Rfault = Rf/Zb;
Transformer_imp=Zt/Zb;
line_impedance1=ZL1/Zb;
line_impedance0=ZL0/Zb;
S2=Zs/Zb;


if Fault_Type == 1
%Line to ground fault
V_th=(curr*((1-m)*line_impedance1+S2))+V2;
Z_1_thev=(S2+(1-m)*line_impedance1);
Z_0_thev=(1/(1/(S2+(1-m)*line_impedance0)+1/(Transformer_imp+m*
   line_impedance0)));
Z_2_thev=Z_1_thev;

I_a1=V_th/(Z_1_thev+Z_2_thev+Z_0_thev+3*Rfault);
I_fault=3*I_a1;
```

```
91  %% The sets of current angles we inject when using zero sequence
       currents to make relay errors resistive
92  % curr(1)=1*exp(1i*(-41.9)*pi/180);
93  % curr(2)=1*exp(1i*(-40.4025)*pi/180);
94  % curr(3)=1*exp(1i*(-38.96)*pi/180);
95  % curr(4)=1*exp(1i*(-37.57)*pi/180);
96  % curr(5)=1*exp(1i*(-36.23)*pi/180);
97  % curr(6)=1*exp(1i*(-34.95)*pi/180);
98  % curr(7)=1*exp(1i*(-33.71)*pi/180);
99  % curr(8)=1*exp(1i*(-32.521)*pi/180);
100 % curr(9)=1*exp(1i*(-31.386)*pi/180);
101
102 I_r0=I_a1*(S2+(1-m)*line_impedance0)/(Transformer_imp+S2+
       line_impedance0);
103 %% Our relay voltage assuming a current angle of 0
104 % V_r1_test=(1*m*line_impedance1)+(V_th-I_a1*Z_1_thev);
105 V_r2=-I_a1*Z_2_thev;
106 V_r0=I_r0*m*line_impedance0-I_a1*Z_0_thev;
107
108 %% Code for angle injections mimicking synchronous generstor operation
109 % V_synch=1*(Transformer_imp +S2+line_impedance1)+V2-(V_r1_test);
110
111 % curr=1*exp(1i*((angle(V_synch)-pi/2)));
112
113 I_r1=curr;
114 I_r2=0;
115
116 I_AR=I_r1+I_r2+I_r0;
117
118 V_r1=(I_r1*m*line_impedance1)+(V_th-I_a1*Z_1_thev);
119
120 V_AR=V_r1+V_r2+V_r0;
121
122 Apparent_Impedance1(z)=V_AR/(I_AR+K0*I_r0);
123 %% Code for Simulink relay impedance
124 % true_imp=v_simu(1)/(i_simu(1)+K0*seq_simu(3));
125
126 %% Code that allows detection of fault resistance where relay
       impedance falls outside mho
127 % if angle(reach*line_impedance1-Apparent_Impedance1(z))-angle(
       Apparent_Impedance1(z))>=(pi/2) && limit_LG==0
128 % limit_LG=Apparent_Impedance1(z)
129 % limit_Rf=Rfault*Zb
130 % end
131
132 %% If statements to allow plotting of multiple relay impedances for
       varying line parameters
133 % if p==1
134 %     temp1(z)=Apparent_Impedance1(z);
```

```
% elseif p==2
%     temp2(z)=Apparent_Impedance1(z);
% elseif p==3
%     temp3(z)=Apparent_Impedance1(z);
% elseif p==4
%     temp4(z)=Apparent_Impedance1(z);
%
% end


end
%% Line to line
if Fault_Type==2
Z_1_thev=(S2+(1-m)*line_impedance1);
Z_2_thev=Z_1_thev;

V_th=(curr*((1-m)*line_impedance1+S2))+V2;

I_a1=V_th/(Z_1_thev+Z_2_thev+Rfault);

I_fault=-i*sqrt(3)*I_a1;



V_r2=(I_a1*(Rfault+Z_2_thev)*(Z_2_thev/(Z_2_thev+Rfault)));

%% Angle injection using sequence relay voltage to estimate fault
   current angle
% curr = 1*exp(1i*(angle(V_r2)-angle(line_impedance1)));

%% Angle injection using synchronous generator mimicry
% V_r1_test=(1*m*line_impedance1+(V_th-(I_a1*Z_1_thev)));
% V_synch=1*(line_impedance1+Transformer_imp+S2)+V2-(V_r1_test);
% curr=1*exp(1i*((angle(V_synch))-pi/2));

V_r1=(curr*m*line_impedance1+(V_th-(I_a1*Z_1_thev)));
V_AR=V_r1+V_r2;

I_AR=curr;

Apparent_Impedance2(z)=(V_r1-V_r2)/curr;

% if angle(reach*line_impedance1-Apparent_Impedance2(z))-angle(
   Apparent_Impedance2(z))>=(pi/2) && limit_LL==0
% limit_LL=Apparent_Impedance2(z)
% R_limit=Rfault*Zb
% end

% if p==1
```

```
%     temp1l(z)=Apparent_Impedance2(z);
% elseif p==2
%     temp2l(z)=Apparent_Impedance2(z);
% elseif p==3
%     temp3l(z)=Apparent_Impedance2(z);
% elseif p==4
%     temp4l(z)=Apparent_Impedance2(z);
%
% end

end









end
% end
% error=imp-test_imp;
% percent_error=abs(error)*100/abs(imp)
hold on
%% Plotting true position of fault along line
true=plot(m*line_impedance1,'x','DisplayName','position of fault','Color','black');

%% Plotting the mho
theta=-2*pi:0.00001:2*pi;
x=(reach/2)*(abs(line_impedance1))*(exp(1i*(theta))+exp(1i*angle(line_impedance1)));
%% Plotting the apparent impedances where 1 is the line to ground impedance and 2 is the line to line impedance

plot(x,'Color','black')

plot([0, 1i*reach*abs(line_impedance1)-0.02,1i*reach*abs(line_impedance1)+abs(line_impedance1),abs(line_impedance1)-0.02,0],'Color','black');
% end
test=[0,line_impedance1];
plot(test,'--');
imp1=plot(Apparent_Impedance1,'DisplayName','L-G fault relay impedance (Script)','Color','blue');
%% Relay impedances obtained from Simulink
% plot(0.0174+0.0417i,'x');
% plot(0.0219+0.0444i,'*');
% plot(0.0172+0.047i,'.');
% plot(0.0158+0.0442i,'+');
%R=10;
```

```
225
226 % plot(0.0716+0.0391i,'x');
227 % plot(0.0984+0.0446i,'*');
228 % plot(0.0772+0.0682i,'.');
229 % plot(0.0659+0.0538i,'+');
230
231 %% Line to line
232 % plot(0.0115+0.0027i,'x');
233 % plot(-0.0341+0.0375i,'*');
234 % plot(0.0007+0.0831i,'.');
235 % plot(0.0463+0.0483i,'+');
236
237 %R=0.5
238 % plot(0.0049+0.0327i,'x');
239 % plot(-0.0063+0.0417i,'*');
240 % plot(0.0028+0.0529i,'.');
241 % plot(0.014+0.0438i,'+');
242
243
244 %% PLotting relay impedance values for current angles ranging from 0
       to 360
245 % imp2=plot(Apparent_Impedance2,'DisplayName','L-L fault relay
       impedance (Script)','Color','magenta');
246
247
248
249 % % % % plot(imp,'x');
250 % Res=plot([m*line_impedance1,m*line_impedance1+0.1],'DisplayName','
       Purely resistive fault error')
251 % impMV1=plot(Apparent_Impedance1(1),'*','DisplayName','L-G  relay
       impedance R=1','Color','blue');
252 %
253 % impMV2=plot(Apparent_Impedance1(5),'*','DisplayName','L-G  relay
       impedance R=4','Color','magenta');
254 % impMV3=plot(Apparent_Impedance1(9),'*','DisplayName','L-G  relay
       impedance R=7','Color','Red');
255 % impMV4=plot(temp4,'DisplayName','L-G relay impedance R=0.7','Color
       ','green');
256
257 % impMV1l=plot(Apparent_Impedance2,'--','DisplayName','L-L  relay
       impedance X-R ratio:5','Color','blue');
258 % impMV2l=plot(temp2l,'--','DisplayName','L-L  relay impedance X-R
       ratio:10','Color','magenta');
259 % impMV3l=plot(temp3l,'--','DisplayName','L-L  relay impedance X-R
       ratio:15','Color','red');
260 % impMV4l=plot(temp4l,'--','DisplayName','Line to Line fault relay
       impedance:R=0.7','Color','green');
261
262 %
```

```
%% Plots showing relay impedance values at specific current angles
% imp0g=plot(Apparent_Impedance1(1),'x','DisplayName','phi=0')
% imp1g=plot(Apparent_Impedance1(91),'*','DisplayName','phi=90')
% imp2g=plot(Apparent_Impedance1(181),'.','DisplayName','phi=180')
% imp3g=plot(Apparent_Impedance1(271),'+','DisplayName','phi=270')
%
% imp0l=plot(Apparent_Impedance2(1),'x','DisplayName','phi=0');
% imp1l=plot(Apparent_Impedance2(91),'*','DisplayName','phi=90') ;
% imp2l=plot(Apparent_Impedance2(181),'.','DisplayName','phi=180') ;
% imp3l=plot(Apparent_Impedance2(271),'+','DisplayName','phi=270');
% legend([true imp0g imp1g imp2g imp3g imp3l impMV1 impMV2 impMV3
   impMV1l impMV2l impMV3l ]);
% R=2
% error1=abs(0.0174+0.0417i-Apparent_Impedance1(1))
% error2=abs(0.0219+0.0444i-Apparent_Impedance1(91))
% error3=abs(0.0172+0.047i-Apparent_Impedance1(181))
% error4=abs(0.0158+0.0442i-Apparent_Impedance1(271))
%R=10
%% Absolute magnitude differences between Simulink and Matlab scripts
% error1=abs(0.0716+0.0391i-Apparent_Impedance1(1))
% error2=abs(0.0984+0.0446i-Apparent_Impedance1(91))
% error3=abs(0.0772+0.0682i-Apparent_Impedance1(181))
% error4=abs(0.0659+0.0538i-Apparent_Impedance1(271))

legend([imp2 imp0l imp1l imp2l imp3l])
hold off
```

18.3 Matlab script code for a power converter injecting current at higher order harmonics

```
%% SImulink outputs
% v_simu=out.relay_voltage;
% seq_simu=out.relay_voltage_a;
% i_simu=out.relay_current_a;
% i_grid=out.grid_current;
% imp=(v_simu(1)-v_simu(2))/i_simu(1)
%
% f_curr=i_simu-i_grid;

%% Base parameters
Vb = 315e3;
Sb = 300e6;
Zb = Vb^2/Sb;
Ib = Sb/(sqrt(3)*Vb);
n=4;
freq=n*60;
w = 2*pi*freq;
%% Fault Params
% pos=[0.25  0.5  0.75  0.95]
```

```
%   for p=1:4
m=0.75;
Rf = linspace(0,10,100);
Fault_Type = 1; % LG = 1, LL = 2;


     % Line Parameters Model
    leng = 50; %km
    R10 = [ 0.02715    0.25155];
    L10 = [0.00100    0.00364];
    C10 = [ 1.16622e-08  6.99588e-09];
%     ZL1 = (2.8323 + 1i*77.1077)*leng/100;
%     ZL2 = ZL1;
%     ZL0 = (27.651+288.38i)*leng/100;
ZL1=(3.251+165.7i)*leng/100;
ZL2 = ZL1;
ZL0=(38.95+686.43i)*leng/100;
    ZL = [ZL1; ZL2; ZL0];
    K0 = (ZL0/ZL1-1);


% Grid Impedance
Psc = 5000e6; % Short Circuit level
ZG_abs = Vb^2/Psc;
XR_ratio = 10;
Rs = ZG_abs/sqrt(1+XR_ratio^2);
Ls = (Rs*XR_ratio)/(2*pi*60);
Zs = Rs + 1i*Ls*w;

% Transformer Winding Impedance
Rt_pu = 0;
Lt_pu = 0.04;

Lt=0.04*Zb/(2*pi*60);
Zt = 2*(Rt_pu + 1i*w*Lt); % 2 x because of two windings

% Mho Setting
reach = 0.8;


%phase
limit_LG=0;
limit_LL=0;
V2=1;

z=1;
PhaseA=-30 + z-1;
PhaseB=210 + z-1;
PhaseC=90 + z-1;
```

```
69
70 %% Theory
71 for phi=1:100
72 Rfault = Rf(phi)/Zb;
73 Transformer_imp=Zt/Zb;
74 line_impedance1=ZL1/Zb;
75 line_impedance0=ZL0/Zb;
76 S2=Zs/Zb;
77 curr = 0.25*exp(1i*0*pi/180);
78 %% Line to ground fault
79 if Fault_Type==1
80 V_th=(curr*((1-m)*line_impedance1+S2));
81 Z_1_thev=(S2+(1-m)*line_impedance1);
82 Z_0_thev=(1/(1/(S2+(1-m)*line_impedance0)+1/(Transformer_imp+m*
      line_impedance0)));
83 Z_2_thev=Z_1_thev;
84
85 I_a1=V_th/(Z_1_thev+Z_2_thev+Z_0_thev+3*Rfault);
86 I_fault=3*I_a1;
87 I_r1=curr;
88 I_r2=0;
89 I_r0=I_a1*(S2+(1-m)*line_impedance0)/(Transformer_imp+S2+
      line_impedance0);
90 I_AR=I_r1+I_r2+I_r0;
91
92 V_r1=(I_r1*m*line_impedance1)+(V_th-I_a1*Z_1_thev);
93
94 V_r2=-I_a1*Z_2_thev;
95
96 V_r0=I_r0*m*line_impedance0-I_a1*Z_0_thev;
97
98
99 V_AR=V_r1+V_r2+V_r0;
100
101 Apparent_Impedance1(phi)=V_AR/(I_AR+K0*I_r0);
102 true_imp=v_simu(1)/(i_simu(1)+K0*seq_simu(3));
103 %% Code to identify fault resistance where classical mho is exceeded
104 % if angle(reach*line_impedance1-Apparent_Impedance1(phi))-angle(
      Apparent_Impedance1(phi))>=(pi/2) && limit_LG==0
105 % limit_LG=Apparent_Impedance1(phi)
106 % limit_Rf=Rfault*Zb
107 % end
108 %% If statement to allow plotting of multiple relay impedances with
      varying fault resistances for varying network parameters
109 % if p==1
110 %     temp1(phi)=Apparent_Impedance1(phi);
111 % elseif p==2
112 %     temp2(phi)=Apparent_Impedance1(phi);
113 % elseif p==3
```

```
%     temp3(phi)=Apparent_Impedance1(phi);
% elseif p==4
%     temp4(phi)=Apparent_Impedance1(phi);
%
% end


end
%% Line to line fault
if Fault_Type==2
Z_1_thev=(S2+(1-m)*line_impedance1);
Z_2_thev=Z_1_thev;

V_th=(curr*((1-m)*line_impedance1+S2));

I_a1=V_th/(Z_1_thev+Z_2_thev+Rfault);

I_fault=-i*sqrt(3)*I_a1;

V_r1=(curr*m*line_impedance1+(V_th-(I_a1*Z_1_thev)));

V_r2=(I_a1*(Rfault+Z_2_thev)*(Z_2_thev/(Z_2_thev+Rfault)));

V_AR=V_r1+V_r2;

I_AR=curr;

Apparent_Impedance2(phi)=(V_r1-V_r2)/curr;

if angle(reach*line_impedance1-Apparent_Impedance2(phi))-angle(
   Apparent_Impedance2(phi))>=(pi/2) && limit_LL==0
limit_LL=Apparent_Impedance1(phi)
limit_Rf_LL=Rfault*Zb
end
% if p==1
%     temp1l(phi)=Apparent_Impedance2(phi);
% elseif p==2
%     temp2l(phi)=Apparent_Impedance2(phi);
% elseif p==3
%     temp3l(phi)=Apparent_Impedance2(phi);
% elseif p==4
%     temp4l(phi)=Apparent_Impedance2(phi);
%
% end



end

```

```
162 end
163 %% Plotting circular mho
164 theta=-2*pi:0.00001:2*pi;
165 x=(reach/2)*(abs(line_impedance1))*(exp(i*(theta))+exp(i*angle(
       line_impedance1)));
166
167 %% Plotting quadrilateral mho
168 plot([0, i*reach*abs(line_impedance1)-0.02,i*reach*abs(line_impedance1
       )+abs(line_impedance1),abs(line_impedance1)-0.02,0],'black');
169
170 hold on
171 plot(x,'black')
172 test=[0,line_impedance1];
173 plot(test,'--');
174 true=plot(m*line_impedance1,'X','DisplayName','Position of fault along
        line');
175 %       end
176 imp1=plot(Apparent_Impedance1,'DisplayName','L-G fault relay impedance
       ');
177
178 %% Plotting values given by Simulink for verification purposes
179 %% lg
180 % plot(0.00837094111720902 + 0.0852783130100865i,'x');
181 % plot(0.0137260077887392 + 0.0859687544437430i,'*');
182 % plot(0.0189673292199148 + 0.0870209207994856i,'.');
183 % plot(0.0238595469764596 + 0.0883530830634956i,'+');
184 %% ll
185 % plot(0.0069 + 0.0858i,'x');
186 % plot(0.0107635752848137 + 0.0861359682261649i,'*');
187 % plot(0.0145480425008113 + 0.0866122688135489i,'.');
188 % plot(0.0181326851517763 + 0.0872423464053490i,'+');
189 %% 240 Hz
190 %lg
191 % plot(0.00780510096069457 + 0.165433349700472i,'x');
192 % plot(0.0132885301281304 + 0.165768066617194i,'*');
193 % plot(0.0187458377393607 + 0.166276774870447i,'.');
194 % plot(0.0239523038837554 + 0.166926815124635i,'+');
195
196
197
198 % impMV1=plot(temp1,'DisplayName','L-G fault relay impedance 25%','
       Color','blue');
199 % impMV2=plot(temp2,'DisplayName','L-G fault relay impedance 50%','
       Color','magenta');
200 % impMV3=plot(temp3,'DisplayName','L-G fault relay impedance 75%','
       Color','Red');
201 % impMV4=plot(temp4,'DisplayName','L-G fault relay impedance 95%','
       Color','Green');
202 %
```

```
203
204
205
206 % imp2=plot(Apparent_Impedance2,'--','DisplayName','Line to Line fault
      relay impedance','Color','BLue');
207 % impMV1l=plot(temp1l,'--','DisplayName','L-L fault relay impedance
    25%','Color','blue');
208 % impMV2l=plot(temp2l,'--','DisplayName','L-L fault relay impedance
    50%','Color','magenta');
209 % impMV3l=plot(temp3l,'--','DisplayName','L-L fault relay impedance
    75%','color','Red');
210 % impMV4l=plot(temp4l,'--','DisplayName','L-L fault relay impedance
    95%','Color','Green');
211 % % plot(imp,'X');
212 impMV1x=plot(Apparent_Impedance1(26),'x','DisplayName','L-L fault
    relay impedance R=2.5','Color','black');
213 % plot(temp2(20),'x','DisplayName','L-G fault relay impedance R=2','
    Color','black');
214 impMV1y=plot(Apparent_Impedance1(51),'*','DisplayName','L-L fault
    relay impedance R=5');
215 impMV1z=plot(Apparent_Impedance1(76),'.','DisplayName','L-L fault
    relay impedance: R=7.5');
216 impMV1q=plot(Apparent_Impedance1(100),'+','DisplayName','L-L fault
    relay impedance: R=10');
217
218
219
220 legend([ imp1 true impMV1x impMV1y impMV1z impMV1q])
221 hold off
```